Molecular phylogenetics, morphological evolution, and speciation of Chinese stout newts (Salamandridae: Pachytriton)

Dissertation Advisor: Dr. James Hanken Yunke Wu

Molecular phylogenetics, morphological evolution, and speciation of Chinese stout newts (Salamandridae: *Pachytriton*)

Abstract

China harbors 10% of the world's salamander species. Studying their evolutionary history provides critical insights into the evolution of the fauna of the Far East. The stout newts (*Pachytriton*, also known as paddle-tailed newts) are a genus of aquatic montane salamanders that are widely distributed in southeastern China. Despite their longstanding popularity among the global pet trade, little is known of their biology beyond external morphology. My thesis presents the first systematic study to elucidate phylogenetic relationships, character evolution, biogeographic patterns, species delimitation, and speciation mechanisms in this genus.

Chapter 1 constructs the molecular phylogeny of *Pachytriton* based on mitochondrial and nuclear genes. The two geographically isolated populations of *P. inexpectatus* are paraphyletic. Rampant convergence of external color pattern likely resulted from habitat selection. Ancestral range reconstruction indicates that the genus originated in the Nanling Mountain Range and subsequently colonized northern mountainous regions.

Chapter 2 describes aquatic specializations in *Pachytriton* through an osteological study. Adaptations include a modified hyobranchial apparatus (specialized for suction feeding), a reduced frontosquamosal arch (correlated with absence of predators in

shallow streams), and deep neural and haemal arches on caudal vertebrae (associated with powerful swimming). Intrageneric comparisons further support the phylogeny from Chapter 1.

Chapter 3 investigates the impact of paleoclimatic changes on *Pachytriton*. Initial speciation occurred after the substantial intensification of the East Asian summer monsoon during the late Miocene. Monsoonal rains facilitate range expansion in the genus. Species likely were formed through subsequent vicariant isolation. A novel temperature buffer-zone model suggests widespread physiological stress of *Pachytriton* populations during the Pliocene warming period and identifies Huangshan Mountain as a potential climatic refugium.

Chapter 4 evaluates the evolutionary independence of three recently described species, which until recently were considered conspecific populations of *P. brevipes*. Species status is supported for each new species by coalescent-based species delimitation methods, despite signals of interspecific gene flow. Ecological niche modeling and multivariate analysis reveal significant niche differentiation among species. Yet, niches are more similar than expected given the different environmental backgrounds, implicating a high degree of niche conservatism. Speciation most likely occurred through isolation of lineages on different montane peaks.

Table of Contents

List of Figures

I. **Chapter 1**

II. **Chapter 2**

IV. **Chapter 4**

List of Tables and Appendices

I. **Chapter 1**

II. **Chapter 2**

III. **Chapter 3**

IV. **Chapter 4**

Acknowledgements

I owe my deepest gratitude to my advisor, Dr. James Hanken, for his masterly guidance throughout my graduate study. Jim provides me the precious opportunity to work on taxa that I am most interested in—Chinese salamanders. I still remember the first day we discussed about my potential Ph.D. project in his office. We simultaneously pointed to the bizzare distribution map of the Chinese stout newts (*Pachytriton*), which become a major component of my life in the past several years. This dissertation would not have been possible without Jim's constant support from all aspects—mentally, academically, and financially. He always stands behind me when I am hesitated. He makes every effort to help me establish connections with Chinese institutes in order to make my research going smoothly. All my field works in China were funded by his grants. Jim is always available to discuss the progress of my study and revisions of manuscripts. Particularly, I benefit tremendously from his unparalleled writing skill, which forces me to think about the wording carefully before writing. Otherwise I see a red "awk" gradually appearing in front of my eyes.

I am also very grateful to my other two committee members, Dr. Scott Edwards and Dr. Jonathan Losos, who have supported me during the course of the project in countless ways. Scott teaches me molecular phylogenetics and population ecology and expands my horizon into the new era of phylogenomics. He provides valuable comments that drive me to refine the analyses in this dissertation. Scott always welcomes me when I interrupted his work by directly walking into his office and looking for advice. During my years at the Museum of Comparative Zoology, Jonathan passes me his great passion for amphibians and reptiles, which becomes my inspiration and motivation. It is also my

biggest honor to be a student and then a teach fellow with Jonathan in the fun classroom of Herpetology. Lastly, both Jonathan and Scott generously allow their students to help me with questions in my research.

I would like to thank José Rosado, Joe Martinez, Tsuyoshi Takahashi, and Jonathan Woodward in the Herpetology Department for their kindly assist with specimen loans, both for my Ph.D. project and the course of Herpetology. I would also thank Ermi Zhao, Yuezhao Wang, Yueying Chen, and Shunquan Li from Chengdu Institute of Biology, the Chinese Academy of Sciences for their enormous assist with specimen transportation from China to Harvard. I would thank Yaping Zhang and Jing Che from Kuming Insitutute of Zoology, the Chinese Academy of Sciences for their generosity to loan tissue samples to me. I would extend my sincere thanks to all other staffs in the Department of Organismic and Evolutionary Biology and the Museum of Comparative Zoology. Particularly, Melissa Aja patiently helped me countless times with purchase and reimbursement. Chris Preheim from the administration office helped me with all sorts of administrative issues. Ronnie Broadfoot and Mary Sears of the Enrst Mayr Library assisted me numerous times in search of literatures. My special thanks go to Marie Studer, Jeffrey Holmes, and Tracy Barbaro at the office of Encyclopedia of Life (EOL), who offered me the opportunity to share my expertise in Chinese salamanders to a broad audience of EOL.

I am fortunate to be able to work with so many sweet people in the Hanken Lab. The past and present lab members are my lifetime treasure. Anne Everly, Breda Zimkus, Zachary Lewis, Elizabeth Sefton, Nadine Piekarski, Hillary Maddin, David Blackburn, Carlos Infante, Ryan Kerney and many others have made their contributions into this

dissertation. More importantly, over those past years when I was alone in a foreign country, they are my family. I am also grateful to members from the Losos Lab and Edwards Lab, who have helped me unselfishly. I would thank Max Sparreboom from Amsterdam, who shares with me his expertise in Asian salamanders. I owe a lot of gratitude to my Chinese colleagues. They have accompanied me to the most remote mountains in southeastern China by train, by bus, by motorcycle, and by foot. First and foremost, I would thank Ke Jiang, a passionate, young herpetologist who I have admired for the past ten years since we first met. Without his field experience and social network, I could not have completed my five field trips to China. Ke Jiang further helped me to acquire specimens from other institutes or individuals. I would never forget the help I got from Mian Hou, Xin Chen, Zhuocheng Zhou, Xu Zhang, Yuhong Guo, Gang Bai, Ziyu Ma and others for assistance in the field.

Above all, I am deeply indebted to my parents, Xiansheng Wu and Ping Wang, for their lifetime support to my research career without any reservations, even though they know that this career would not make a big profit as some others do. But they also know that I love animals since I was a kid, so they brought me to the zoo and tolerated every strange, live or dead, animal at home. They know that I am happy to do such kind of research, so they encourage me to follow my passion. I could not ask for better parents, and I know that I would never be able to pay back what they have done for me. Although words can barely describe my gratitude, I still want to say thank you! I am also grateful to other family members for their constant support.

Finally, I would like to thank Jie Fang, my beloved wife, who has made so many sacrifices to help me pursue my research career. She had to leave her family and friends

and to quit her high-paid job to follow me to the US. She takes good care of our daily lives so that I can concentrate on the research. Whenever I am at the low tide of my enthusiasm for the work, she always encourages me to keep my spirits high. I am fortunate and proud to have Jie as my companion and would share with her the sweetness and bitterness of every moment of my life.

I dedicate this work to my parents, who have raised, indulged, and supported a child with a born affection for the nature.

Chapter 1

Homoplastic evolution of external coloration in Chinese stout newts (Salamandridae: *Pachytriton*) inferred from molecular phylogeny[1]

[1] Partial results presented in this chapter are published in Zoologica Scripta (2010).

Abstract

The Asian stout newts of the genus *Pachytriton* inhabit montane streams in southeastern China. Despite their abundance in the pet trade, the phylogeny and systematics of this genus are poorly understood. Coloration is often used to delimit species under the assumption that consistent chromatic differences characterize independent evolutionary lineages. I present the first phylogenetic study of *Pachytriton* that incorporates mitochondrial and nuclear DNA along with morphometric characters, to infer intrageneric evolutionary relationships, patterns of color evolution, and likely geographic origin of the genus. My results support the monophyly of *Pachytriton* and recover *P. archospotus* as the sister taxon to *P. brevipes*[2]. Monophyly of *P. inexpectatus* is significantly rejected: southwestern populations are sister to the group of *P. brevipes* plus *P. archospotus*, whereas northeastern populations are nested within *P. brevipes*. The two geographic units are further separated by multivariate morphological analyses. Southwestern *P. inexpectatus* is the type species; misidentification of northeastern populations as *P. inexpectatus* results from their similar coloration. The unspotted, dark brown dorsal coloration is the likely ancestral state for the genus. Small black spots, which characterize *P. brevipes* and *P. archospotus*, were acquired independently numerous times. Reversal from the black-spotted coloration to the unspotted coloration also occurred in multiple populations. Color pattern in the genus is correlated with stream substrate type; change of the latter leads to change in coloration. Coloration in *Pachytriton* evolves at a high transitional rate and is an unreliable character for species diagnosis. My analyses demonstrate the importance of comprehensive sampling in

[2] Discussion is based on the taxonomy that was widely accepted before the start of my doctorate study (see Zhao & Hu 1984 and Fei *et al.* 2006). This chapter provides evidence for taxonomic revision (for updated taxonomy, see Chapters 3 and 4).

ancestral character reconstruction. *Pachytriton* most likely originated in the Nanling Mountain Range and subsequently colonized northern mountainous regions. *Pachytriton* is under the threat of human collection and habitat destruction and is in urgent need of conservation protection.

Introduction

The booming utilization of molecular techniques and associated analytical tools has facilitated reassessment of evolutionary relationships that previously were inferred mainly by analysis of phenotypic variation. Phylogenies derived from molecular data may confirm, supplement, and sometimes reject traditional taxonomic assessments. The latter instance often yields new evolutionary hypotheses to explain the incongruence between molecular data and other phenotypic characters (e.g., Schaefer *et al.* 2002; García-París *et al.* 2003; Babik *et al.* 2005). In vertebrate phylogenetics, mitochondrial DNA (mtDNA) is a frequently used marker for molecular analysis because it generally evolves faster than nuclear genes (Ballard & Whitlock 2004). The typically one-fourth coalescent time of mtDNA, in comparison to autosomal nuclear genes, offers an advantage for studies of closely related species in which lineage sorting of ancestral gene copies may confound the gene tree with the true species tree (Moore 1995). However, in most cases mitochondrial genes are all linked as a single molecule, which provides only one independent estimate of the phylogeny, and such results may be misleading if there has been mitochondrial introgression. As advocated by integrative taxonomists, the combination of multiple lines of evidence, including independent molecular markers, morphology, behavior, ecology, etc., yields the most informative and insightful evaluation of evolutionary relationships among species (Padial *et al.* 2009).

The Asian stout newts of the genus *Pachytriton* are popular in the global pet trade. In nature they inhabit tiny shallow montane streams across southeastern China, a large geographic area that is characterized by mountain ranges exceeding 2000 m in elevation. These mountains were uplifted by folding and deformation of the Earth's crust in

polyphasic inherited orogenies from the Late Permian through the Cenozoic (Guo 1998). Between adjacent mountain ranges lie lower plains and large river systems, which constitute zoogeographic barriers to montane salamanders (Fu & Zeng 2008; Shepard & Burbrink 2008). Additionally, most areas of East Asia were not glaciated during the Pleistocene (Williams *et al.* 1998). In situations such as this, I can expect that the combination of complex topography and long-term persistence of populations on isolated mountain peaks may promote significant levels of interspecific and intraspecific genetic differentiation, as well as geographically based phenotypic divergence.

For a long time, *Pachytriton* was believed to comprise just two species: *P. brevipes*, the black-spotted stout newt, and *P. labiatus*, the unspotted stout newt (Zhao & Hu 1984; Fei *et al.* 2006). As their common names imply, these two species are distinguished mainly by external color pattern. Recently, *P. archospotus* was described from a population previously regarded as *P. brevipes*, which it resembles in coloration (Shen *et al.* 2008). Another recent study suggests that the lectotype of *P. labiatus* is actually a member of the closely related genus *Paramesotriton* (Nishikawa *et al.* 2011). Consequently, the specific epithet *labiatus* has been assigned to *Paramesotriton*, and the *Pachytriton* species originally known as *P. labiatus* given a new name, *P. inexpectatus* (Nishikawa *et al.* 2011). I adopt this nomenclature change hereafter.

While phylogenetic relationships of *Pachytriton* to other Asian salamandrids are well resolved—the genus forms a well-supported, monophyletic group with *Laotriton*, *Paramesotriton*, and *Cynops* (Titus & Larson 1995; Chan *et al.* 2001; Weisrock *et al.* 2006; Steinfartz *et al.* 2007; Zhang *et al.* 2008)—phylogenetic relationships within *Pachytriton* have not been assessed in detail, largely due to the difficulty of obtaining

specimens with verified locality data. Interestingly, only two previous molecular studies analyzed more than one specimen of *Pachytriton*, yet each study revealed substantial genetic divergence in the genus. In Chan *et al.* (2001), one commercially obtained *P. inexpectatus* was so different from two other conspecific specimens in cytochrome *b* sequences that Chan *et al.* concluded that *P. inexpectatus* could comprise more than one species. Another extensive work on Salamandridae by Weisrock *et al.* (2006) revealed the possible paraphyly of *P. brevipes*, with one specimen of this species grouping with *P. inexpectatus* rather than with other *P. brevipes*. The three named species of *Pachytriton* are mainly distributed in allopatry, occupying three isolated regions with mountains ranges oriented roughly from north to south. Interestingly, the southern ends of these three regions converge to form the the east-west oriented Nanling Mountain Range, where all three species occur. Given this unique distributional pattern, I can also test whether the Nanling Mountain Range, which is one of the three centers of amphibian diversity in China (Xie *et al.* 2007), represents as the center of origin for this salamander genus.

Here I present the first phylogenetic study of the genus *Pachytriton*, based on complete mitochondrial gene sequences that code for cytochrome *b* (cty*b*) and subunit two of NADH dehydrogenase (*ND2*), as well as partial nuclear-coding sequences from recombination activating gene 1 (*RAG-1*). I reconstruct a resolved phylogeny of samples from populations of *P. archospotus*, *P. brevipes*, and *P. inexpectatus*. The current distribution of *P. inexpectatus* comprises two allopatric areas separated by a gap of at least 600 km (Fei *et al.* 2006). I assess the evolutionary relationship between populations of these two areas from molecular phylogenetic and additional morphometric data. Based

Figure 1-1[3]. Distribution of *Pachytriton brevipes* (solid line), *P. inexpectatus* (long-dashed line), and *P. archospotus* (short-dashed line) in southeastern China (Zhao & Hu 1984; Fei *et al.* 2006; Shen *et al.* 2008), with representative animals collected from the corresponding ranges. *Pachytriton inexpectatus* has a disjunct distribution. Solid circles denote sampled localities.

[3] This distribution map represents people's understanding of *Pachytriton* before the start of my doctorate study. The taxonomy has been revised recently (see Figure 4-1 in Chapter 4).

on the inferred phylogeny, I discuss how different color patterns may have evolved within *Pachytriton*. I further estimate the likely geographic origin for the genus and the routes by which it colonizes the southeastern China. Finally, I highlight the need for conservation efforts to end overexploitation and habitat destruction, which are the most serious factors leading to amphibian declines in east Asia (Collins & Storfer 2003; Stuart *et al.* 2004).

Materials and methods

Data collection

Specimens of *Pachytriton* were collected in two periods. During the first period (2007–2008), I sampled three populations of *Pachytriton brevipes*[4], three *P. inexpectatus* populations from the northeastern distribution (NE), three *P. inexpectatus* populations from the southwestern distribution (SW), and one population of *P. archospotus* (Fig. 1-1; Table 1-1). Type localities of all three species were included to ensure correct phylogenetic inference. I also included five market-obtained *P. inexpectatus* to identify the source of commercial exploitation. Specimens were sampled from pet stores in Chengdu during May 2007 and in Hangzhou during August 2007. These five specimens are morphologically similar to *P. inexpectatus* from Zhejiang province. An additional 34 populations from several species were sampled in the second period (2009–2011; Table 4-1). Because samples collected during the first period are sufficient to reveal major phylogenetic patterns within the genus, the additional populations are only used in reconstruction of ancestral color patterns and the geographic range of the genus. Fresh liver or muscle was dissected from euthanized animals and preserved in 100% ethanol,

[4] Species designation follows the taxonomy in Zhao & Hu (1984) and Fei *et al.* (2006).

Table 1-1. Taxon sampling and specimens used in this study.

Sampling	**Museum No.**	**Genebank Accession No.**		
Pachytriton inexpectatus		*ND2*	*cytb*	*RAG-1*
Dayaoshan, Guangxi	CIB88165	GQ303602	GQ303639	GQ303680
Mao'ershan, Guangxi1	CIB88182	GQ303594	GQ303631	GQ303672
Mao'ershan, Guangxi2	CIB88173	GQ303595	GQ303632	GQ303673
Mao'ershan, Guangxi3	CIB88158	GQ303596	GQ303633	GQ303674
Mao'ershan, Guangxi4	CIB88156	GQ303597	GQ303634	GQ303675
Leigongshan, Guizhou1	CIB88162	GQ303598	GQ303635	GQ303676
Leigongshan, Guizhou2	CIB88148	GQ303600	GQ303637	GQ303678
Leigongshan, Guizhou3	CIB88170	GQ303601	GQ303638	GQ303679
Leigongshan, Guizhou4	CIB88147	GQ303599	GQ303636	GQ303677
Tianmushan, Zhejiang1	CIB88145	GQ303606	GQ303643	GQ303684
Tianmushan, Zhejiang2	CIB88137	GQ303607	GQ303644	GQ303685
Tianmushan, Zhejiang3	CIB88152	GQ303608	GQ303645	GQ303686
Tianmushan, Zhejiang4	CIB88139	GQ303609	GQ303646	GQ303687
Tiantaishan, Zhejiang1	CIB88143	GQ303610	GQ303647	GQ303688
Tiantaishan, Zhejiang2	CIB88161	GQ303611	GQ303648	GQ303689
Tiantaishan, Zhejiang3	CIB88169	GQ303612	GQ303649	GQ303690
Jinhua, Zhejiang1	CIB95997	GQ303624	GQ303661	GQ303702
Jinhua, Zhejiang2	CIB95996	GQ303625	GQ303662	GQ303703
Pet Trade, Chengdu1	CIB88138	GQ303603	GQ303640	GQ303681
Pet Trade, Chengdu2	CIB88181	GQ303604	GQ303641	GQ303682
Pet Trade, Chengdu3	CIB88135	GQ303605	GQ303642	GQ303683
Pet Trade, Hangzhou1	CIB88142	GQ303613	GQ303650	GQ303691
Pet Trade, Hangzhou2	CIB88168	GQ303614	GQ303651	GQ303692
Pachytriton brevipes				
Junfengshan, Jiangxi1	CIB95926	GQ303626	GQ303663	GQ303704
Junfengshan, Jiangxi2	CIB95930	GQ303627	GQ303664	GQ303705
Wuyishan, Fujian1	CIB88221	GQ303615	GQ303652	GQ303693
Wuyishan, Fujian2	CIB88194	GQ303616	GQ303653	GQ303694
Wuyishan, Fujian3	CIB88188	GQ303617	GQ303654	GQ303695
Wuyishan, Fujian4	CIB88197	GQ303618	GQ303655	GQ303696
Wuyishan, Fujian5	CIB88192	GQ303619	GQ303656	GQ303697
Youxi, Fujiang1	CIB88207	GQ303620	GQ303657	GQ303698
Youxi, Fujiang2	CIB88189	GQ303621	GQ303658	GQ303699
Youxi, Fujiang3	CIB88190	GQ303623	GQ303660	GQ303701
Youxi, Fujiang4	CIB88185	GQ303622	GQ303659	GQ303700
Pachytriton archospotus				
Qiyunshan, Hunan1	CIB95953	GQ303628	GQ303665	GQ303706
Qiyunshan, Hunan2	CIB95950	GQ303629	GQ303666	GQ303707
Qiyunshan, Hunan3	CIB95949	GQ303630	GQ303667	GQ303708

Table 1-1 (continued)

Sampling	**Museum No.**	**Genebank Accession No.**		
*Paramesotriton ermizhaoi*1	CIB88141	FJ744601	GQ303670	GQ303711
*Paramesotriton ermizhaoi*2	CIB88140	FJ744602	GQ303671	GQ303712
*Paramesotriton deloustali*1	MVZ223628	FJ744599	GQ303668	GQ303709
*Paramesotriton deloustali*2	MVZ223629	FJ744600	GQ303669	GQ303710

then stored at 4 °C before final transfer to permanent storage at -80 °C. *Paramesotriton* was chosen as a phylogenetic outgroup based on its known close relationship to *Pachytriton* (Chan *et al.* 2001; Weisrock *et al.* 2006; Steinfartz *et al.* 2007).

Extraction, amplification, and sequencing

Genomic DNA was extracted from preserved liver or muscle tissue using a QIAGEN DNeasy blood and tissue kit following the manufacturer's protocol. Amplifications of mitochondrial fragments were conducted under the condition of initial denaturation at 94 °C for 2 min, followed by 35 cycles of denaturation at 94 °C for 30 s, annealing at 52 °C for 45 s, extension at 72 °C for 90 s, and a final extension at 72 °C for 5 min. Cycle annealing temperature was raised to 56 °C and final extension was increased to 7 min for the nuclear *RAG-1* gene, with other conditions unchanged. Negative controls were added to detect contamination. Amplified products were examined on 1% agarose gels and successively purified with a QIAquick PCR purification kit, and then sequenced on an ABI 3730. All regions were sequenced in both directions. PCR primers (Table 1-2) were designed specifically to *Pachytriton* and *Paramesotriton* for successful amplification and sequencing. Internal primers were applied to improve sequence quality. Sequences are deposited in GenBank.

Phylogenetic analyses based on samples from 2007–2008

Mitochondrial sequences were amplified for the complete *ND2* and flanking tRNAs (hereafter, "*ND2*") and the complete *cytb* and flanking tRNAs ("*cytb*"). The nuclear fragment was amplified for the *RAG-1* gene. Sequences were imported into Se-Al 2.0 (Rambaut 1995) and aligned manually. Codon positions were determined according to

reference sequences from the *Paramesotriton hongkongensis* mitochondrial genome (Zhang *et al.* 2005) and the complete *RAG-1* coding sequence from *Pleurodeles waltl* (Frippiat *et al.* 2001). To assess the extent of substitution saturation, uncorrected pairwise distances (*p*-distance) were plotted against K2p-corrected distances (Kimura two-parameter model; Kimura 1980) for both transitions and transversions at each codon position in each gene. If a corrected distance is excessively larger than the corresponding uncorrected distance, then more than one substitution has occurred at some sites, thus increasing the chance of homoplasy. Saturation was further evaluated by Xia's (2003) saturation index in the program DAMBE (Xia & Xie 2001). Mitochondrial divergences among populations are represented by net uncorrected pairwise distances in MEGA 4 (Tamura *et al.* 2007). To assess phylogenetic congruence between genes, Partition Homogeneity Tests (Farris *et al.* 1995) implemented in PAUP 4.0b10 (Swofford 2002) were conducted for 100 replicates.

Phylogenetic topologies were reconstructed under the maximum-likelihood (ML) criterion. The best-fit substitution model was determined by Akaike Information Criterion (AIC) implemented in MODELTEST 3.7 (Posada & Crandall 1998). The resultant model parameters were input into Garli v.0.951 (Zwickl 2006). The search for the ML tree was terminated when the likelihood score had not been improved for 500,000 generations. Bootstrap values were calculated for 100 replicates with the termination generation reducing to 100,000. For the maximum parsimony (MP) analysis, heuristic searches were performed for 1000 replicates of random sequence additions with tree-bisection-reconnection (TBR) as the branch-swapping algorithm in PAUP 4.0b10. Gaps were treated as missing data and ambiguous nucleotides were interpreted as

Table 1-2. Primers designed in this study. MtDNA primers are named by their 5' position in the mitochondrial genome of *Paramesotriton hongkongensis* (AY458597; Zhang *et al.* 2005); nuclear primers are named by their 5' position in the *RAG-1* coding sequence of *Pleurodeles waltl* (AJ010258; Frippiat *et al.* 2001).

Gene	Primer	Sequences 5'-3'
ND2	3787F	TCGTGCGCCCACTACACTAT
	5081R	GTCGTAGGGTCAAAGCCTGC
	4416F	ATAGCATACTCATCCATTGCACA
cytb	14052F	CCTGGGCTCTAACCAAGACC
	15293R	TCGGCTTACAAGACCGATGT
	14590F	TCCCTAGTAGAGTGAGTCTGG
RAG-1	1738F	CTGGTGCAGTCTGTTGATGA
	3049R	GCCTGGCATTCATTTTCCTG

uncertainty. Non-parametric bootstrap values were calculated for 1000 replicates, each of which included 100 replicates of random sequence additions. Bayesian inference (BI) was performed in MrBayes 3.1.2 (Huelsenbeck & Ronquist 2001). I partitioned the mitochondrial data according to gene functions and codon positions, following the suggestion from Zhang *et al.* (2008) based on a mitogenomic study of Salamandridae. Nuclear *RAG-1* data were not partitioned for its low level of variation. The best-fit substitution model was selected by AIC implemented in MrModeltest 2.2 (Nylander 2004). Markov chain Monte Carlo (MCMC) analyses were carried out simultaneously in two independent runs with default heating and sample frequency for 2 million generations. Convergence between runs is determined by the average standard deviation of split frequencies. The first one-fourth of the runs was discarded as burn-in.

To evaluate competing phylogenetic hypotheses, alternative phylogenies of highest likelihood were reconstructed under topological constraints in Garli v.0.951 with the same substitution model used in the ML analysis. These topologies were then loaded into PAUP 4.0b10 and statistically compared with the ML tree by using a Templeton test (Templeton 1983), a one-tailed KH test (Kishino & Hasegawa 1989), and a one-tailed SH test (Shimodaira & Hasegawa 1999). Tests were performed for both mitochondrial and nuclear genes. The KH and SH tests were done with 100 bootstrap replicates under full optimization. To trace the evolutionary history of color pattern changes in *Pachytriton*, I coded the observed patterns of sampled populations into binary characters (unspotted vs. black-spotted). I employed a statistical approach using Bayesian mutational mappings in the ancestral state reconstruction to accommodate uncertainty in the phylogeny by sampling Bayesian trees and associated parameters in proportion to their posterior

probabilities (PP) (Bollback 2006). The posterior distributions of ancestral states are calculated from 20 sets of substitution rate priors drawn from the prior distribution for 20,000 post-burn-in phylogenies from MrBayes. By setting the bias prior on two-state character to the bell-shaped beta distribution (alpha = 5), I assumed that the prior probability for each state is close to 0.5. This analysis was carried out using the program SIMMAP (Bollback 2006).

Phylogenetic analyses based on samples from both periods

Because ancestral state reconstruction can benefit from increased sampling, especially when ML or Bayesian methods are used (Heath *et al.* 2008; Litsios & Salamin 2012), I performed additional reconstruction of the ancestral color patterns in *Pachytriton* using all populations (44 in total) collected from both periods. Instead of using SIMMAP, I employed a second ML method in MESQUITE (Maddison & Maddison 2006) and a third Bayesian method in BayesTraits (Pagel *et al.* 2004) to independently infer the evolutionary history.

The two mitochondrial genes, *ND2* + *cytb*, were sequenced from one specimen per population. The ML tree was estimated by RAxML-HPC 7.3.1 (Stamatakis 2006; Stamatakis *et al*. 2008) with the substitution model chosen in MODELTEST 3.7. The tree and the character matrix of color patterns were imported into MESQUITE, which estimates rates of color change and reconstructs ancestral states to maximize the probability of generating observed states in terminal taxa (Schluter *et al.* 1997; Pagel 1999). Four populations sampled during 2009–2011 exhibit both unspotted and black-spotted colorations; the pattern observed in the majority of specimens was taken as

the coloration of the population. I compared the fitness of the one-rate model (a single rate of change) to the two-rate model (one rate for the change from unspotted to black-spotted coloration and a second rate for change in the opposite direction) using a likelihood ratio test (LRT) with one degree of freedom (*d.f.*).

I also inferred the evolution of color patterns in BayesMultiState (Pagel *et al.* 2004) implemented in BayesTraits. Partitioned BI was performed in MrBayes 3.1.2 with the best-fit substation model chosen in MrModeltest 2.2. The MCMC was run for 10 million generations with sampling at every 1000 generations. The last 5000 trees from the post-burn-in period were used in ancestral state reconstruction in BayesMultiState to accommodate uncertainty in the phylogeny. The character matrix of color patterns was the same as the one used in MESQUITE. Priors for rate of change were set to a uniform distribution (0, 20). The MCMC of BayesMultiState was run for 10 million generations and sampled every 2000 generations. The first one million generations were discarded as burn-in. Probability of either color pattern at each ancestral node is obtained as the arithmetic mean of the corresponding posterior probabilities calculated from 4,500 post-burn-in samples.

During fieldwork, I observe that unspotted populations are often found in streams in which the substrate consist of fine sand or mud, whereas black-spotted populations are more often associated with stream beds that are covered by gravel and small rocks. To test whether color pattern is statistically correlated with stream substrate type, I performed a correlation test in BayesDiscrete (Pagel & Meade 2006) implemented in BayesTraits. The null model in which the two characters evolve independently is compared to the alternative model in which change of one character is dependent on the

state of the other character. Bayes Factor (BF) was used to discriminate models: BF > 2 is conventionally considered as positive evidence in favor of the better model, whereas BF > 6 indicates strong evidence (Kass & Raftery 1995). If evolution of the two characters is correlated, it is possible to test whether stream substrate type changed before or after the change of color pattern. The dependent model is compared to a model in which $q_{12} = q_{13}$ (q_{12} and q_{13} are rates of acquisition for the two characters, respectively) in the transition matrix of Pagel (1994). The MCMC was run on the 5000 post-burn-in trees obtained from MrBayes for 10 million generations and sampled every 2000 generations. The first one million generations were discarded as burn-in.

To determine the geographic origin of *Pachytriton* and subsequent routes of range expansion, I applied the dispersal–extinction–cladogenesis (DEC) model implemented in Lagrange (Ree & Smith 2008). Likelihoods of range inheritance scenarios at cladogenesis events were estimated along with rates of dispersal and local extinction. The geographic distribution of the genus was divided into six regions: 1) the Nanling Mountain Range (N), 2) the Wuyi Mountain Range (W), 3) the western Plateau (P), 4) the Yunxiao Mountain Range (Y), 5) coastal mountains in Fujian and Zhejiang province (C), and 6) Huangshan[5] and adjacent mountains (H). Each population was assigned to a corresponding geographic region. Because Lagrange requires the input phylogeny to be ultrametric, I inferred an mtDNA chronogram in BEAST 1.7.0 (Drummond & Rambaut 2007) with default priors and 10 million generations of MCMC (25% burn-in). Given the low dispersal ability of salamanders, I assume that dispersal events only occurred between neighboring regions. It is also unlikely that the ancestor of the genus was widely

[5] I use suffix -*shan* (Chinese pinyin for mountain) to refer to a single mountain, and the capitalized plural *Mountains* to refer to a large mountain range.

distributed in southeastern China as a single species. Therefore, I restricted the geographic range at the root of the chronogram to include at most two of the above six regions.

Morphometric analysis

I use morphometric analysis to assess the similarity of external morphology between *P. inexpectatus* from the two allopatric regions. Fifteen linear measurements were taken from museum specimens in the Chengdu Institute of Biology, Chinese Academy of Sciences (CIB): total length, snout-to-vent length, head length, head width, head depth, snout-to-axilla length, snout length, interocular distance, internostril distance, shoulder width, tail length, tail depth, tail width, forelimb length, and hind limb length. Approximately 15 sexually mature specimens were measured per population. These populations correspond to sampling from the first period and are available from museum collections. Animals obtained from the pet trade were also measured. Each linear measurement was taken multiple times using a digital caliper to minimize error. To reduce dominance of a few variables, such as total length (Manly 2004), measurements were normalized prior to principal-components analysis in SPSS (ver. 13, Chicago, IL). Principal-component (PC) scores were plotted in orthogonal space. I conducted Levene's test (1960) to assess the equality of variances of PC scores among different populations. One-factor analysis of variance (ANOVA) was performed to test if populations are significantly different in PC scores and individual measurements. When variances were heterogeneous among PC scores, Welch's test (1938), which assumes unequal variance, was used instead. Additionally, I applied a multivariate analysis of variance (MANOVA)

to determine if sexual dimorphism contributes to differences among populations.

Results

Characteristics of sequences from 2007–2008

No length variation is observed in the protein-coding region in mitochondrial or nuclear sequences. Only three single-base indels are detected in the mitochondrial tRNA-Trp gene. When K2p-corrected distances are plotted against uncorrected *p*-distances for the mtDNA and *RAG-1* fragments, neither transitions nor transversions show evidence of excessive multiple substitutions, although the third mitochondrial codon position suggests some overprinted substitutions (results not shown). Saturation at the third codon position is significantly rejected by Xia's (2003) saturation index (*ND2*: $P_{\text{symmetrical}} = 0.000$ and $P_{\text{asymmetrical}} = 0.000$; *cytb*: $P_{\text{symmetrical}} = 0.000$ and $P_{\text{asymmetrical}} = 0.000$). Furthermore, downweighting the third codon position does not alter the topology of phylogenetic reconstructions. Both *ND2* and *cytb* exhibit a compositional bias against guanines (12.5% and 14.8%, respectively), while *RAG-1* has a relatively even base composition.

Mitochondrial genes present high levels of interspecific divergence among the three *Pachytriton* species (Table 1-3). Southwestern *P. inexpectatus*, which includes a population sample from its type locality (Dayaoshan), diverges from *P. brevipes* and *P. archospotus* by more than 12.0% and 10.8% in *ND2*, and 7.4% and 8.0% in *cytb*, respectively. Surprisingly, *P. inexpectatus* from the two allopatric ranges exhibit remarkably large genetic differences (12.0–13.4% in *ND2* and 7.4–8.0% in *cytb*), similar to the observed levels of interspecific divergence. Among-population variation is also high within southwestern *P. inexpectatus* (2.1–4.7%), within northeastern *P. inexpectatus*

Table 1-3. Net average uncorrected *p*-distance (in percentage) between and within samples. Lower diagonal: between-group *p*-distance of *ND2*; upper diagonal: between-group *p*-distance of *cytb*. On diagonal before slash: within-group *p*-distance of *ND2*; after slash: within-group *p*-distance of *cytb*.

		Mao'er shan	Leigong shan	Dayao shan[T]	Tianmu shan	Tiantai shan	Jinhua	Wuyi shan	Youxi	Junfeng shan[T]	Qiyun shan[T]
P. inexpectatus (southwestern)	Mao'ershan	0.1/0.1	2.1	2.8	7.6	7.9	7.8	8.7	8.1	8.3	8.5
	Leigongshan	2.8	0.3/0.5	2.7	7.4	7.6	7.5	8.5	7.9	8.1	8.1
	Dayaoshan[T]	4.7	4.3	N/A[§]	7.5	8.0	8.0	8.3	8.1	8.4	8.0
P. inexpectatus (northeastern)	Tianmushan	12.5	12.1	12.0	0.1/0.1	2.5	2.4	6.4	2.2	5.9	6.4
	Tiantaishan	12.8	12.4	12.1	3.8	1/0.7	0.4	6.2	2.8	5.7	7.3
	Jinhua	13.3	13.2	13.0	4.5	0.8	0.2/0.3	6.1	2.8	5.6	7.2
P. brevipes	Wuyishan	12.1	12.2	12.5	7.3	7.9	8.3	0.2/0.2	6.6	0.9	6.8
	Youxi	12.7	12.0	12.0	3.1	3.7	4.5	7.0	0.0/0.0	6.2	6.7
	Junfengshan[T]	12.0	12.3	12.8	7.2	7.9	8.0	1.1	6.9	0.3/0.6	7.0
P. archospotus	Qiyunshan[T]	11.1	10.8	11.0	7.4	8.3	8.5	7.4	7.5	7.3	1.5/1.2

T Type locality
§ Only one specimen is available from Dayaoshan

(0.4–4.5%), and within *P. brevipes* (0.9–7.0%). In contrast, little within-population variation is observed. For *RAG-1* sequences, the average net uncorrected sequence divergence is very limited both among and within *Pachytriton* populations (< 0.9%).

Phylogenetic analyses based on samples from 2007–2008

For ingroup taxa, there are 266 (22.5%) and 206 (17.6%) parsimony-informative sites in the *ND2* (1183 bp) and *cytb* (1172 bp) alignments, respectively. Of 1208 characters in the nuclear *RAG-1* sequences, only 37 are variable and 21 (1.7%) are parsimony-informative. Results from the Partition Homogeneity Test suggest that mitochondrial *ND2* and *cytb* genes are congruent with each other ($P = 0.36$). However, significant incongruence is revealed among *ND2*, *cytb* and *RAG-1* ($P = 0.01$). Removing the third codon position in mitochondrial genes does not result in a homogeneous data set ($P = 0.01$). Therefore, I concatenated the two mitochondrial genes (total 2355 bp) in the phylogenetic inference but analyzed *RAG-1* separately.

The best-fit substitution model was selected as TIM with a proportion of 0.6338 invariable sites for the mitochondrial data in the ML analysis. Nucleotide frequencies were estimated as follows: A = 0.3344, C = 0.2601, G = 0.1225 and T = 0.2829. The ML tree recovers a monophyletic *Pachytriton* with three major clades (Fig. 1-2). Clade A corresponds to southwestern populations of *P. inexpectatus*, which diverged early from other species. Clade B represents the recently described *P. archospotus*. The third lineage (Clade C), which is sister to Clade B, presents an unexpected grouping of northeastern *P. inexpectatus* with *P. brevipes*. Monophyly of northeastern *P. inexpectatus* is not supported statistically. Specimens from the pet trade formed a less-resolved group with northeastern

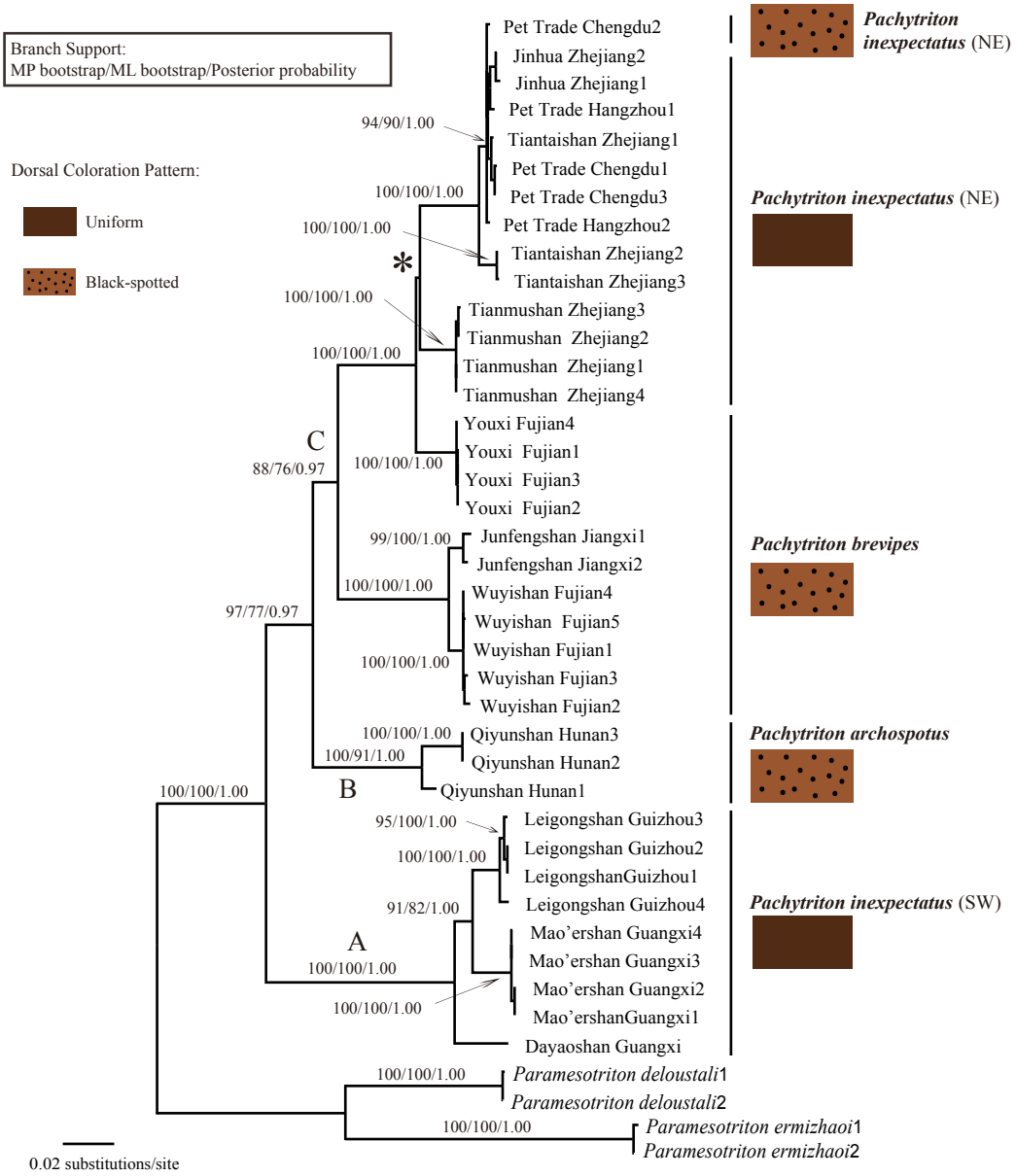

Figure 1-2. Maximum-likelihood gene tree of the genus *Pachytriton* based on combined mitochondrial *ND2* and *cytb* sequence data with bootstrap values and posterior probabilities. Maximum parsimony and Bayesian inference produced very similar topologies. Three principal clades are evident (A, B, C). Dorsal color patterns are mapped to each locality. The asterisk denotes low statistical support for that node. SW, southwestern *P. inexpectatus*; NE, northeastern *P. inexpectatus*.

P. inexpectatus from Tiantaishan and Jinhua. Animals collected at the same locality are either monophyletic or nested with nearby populations. Bayesian inference recovers an identical topology under the GTR+I model for each data partition. Posterior probabilities were high for most major groups, but low again regarding the monophyly of northeastern *P. inexpectatus*. The MP heuristic search against mtDNA found 40 equally parsimonious trees with 1113 steps (CI = 0.6739, RI = 0.9202). The topology of the strict consensus tree resembles that of the ML tree, and relationships between northeastern *P. inexpectatus* and *P. brevipes* from Daiyunshan are unresolved.

The substitution model of TVM with a proportion of 0.9042 invariable sites was selected for *RAG-1* sequences. The ML analysis produced a less-resolved phylogeny than the mtDNA-derived tree. Of the outgroups, *Paramesotriton ermizhaoi* has a long-branch connection to the ingroup taxa (result not shown); the same pattern occurs in the mtDNA ML tree (Fig. 1-2). Long branches reduce the accuracy of outgroup rooting, especially when sequence variation is low, because substitutions on long outgroup branches may converge with those on ingroup branches, resulting in spurious rooting (Graham *et al.* 2002). Therefore, I re-ran the analysis without *Paramesotriton ermizhaoi* and rooted the *RAG-1* phylogenies using only two *Paramesotriton deloustali* (Fig. 1-3). The *RAG-1* ML tree recognizes two main clades: one includes southwestern *P. inexpectatus* and *P. archospotus*; the other groups northeastern *P. inexpectatus* with *P. brevipes*. Maximum parsimony and Bayesian analyses produce similar topologies, although most nodes have low statistical support.

Alternative phylogenetic topologies were compared statistically with the ML trees under both parsimony and likelihood criteria. A monophyletic *P. inexpectatus* as

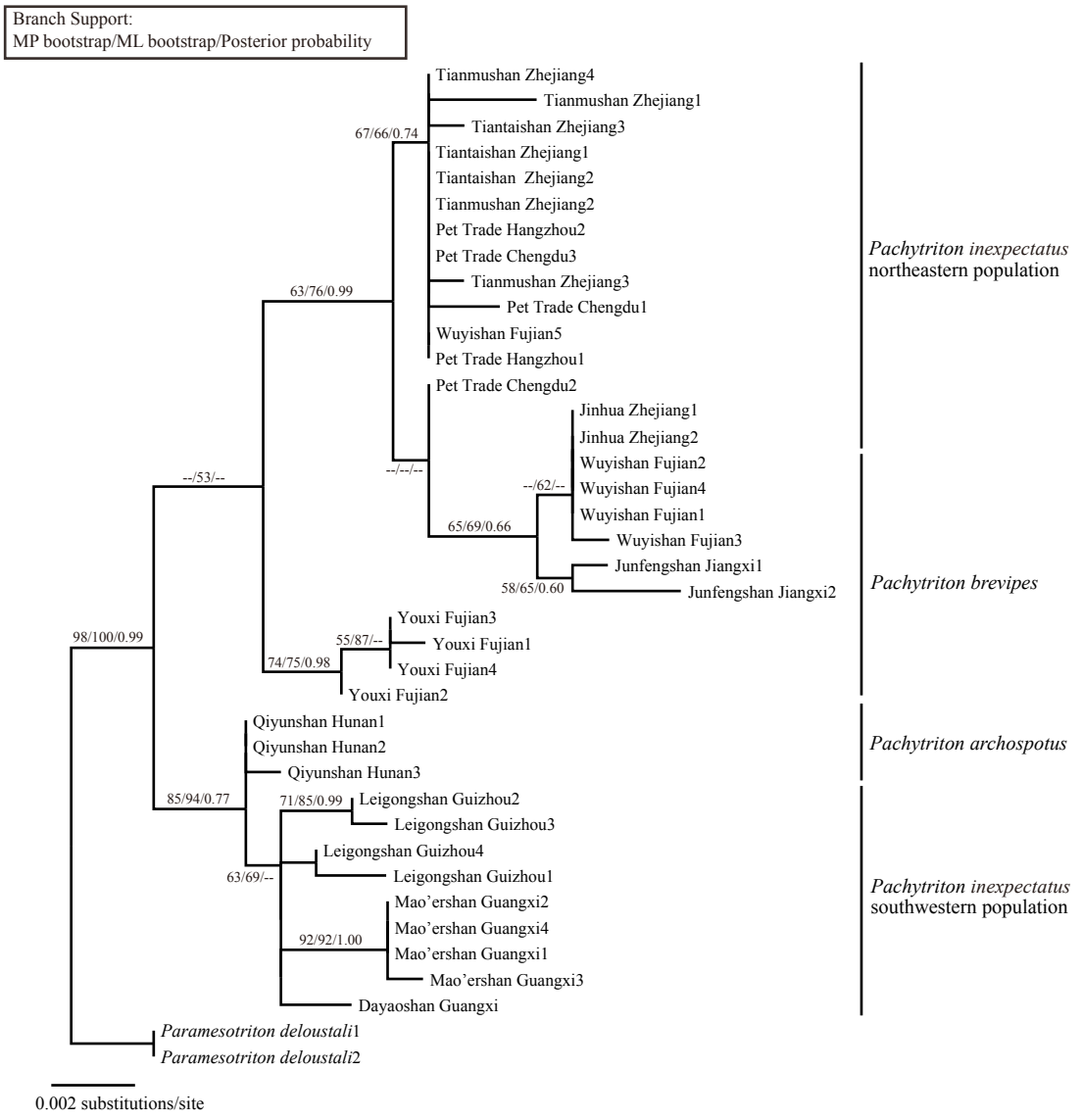

Figure 1-3. Maximum-likelihood gene tree of *Pachytriton* based on *RAG-1* sequences. Levels of statistical support are indicated above or below branches. Double hyphens denote nodes with bootstrap values or posterior probabilities lower than 50 or 0.5. The inferred phylogeny fails to identify the three named *Pachytriton* species as monophyletic clades. The tree is rooted by *Paramesotriton deloustali*.

recognized by Zhao & Hu (1984) and Fei *et al.* (2006) is significantly rejected by the Templeton test, the one-tailed KH test, and the one tailed SH test for both mtDNA and *RAG-1* data (each $P < 0.005$). Reconstruction of the ancestral color pattern with SIMMAP suggests that an unspotted coloration is the likely ancestral state for the genus ($PP_{unspotted} = 0.75$, $PP_{black\text{-}spotted} = 0.25$), which is retained in southwestern *P. inexpectatus* ($PP_{unspotted} = 1.00$, $PP_{black\text{-}spotted} = 0.00$). Black spots likely evolved in the most recent common ancestor (MRCA) of *P. archospotus*, *P. brevipes*, and northeastern *P. inexpectatus* ($PP_{unspotted} = 0.21$, $PP_{black\text{-}spotted} = 0.79$), and was retained in the MRCA of *P. brevipes* and northeastern *P. inexpectatus* ($PP_{unspotted} = 0.19$, $PP_{black\text{-}spotted} = 0.81$).

Phylogenetic analyses based on more extensive sampling

Ancestral state reconstruction using all populations sampled from both periods yields different insights into the evolution of color pattern. For the ML method in MESQUITE, the two-rate model did not fit the data statistically better than the one-rate model (LRT = 3.52, *d.f.* =1, $P = 0.0606$). Therefore, I estimate a single rate (r = 8.13) of change of coloration along the ML tree (Fig. 1-4). Consistent with the result from SIMMAP, the common ancestor of the genus is reconstructed as most likely having an unspotted external coloration. This ancestral state is retained in southwestern *P. inexpectatus*. However, increased sampling suggests that the MRCA of *P. archospotus*, *P. brevipes*, and northeastern *P. inexpectatus* probably also inherited this unspotted coloration, which is further retained in the MRCA of *P. brevipes* and northeastern *P. inexpectatus*. Instead of a single transition from the unspotted coloration, as suggested by analysis using partial sampling, black spots were acquired at least seven times independently.

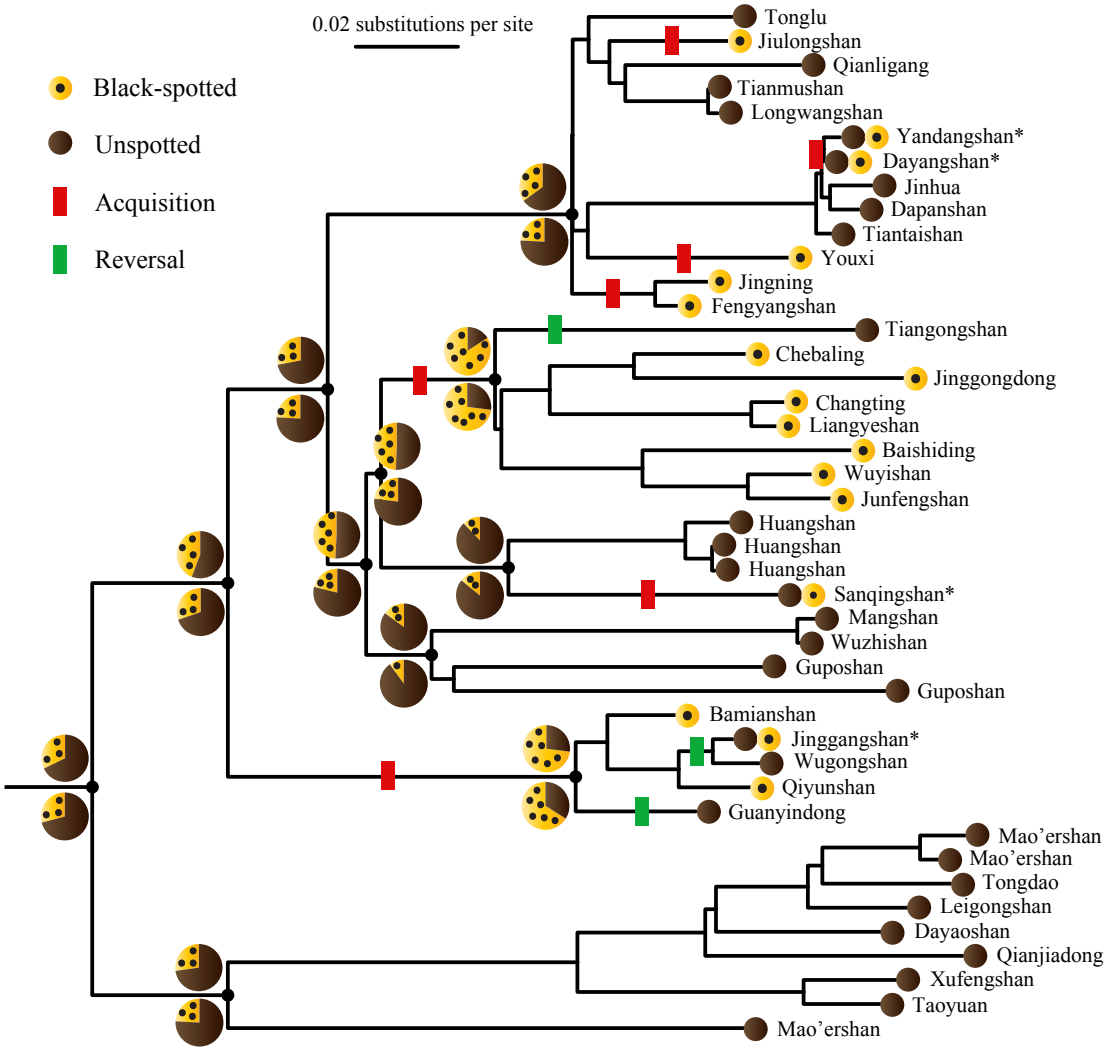

Figure 1-4. Maximum-likelihood mtDNA gene tree of the *Pachytriton* with more extensive sampling. Observed color patterns are mapped to each locality. Asterisks denote populations exhibiting both patterns. Bayesian (up) and maximum-likelihood (below) reconstruction of ancestral states are mapped on internal nodes (black circles). Each red box represents one case of acquisition of the black-spotted coloration; each green box represents a reversal change back to the unspotted coloration.

Reversal from black-spotted to unspotted coloration also occurred at least three times. For the analysis in BayesMultiState, I follow MESQUITE to assume a single transitional rate between colorations. Using 5000 post-burn-in trees, BayesMultiState recovers an evolutionary history similar to that from MESQUITE. Although the support for an unspotted MRCA of *P. archospotus*, *P. brevipes*, and northeastern *P. inexpectatus* is low, this reconstruction is slightly favored over the alternative model in which the MRCA has black spots (BF = 1.44). Similarly, there is positive evidence in favor of the unspotted coloration in the MRCA of *P. brevipes* and northeastern *P. inexpectatus* instead of the black-spotted coloration (BF = 2.15). The correlation test in BayesDiscrete provides strong support for the dependent model over the independent model (BF = 10.76), which demonstrates the association between color pattern and stream substrate type: the unspotted pattern is correlated more often with a sandy or muddy substrate, whereas the black-spotted coloration tends to be associated with a rocky substrate. Among the 4500 post-burn-in samples of the dependent model, 3843 samples (85%) suggest that the rate of acquisition of substrate type exceeds the rate of acquisition of color pattern, indicating that change of substrate type preceded that of color pattern (Pagel 1994). Assuming the two rates are equal ($q_{12} = q_{13}$) results in a significant decrease of the model likelihood (BF = 3.13).

Likelihood estimates of ancestral range evolution yield a dispersal rate of 0.061 and a local extinction rate of 0.038 for *Pachytriton*, which most likely originated in the Nanling Mountain Range (relative probability = 0.41). Given a conventional confidence window of two log-likelihood units (i.e., within 2 log-likelihood units of the maximum; Edwards 1992), the alternative site of origin is the Nanling Mountain Range and Wuyi

Mountain Range combined (relative probability = 0.32) or the Nanling Mountain Range and western Plateau combined (relative probability = 0.12). All three reconstructions implicate the likely role of the Nanling Mountain Range as the geographic origin for the genus. Based on the ML reconstruction on the chronogram (Fig. 1-5), southwestern *P. inexpectatus* dispersed out of the Nanling Mountain Range and subsequently colonized the western Plateau. By similar processes, *P. archospotus* and the MRCA of *P. brevipes* and northeastern *P. inexpectatus* colonized the Yunxiao Mountain Range and the Wuyi Mountain Range, respectively. Northeastern *P. inexpectatus* dispersed further northward into mountains in Fujian and Zhejiang province. The Chebaling-Jiulianshan group of *P. brevipes* re-colonized the Nanling Mountain Range (relative probability = 0.95). Another re-colonization event could have occurred at the MRCA of *P. brevipes* and northeastern *P. inexpectatus* (relative probability = 0.33).

Morphometric analysis

The first three principal components (PC) explain 90% of the total morphological variance among the fifteen variables. These components represent overall body size, body shape (i.e., length versus girth) and relative head size, respectively (Fig. 1-6). Southwestern and northeastern *P. inexpectatus* are significantly different in PC1 and PC3 scores in one-factor ANOVA and Welch's tests (each $P < 0.005$), which indicates that southwestern *P. inexpectatus* have a significantly larger body size and relatively larger head than northeastern *P. inexpectatus*. *Pachytriton brevipes* are intermediate, but still significantly different from the two groups of *P. inexpectatus*. Northeastern *P. inexpectatus* is the most slender *Pachytriton* of all. It has the largest ratio of forelimb

Figure 1-5. Reconstruction of the geographic origin of *Pachytriton* and its subsequent colonization routes. Localities are color-coded according to their geographic regions: 1) the Nanling Mountain Range (N), 2) the Wuyi Mountain Range (W), 3) the western Plateau (P), 4) the Yunxiao Mountain Range (Y), 5) coastal mountains in Fujian and Zhejiang province (C), and 6) Huangshan and adjacent mountains.

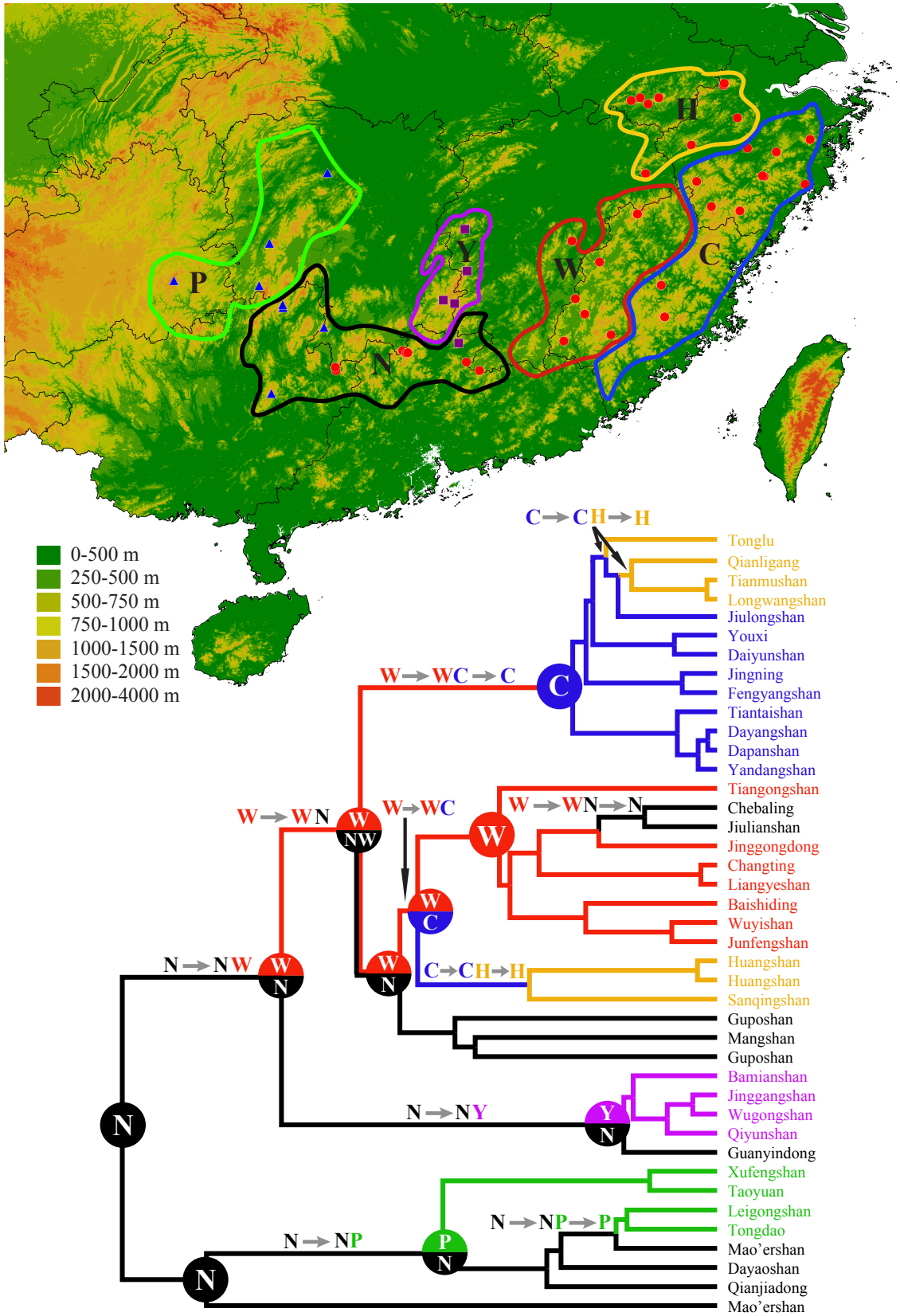

Figure 1-5 (continued)

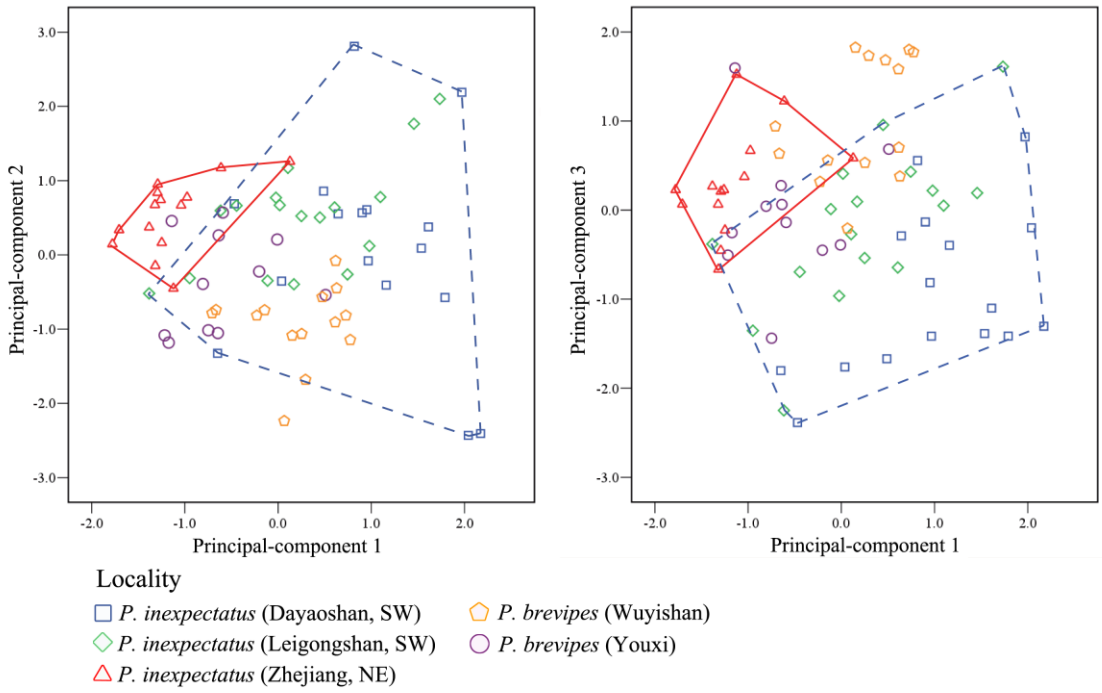

Figure 1-6. Principal-components analysis of morphometric measurements of five populations of *Pachytriton*. Southwestern *P. inexpectatus* (bounded by dashed line) are separated from northeastern *P. inexpectatus* (solid line) in the morphospace.

length to total length ($P = 0.001$) and the smallest ratio of head width to total length ($P < 0.001$). MANOVA suggests no detectable sexual dimorphism among the pooled specimens (Wilks' Lambda $P = 0.306$), and measurement differences between sexes did not contribute significantly to the separation of populations in the PC morphospace. Box's M-test (Box 1949) rejects the equality of covariance matrices, however, so this result should be interpreted with caution.

Discussion

Phylogenetic relationships within Pachytriton

My analysis yields a well-resolved phylogeny for species and populations of *Pachytriton*. Mitochondrial gene trees derived from partial (2007–2008) and more extensive (2007–2011) samplings are entirely congruent. Three major lineages are identified on the ML tree based on populations collected during 2007–2008 (Fig. 1-2). The first clade, A, comprises three populations of *P. inexpectatus* from its southwestern distribution, which includes Dayaoshan, the species' type locality. This clade, which should retain the name *P. inexpectatus*, was the first branching clade of *Pachytriton*. Monophyly of this clade is well supported by mitochondrial data. When *P. inexpectatus* was described (Unterstein 1930), many authors regarded it as a synonym of *P. brevipes*, which is similar morphologically except for coloration (Pope 1931; Chang 1936). Hu *et al.* (1973) confirmed the color difference between the two forms, but they choose instead to classify *P. inexpectatus* as a subspecies of *P. brevipes*. Then Zhao & Hu (1984) once again elevated *P. inexpectatus* to species level. In my study, southwestern *P. inexpectatus* exhibits considerable mitochondrial sequence divergence from other populations of

Pachytriton. Uncorrected pairwise distances to Clade B (*P. archospotus*) are over 10.8% in *ND2* and 8.0% in *cytb*. It differs from *P. brevipes* by over 12.0% in *ND2* and 7.9% in *cytb*. These levels of mitochondrial divergences are comparable to or greater than interspecific differences within other salamander genera, such as species of *Lyciasalamandra* (7.6–10.1%; Weisrock *et al.* 2001), *Triturus* (5–6.8%; Steinfartz *et al.* 2007), *Lissotriton* (~5%; Babik *et al.* 2005), and another Asian stream salamander *Batrachuperus (*6.05–10.89%, Fu & Zeng 2008). The geographic distribution of southwestern *P. inexpectatus* does not overlap with the other two clades. According to the general lineage species concept, species are regarded as separately evolving metapopulations (de Queiroz 2005; de Queiroz 2007). Therefore, I consider *P. inexpectatus*, which comprises only its southwestern populations, a valid species based on available evidence.

Clade B, the second lineage in the mtDNA phylogeny, corresponds to *P. archospotus*, a recently described species that was long misidentified as *P. brevipes* due to similar external morphology and coloration (Shen *et al.* 2008). The new species exhibits a unique osteological feature: straight epibranchial bones in the hyobranchial skeleton. Epibranchial bones are highly curved and flared in both *P. inexpectatus* and *P. brevipes* (Shen *et al.* 2008). My mitochondrial data indicates that the *P. archospotus* forms the sister taxon to the group of northeastern *P. inexpectatus* and *P. brevipes*. Based on the above osteological feature and its large genetic divergence from congeners (Table 1-3), I accept the validity of *P. archospotus*. Interestingly, the phylogenetic hypothesis, which places *P. archospotus* in a non-basal position within *Pachytriton*, suggests the unique evolution of straight epibranchial bones in this species.

Phylogenetic relationships of Clade C are more complicated. Northeastern *P. inexpectatus* is nested within *Pachytriton brevipes*. The result indicates that *P. inexpectatus*, as current taxonomy defined, is paraphyletic. Northeastern *P. inexpectatus* diverges substantially from southwestern *P. inexpectatus*. Monophyly of *P. inexpectatus* is significantly rejected in parsimony-based and likelihood-based topological tests. Morphometric analysis further supports the separation of the two groups. Southwestern *P. inexpectatus* are significantly larger than northeastern *P. inexpectatus* and have a much wider head. The result agrees with the overall impression that northeastern *P. inexpectatus* is a small and gracile newt even as adults, whereas adults of congeners are larger and more bulky. Northeastern *P. inexpectatus* may in fact consist of several lineages that are similar phenotypically, because monophyly of this clade is not supported by either molecular data set.

The phylogeny based on *RAG-1* sequence data failed to identify the same three clades revealed by analysis of mtDNA. Instead, this nuclear gene groups Clade A and B and yields low support for Clade C. Incongruence between *RAG-1* and mitochondrial data is not rare in amphibian phylogenetics, where low levels of genetic variation in *RAG-1* sequences among closely related taxa often defy attempts to obtain a robust phylogeny (e.g., San Mauro *et al.* 2004; Martinez-Solano *et al.* 2007; Kotaki *et al.* 2008). Furthermore, because nuclear autosomal genes typically have an effective population size that is four times larger than maternally inherited mitochondrial DNA, lineage sorting of ancestral polymorphisms may be incomplete in recently diverged species (Moore 1995). Consequently, groupings of nuclear alleles do not necessarily correspond to species boundaries. Nevertheless, my *RAG-1* data provides an independent test of the possibility

of interspecific gene flows. The affinity between northeastern *P. inexpectatus* and *P. brevipes* in the mtDNA-derived phylogeny could be a result of mitochondrial introgression from the latter species followed by fixation. But an introgressed nuclear allele is less likely to reach fixation if assumed neutral (Funk & Omland 2003) and would reveal the true relationship between source and sink species. Despite low level of support at major nodes, southwestern *P. inexpectatus* and northeastern *P. inexpectatus* are consistently placed in separate parts of the nuclear-gene trees in the MP, ML, and BI analyses. In contrast, moderate bootstrap values and posterior probabilities support the grouping of northeastern *P. inexpectatus* with *P. brevipes*. Topological tests significantly reject the monophyly of the two *P. inexpectatus* groups. Several unambiguous substitutions are shared between *P. brevipes* and northeastern *P. inexpectatus*, to the exclusion of southwestern *P. inexpectatus*. A second, independent nuclear POMC gene also unequivocally supports the close relationship between *P. brevipes* and northeastern *P. inexpectatus* (unpubl. data from Yunke Wu). Hence, my analyses are unlikely to reflect past hybridization events, and the inferred relationship among southwestern *P. inexpectatus*, northeastern *P. inexpectatus*, and *P. brevipes* should be robust.

Evolution of color pattern

Until the discovery of *P. archospotus*, the other two species of *Pachytriton*, are identified and differentiated mainly by their external colorations (Fei *et al.* 2006). In general, *P. brevipes* exhibits numerous black, rounded spots on its yellow to brown dorsal side (Sauvage 1876; Fei *et al.* 2006). On the other hand, *P. inexpectatus* has a chocolate-to-dark-brown dorsum that lacks any black spots (Unterstein 1930; Fei *et al.*

2006). Southwestern and northeastern *P. inexpectatus* have nearly identical coloration. This shared coloration is perhaps the most compelling reason for recognizing the two allopatric *P. inexpectatus* as a single species. *Pachytriton archospotus* is chromatically similar to *P. brevipes*. A systematic key based on color pattern was provided by Fei *et al.* (2006).

Mitochondrial and nuclear sequence data reveal unexpected evolutionary relationships by grouping northeastern *P. inexpectatus* with *P. brevipes* and separating southwestern *P. inexpectatus* as a different species. According to this scheme, the color pattern shared by the two groups of *P. inexpectatus* does not constitute a synapomorphy by which this species can be delimited. Color pattern variation has been studied in other salamander species, mostly as intraspecific polymorphisms (e.g., Baird *et al*. 2006; Wake 2006; McKnight & Nelson 2007). There are fewer documented instances of interspecific homoplasy of external coloration. One example involves the European *Salamandra lanzai* and *S. atra*, which achieve melanistic color by convergent evolution (Veith 1996; Bonato & Steinfartz 2005). I provide the first example of interspecific color homoplasy in Asian newts.

Regardless of which samples or analytical approaches were used, reconstruction of the ancestral color pattern suggests the common ancestor of *Pachytriton* most likely had an unspotted dark dorsum, which is retained by southwestern *P. inexpectatus*. However, subsequent evolutionary history among *P. archospotus*, *P. brevipes*, and northeastern *P. inexpectatus* is reconstructed differently depending on which samples were considered. Using only populations collected in 2007–2008, the reconstruction suggests a single evolution of black spots at the MRCA of these three groups and a reversal in northeastern

P. inexpectatus (Fig. 1-2). However, using those samples as well as those collected in 2009–2011, I conclude instead that this MRCA, as well as that of *P. brevipes* and northeastern *P. inexpectatus*, likely retained the unspotted coloration (Fig. 1-4). The latter evolutionary history is more plausible given the recent discovery of multiple unspotted populations in both *P. archospotus* and *P. brevipes*, which originally were thought to only have the black-spotted color pattern. These unspotted populations are critical to ancestral state reconstruction because many represent early branches in one species or another, thus suggesting that black spots were acquired more recently. Furthermore, using only populations collected in 2007–2008 would imply that the chromatic similarity between northeastern and southwestern *P. inexpectatus* is due to secondary loss of black spots in the former group. In contrast, more extensive sampling supports an alternative hypothesis that the unspotted color pattern in northeastern *P. inexpectatus* represents an ancestral state shared with southwestern *P. inexpectatus* (i.e., symplesiomorphy). Therefore, dense taxon sampling enables a more accurate ancestral state reconstruction (Heath *et al.* 2008; Litsios & Salamin 2012).

External coloration in *Pachytriton* provides an example of characters with high rates of transition. Based on more extensive sampling, black spots evolved independently at least seven times across a large geographic distance. In addition, there are three times of reversals from black-spotted to unspotted coloration. Four populations have both unspotted and spotted individuals inhabiting the same stream. *Pachytriton* is restricted to montane streams at high elevations, which are isolated by intervening lowlands. Under such a “sky island” distribution, rampant acquisition of the same chromatic trait in multiple separated populations indicates that this trait may not be selectively neutral.

Natural selection may favor certain types of coloration due to environmental and biotic interactions (Schaefer *et al.* 2002; Chiari *et al.* 2004). This hypothesis is supported by the correlation test, which demonstrates a strong association between coloration and stream substrate type. The uniformly brown, unspotted color pattern is more likely to be found in streams with dark sandy or muddy substrate, whereas the black-spotted color pattern is always associated with streams in which the sediment is composed of rocks and boulders. One potential explanation is camouflage, because the two colorations seem to blend into their respective habitats. Furthermore, the transition from sandy or muddy substrate to rocky substrate likely preceded the transition of color pattern. Therefore, habitat change may promote local phenotypic adaptation in *Pachytriton*.

Before recognizing the homoplastic evolution of dorsal coloration in *Pachytriton*, some authors have proposed using both dorsal and ventral color pattern to diagnose species (Fei *et al.* 2006). I regard this strategy as problematic, because ventral color pattern is subject to large intraspecific variation. In both groups of *P. inexpectatus*, it varies with age of an animal. Juveniles have clearly defined red ventral blotches, which become connected and then blurred in subadults and gradually fade away in older animals. On the other hand, whereas *P. archospotus* and *P. brevipes* generally possess black ventral spots, they vary greatly in density. Many specimens are spotless, which renders them less distinct from older *P. inexpectatus*. In addition, subadults of *P. brevipes* from Junfengshan, the type locality of *P. brevipes*, have a very similar ventral color pattern to subadults of *P. inexpectatus*. Overall, external coloration is not a reliable character to delimit species boundaries in *Pachytriton*.

Historical biogeography

Ancestral range reconstruction suggests that *Pachytriton* originated in the Nanling Mountain Range. This mountain range is regarded as a diversity hotspot for Chinese amphibians and a major center of endemism for Chinese plants (Xie *et al.* 2007; Li *et al.* 2009; López-Pujol *et al.* 2011). As the largest east-west oriented mountain range in southern China, the Nanling Mountain Range connects three northern mountainous regions that are otherwise isolated: the western Plateau, the Yunxiao Mountain Range, and the Wuyi Mountain Range. Because mountain orogeny in southern China largely predates the origin of *Pachytriton* (e.g., Nanling began to uplift in the Cretaceous; López-Pujol *et al.* 2011), this connection probably facilitated colonization of all three regions by *Pachytriton*. For example, the phylogeny of *P. archospotus* is consistent with a south-to-north colonization route into the Yunxiao Mountain Range, as the branching order matches the gradual increase in latitude of the corresponding population. Initial speciation events likely occurred within the Nanling Mountain Range prior to northwards colonization (i.e., divergence oocurred *in situ*), because both *P. archospotus* and *P. inexpectatus* have populations that represent early phylogenetic branches sampled from the Nanling Mountain Range. After the northwards range expansion, at least one clade of *P. brevipes* (Chebaling-Jiulianshan) returned to the Nanling Mountain Range. It is possible that another, and earlier, re-colonization occurred at the MRCA of *P. brevipes* and northeastern *P. inexpectatus*, but the probability of this event is low, which suggests that the reconstruction is indecisive at this node. If the lowlands that contemporarily isolate Huangshan from the Wuyi Mountain Range have represented geographic barriers for *Pachytriton* throughout geologic times, then the coastal mountains in Zhejiang

province must have served as stepping stones for two independent colonization events to Huangshan and adjacent mountains.

Conservation implications

Pachytriton is a widely available newt in the commercial pet trade. Large numbers of animals are collected in the wild each year and exported from China to Europe, North America and other continents. It also is a popular amphibian pet in China (Fei *et al.* 2006). In addition, many animals are collected from certain localities and deposited in the nation's museums. Over-exploitation has been the most serious crisis faced by East Asian amphibians (Stuart *et al.* 2004), and it is worth considering if *Pachytriton* is susceptible to a similar fate.

In sample 2007–2008, *Pachytriton* purchased in several Chinese cities on different dates are genetically similar to northeastern *P. inexpectatus* from Zhejiang province. Analysis of other published DNA sequences in GenBank further implicates mountains in eastern Zhejiang as the major source of traded northeastern *P. inexpectatus* (data not shown). Tourism and tunnel construction have damaged the natural environment in this region. Montane streams, the vital habitats for *Pachytriton* and other aquatic organisms, have been polluted or dried out. Xie *et al.* (2007) suggest that stream-breeding, high-elevation forest amphibians, which include *Pachytriton*, have the highest risk of declining. However, we are just beginning to resolve phylogenetic relationships and evolutionary evolutions in this genus, which are much more complex than previously thought. Adult size decrease in northeastern *P. inexpectatus*, for example, which typically occur at much lower elevation than other species, provides excellent opportunities to

study the interactions among amphibian ontogeny, morphology and environmental factors. Sustaining, and in some instances restoring northeastern *P. inexpectatus* populations are crucial for continuing research. I should also protect habitat in the Nanling Mountain Range, where unknown populations could still be discovered. Those populations may represent early branches in the phylogeny and are crucial to improve our understanding of the evolutionary history of the genus. Therefore, I urge the imposition of legal restrictions that would limit habitat destruction and human exploitation.

Conclusions

Phylogenetic relationships within *Pachytriton* are inferred for the first time with molecular and morphometric data. Mitochondrial genes reveal considerable interspecific divergence and identify three major clades that correspond to known species. *Pachytriton inexpectatus* and *P. archospotus* are recognized as valid species. Northeastern *P. inexpectatus* is nested within *P. brevipes*, whereas southwestern *P. inexpectatus* represents the authentic nominal species. Ancestors of the genus likely had an unspotted color pattern as currenly seen in *P. inexpectatus*. The black-spotted coloration that characterizes *P. brevipes* and *P. archospotus* was acquired independently at least seven times. Reversal to the ancestral coloration also occurred multiple times. Such a high rate of transition between color patterns makes chromatic traits unreliable characters in species diagnosis. Coloration in *Pachytriton* is correlated with stream substrate type. The genus likely originated in the Nanling Mountain Range and subsequently colonized northern mountainous regions. This mountain range is not only a biodiversity hotspot but also a diversification center for Chinese amphibians.

References

Babik W, Branicki W, Cranobrnja-Isailovic J, Cogalniceanud D, Sas I, Olgun K, Poyarkov NA, Garcia-Paris M, Arntzen W (2005) Phylogeography of two European newt species – discordance between mtDNA and morphology. Molecular Ecology, 14, 2475–2491.

Baird AB, Krejca JK, Reddell JR, Peden CE, Mahoney MJ, Hillis DM (2006) Phylogeographic structure and color pattern variation among populations of *Plethodon albagula* on the Edwards Plateau of Central Texas. Copeia, 2006, 760–768.

Ballard JW, Whitlock MC (2004) The incomplete natural history of mitochondria. Molecular Ecology, 13, 729–744.

Bollback JP (2006) SIMMAP: Stochastic character mapping of discrete traits on phylogenies. BMC Bioinformatics, 7, 88.

Bonato L, Steinfartz S (2005) The evolution of the melanistic colour in the Alpine Salamander *Salamandra atra* as revealed by a new subspecies from the Venetian Prealps. Italian Journal of Zoology, 72, 253–260.

Box GEP (1949) A general distribution theory for a class of likelihood criteria. Biometrika, 36, 317–346.

Chan LM, Zamudio KR, Wake DB (2001) Relationships of the salamandrid genera *Paramesotriton*, *Pachytriton*, and *Cynops* based on mitochondrial DNA sequences. Copeia, 2001, 997–1009.

Chang MLY (1936) Amphibiens urodèles de la Chine. Facsimile Reprint (1968) Society for the Study of Amphibians and Reptiles, 99–103.

Chiari Y, Vences M, Vieites DR, Rabemananjara F, Bora P, Ravoahangimalala OR, Meyer A (2004) New evidence for parallel evolution of colour patterns in Malagasy poison frogs (*Mantella*). Molecular Ecology, 13, 3763–3774.

Collins J, Storfer A (2003) Global amphibian declines: sorting the hypotheses. Diversity

and Distributions, 9, 89–98.

de Queiroz K (2005) Ernst Mayr and the modern concept of species. Proceedings of the National Academy of Sciences of the United States of America, 102, 6600–6607.

de Queiroz K (2007) Species concepts and species delimitation. Systematic Biology, 56, 879–886.

Drummond AJ, Rambaut A (2007) BEAST: Bayesian evolutionary analysis by sampling trees. BMC Evolutionary Biology, 7, 214.

Edwards AWF (1992) Likelihood. Johns Hopkins University Press, Baltimore.

Farris JS, Kallersjo M, Kluge AG, Bult C (1995) Testing significance of incongruence. Cladistics, 10, 315–319.

Fei L, Hu S, Ye C, Huang Y *et al.* (2006) Fauna Sinica, Amphibia Vol. 1. Beijing: Science Press, 314–323.

Frippiat C, Kremarik P, Ropars A, Dournon C, Frippiat JP (2001) The recombination-activating gene 1 of *Pleurodeles waltl* (urodele amphibian) is transcribed in lymphoid tissues and in the central nervous system. Immunogenetics, 52, 264–275.

Fu J, Zeng X (2008) How many species are in the genus *Batrachuperus*? A phylogeographical analysis of the stream salamanders (family Hynobiidae) from southwestern China. Molecular Ecology, 17, 1469–1488.

Funk DJ, Omland KE (2003) Species–level paraphyly and polyphyly: frequency, causes, and consequences, with insights from animal mitochondrial DNA. Annual Review of Ecology Evolution and Systematics, 34, 397–423.

García-París M, Alcobendas M, Buckley D, Wake DB (2003) Dispersal of viviparity across contact zones in Iberian populations of Fire salamanders (*Salamandra*) inferred from discordance of genetic and morphological traits. Evolution, 57, 129–143.

Graham SW, Olmstead RG, Barrett SCH (2002) Rooting phylogenetic trees with distant outgroups: a case study from the commelinoid monocots. Molecular Biology and Evolution, 19, 1769–1781.

Guo F (1998) Meso–Cenozoic Nanhua (South China) orogenic belt: subaerial tridirectional orogeny. Acta Geologica Sinica, 72, 22–33.

Heath TA, Hedtke SM, Hillis DM (2008) Taxon sampling and the accuracy of phylogenetic analyses. Journal of Systematics and Evolution, 46, 239–257.

Hu S, Zhao E, Liu C (1973) A survery of amphibians and reptiles in Kweichow province, including a herpetofaunal analysis. Acta Zoologica Sinica, 19, 149–178.

Huelsenbeck JP, Ronquist F (2001) MRBAYES: Bayesian inference of phylogenetic trees. Bioinformatics, 17, 754–755.

Kass RE, Raftery AE (1995) Bayes factors. Journal of the American Statistical Association, 90, 773–795.

Kimura M (1980) A simple method for estimating evolutionary rates of base substitutions through comparative studies of nucleotide sequences. Journal of Molecular Evolution, 16, 111–120.

Kishino H, Hasegawa M (1989) Evaluation of the maximum likelihood estimate of the evolutionary tree topologies from DNA sequence data, and the branching order in Hominoidea. Journal of Molecular Evolution, 29, 170–179.

Kotaki M, Kurabayashi A, Matsui M, Khonsue W, Djong TH, Tandon M, Sumida M (2008) Genetic divergences and phylogenetic relationships among the *Fejervarya limnocharis* complex in Thailand and neighboring countries revealed by mitochondrial and nuclear genes. Zoological Science, 25, 381–390.

Levene H (1960) Robust test for equality of variances. In: Olkin, I., Ghurye, S.G., Hoeffding, W., Madow, W.G., Mann, H.B., (Eds) Contributions to Probability and Statistics: Essays in Honour of Harold Hotelling (pp. 278–292) Stanford: Stanford

University Press.

Li G, Shen Z, Ying T, Fang J (2009) The spatial pattern of species richness and diversity centers of gymnosperm in China. Biodiversity Science, 17, 272–279.

Litsios G, Salamin N (2012) Effects of phylogenetic signal on ancestral state reconstruction. Systematic Biology, 61, 533–538.

López-Pujol J, Zhang MF, Sun HQ, Ying TS, Ge S (2011) Centres of plant endemism in China: Places for survival or for speciation? Journal of Biogeography, 38, 1267–1280.

Maddison WP, Maddison DR (2006) MESQUITE: A Modular System for Evolutionary Analysis, Version 1.12, http://mesquiteproject.org.

Manly BFJ (2004) Multivariate Statistical Methods: a Primer, 3rd edn. Boca Raton, Chapman, Hall/CRC Press.

Martinez-Solano I, Jockusch EL, Wake DB (2007) Extreme population subdivision throughout a continuous range: phylogeography of *Batrachoseps attenuatus* (Caudata: Plethodontidae) in western North America. Molecular Ecology, 16, 4335–4355.

McKnight ML, Nelson NA (2007) Life history and color variants in a matriline of Oklahoma Salamander (*Eurycea tynerensis*) Southeastern Naturalist, 6, 727–736.

Moore WS (1995) Inferring phylogenies from mtDNA variation: mitochondrial-gene trees versus nuclear-gene trees. Evolution, 49, 718–726.

Nishikawa K, Jiang J, Matsui M, Mo Y (2011) Unmasking *Pachytriton labiatus* (Amphibia: Urodela: Salamandridae), with description of a new species of *Pachytriton* from Guangxi, China. Zoological Science, 28, 453–461.

Nylander JAA (2004) MrModeltest v2. Program distributed by the author. Evolutionary Biology Centre, Uppsala University. Available via http://www.abc.se/~nylander/.

Padial JM, Castroviejo-Fisher S, Köhler J, Vilà C, Chaparro JC, De la Riva I (2009) Deciphering the products of evolution at the species level: the need for an integrative taxonomy. Zoologica Scripta, 38, 431–447.

Pagel M (1994) Detecting correlated evolution on phylogenies: a general method for the comparative analysis of discrete characters. Proceedings of the Royal Society B: Biological Sciences, 255, 37–45.

Pagel M (1999) The maximum likelihood approach to reconstructing ancestral character states of discrete characters on phylogenies. Systematic Biology, 48, 612–622.

Pagel M, Meade A (2006) Bayesian analysis of correlated evolution of discrete characters by reversible-jump Markov chain Monte Carlo. American Naturalist, 167, 808–825.

Pagel M, Meade A, Barker D (2004) Bayesian estimation of ancestral character states on phylogenies. Systematic Biology, 53, 673–684.

Pope CH (1931) Notes on amphibians from Fukien, Hainan, and other parts of China. Bulletin of the American Museum of Natural History, 61, 397–611.

Posada D, Crandall KA (1998) MODELTEST: testing the model of DNA substitution. Bioinformatics, 14, 817–818.

Rambaut A (1995) Se–Al: Sequence alignment program. Oxford University, Oxford, U.K. Available via http://tree.bio.ed.ac.uk/software/seal/.

Ree RH, Smith SA (2008) Maximum-likelihood inference of geographic range evolution by dispersal, local extinction, and cladogenesis. Systematic Biology, 57, 4–14.

Salisbury BA, Kim J (2001) Ancestral state estimation and taxon sampling density. Systematic Biology, 50, 557–564.

San Mauro D, Gower DJ, Oommen OV, Wilkinson M, Zardoya R (2004) Phylogeny of caecilian amphibians (Gymnophiona) based on complete mitochondrial genomes and nuclear RAG1. Molecular Phylogenetics and Evolution, 33, 413–427

Sauvage HE (1876) Sur quelques Batraciens de la Chine. L' Institut (N. S.) IV. Paris, 274–275.

Schaefer HC, Vences M, Veith M (2002) Molecular phylogeny of Malagasy poison frogs, genus *Mantella* (Anura: Mantellidae): homoplastic evolution of color pattern in aposematic amphibians. Organisms Diversity and Evolution, 2, 97–105.

Schluter D, Price T, Mooers AO, Ludwig D (1997) Likelihood of ancestor states in adaptive radiation. Evolution, 51, 1699–1711.

Shen Y, Shen D, Mo X (2008) A new species of salamander *Pachytriton archospotus* from Hunan Province, China (Amphibia, Salamandridae) *Acta zoologica Sinica*, 54, 645–652.

Shepard DB, Burbrink FT (2008) Lineage diversification and historical demography of a sky island salamander, *Plethodon ouachitae*, from the Interior Highlands. Molecular Ecology, 17, 5315–5335.

Shimodaira H, Hasegawa M (1999) Multiple comparisons of Log–likelihoods with applications to phylogenetic inference. Molecular Biology and Evolution, 16, 1114–1116.

Stamatakis A (2006) RAxML-VI-HPC: maximum likelihood-based phylogenetic analyses with thousands of taxa and mixed models. Bioinformatics, 22, 2688–2690.

Stamatakis A, Hoover P, Rougemont J (2008) A rapid bootstrap algorithm for the RAxML web servers. Systematic Biology, 57, 758–771.

Steinfartz S, Vicario S, Arntzen JW, Caccone A (2007) A Bayesian approach on molecules and behavior: Reconsidering phylogenetic and evolutionary patterns of the Salamandridae with emphasis on *Triturus* newts. Journal of Experimental Zoology (Molecular and Developmental Evolution), 308B, 139–162.

Stuart SN, Chanson JS, Cox NA, Young BE, Rodrigues ASL, Fischman DL, Waller RW (2004) Status and trends of amphibian declines and extinctions worldwide. Science, 306, 1783–1786.

Swofford DL (2002) PAUP*: phylogenetic analysis using parsimony (*and other methods), Version 4. Sinauer Associates, Sunderland, MA.

Tamura K, Dudley J, Nei M, Kumar S (2007) MEGA4: Molecular Evolutionary Genetics Analysis (MEGA) software version 4.0. Molecular Biology and Evolution, 24, 1596–1599.

Templeton AR (1983) Phylogenetic inference from restriction endonuclease cleavage site maps with particular reference to the evolution of humans and the apes. Evolution, 37, 221–244.

Titus TA, Larson A (1995) A molecular phylogenetic perspective on the evolutionary radiation of the salamander family Salamandridae. Systematic Biology, 44, 125–151.

Unterstein W (1930) Beiträge zur Lurch und Kriechiterfauna Kwangsi's: II. Schwanzlurche. Sitzungsbericht Gesellschaft Naturforschender Freunde. Berlin 2, 313–315.

Veith M (1996) Are *Salamandra atra* and *S. lanzai* sister species? Amphibia-Reptilia, 17, 174–177.

Wake DB (2006) Problems with species: Patterns and processes of species formation in salamanders. Annals of the Missouri Botanical Garden, 93, 8–23.

Weisrock DW, Macey JR, Ugurtas IH, Larson A, Papenfuss TJ (2001) Molecular phylogenetics and historical biogeography among salamandrids of the "true" salamander clade: rapid branching of numerous highly divergent lineages in *Mertensiella luschani* associated with the rise of Anatolia. Molecular Phylogenetics and Evolution, 18, 434–448.

Weisrock DW, Papenfuss TJ, Macey JR, Litvinchuk SN, Polymeni R, Ugurtas IH, Zhao E, Jowkar H, Larson A (2006) A molecular assessment of phylogenetic relationships and lineage accumulation rates within the family Salamandridae (Amphibia, Caudata) Molecular Phylogenetics and Evolution, 41, 368–383.

Welch BL (1938) The significance of the difference between two means when the

population variances are unequal. Biometrika, 29, 350–362.

Williams MAJ, Dunkerley DL, de Deckker P, Kershaw AP, Chappel J (1998) Quaternary Environments. Arnold, London.

Xia X, Xie Z (2001) DAMBE: data analysis in molecular biology and evolution. Journal of Heredity, 92, 371–373.

Xia X, Xie Z, Salemi M, Chen L, Wang Y (2003) An index of substitution saturation and its application. Molecular Phylogenetics and Evolution, 26, 1–7.

Xie F, Lau MWN, Stuart SN, Chanson JS, Cox NA, Fischman DL (2007) Conservation needs of amphibians in China: a review. Science in China Series C, Life Sciences, 50, 265–276.

Zhang P, Papenfuss TJ, Wake MH, Qu L, Wake DB (2008) Phylogeny and biogeography of the family Salamandridae (Amphibia: Caudata) inferred from complete mitochondrial genomes. Molecular Phylogenetics and Evolution, 49, 586–597.

Zhang P, Zhou H, Chen YQ, Liu, YF, Qu LH (2005) Mitogenomic perspectives on the origin and phylogeny of living amphibians. Systematic Biology, 54, 391–400.

Zhao E, Hu Q (1984) Studies on Chinese tailed amphibians. Chengdu: Sichuan Scientific and Technical Publishing House.

Zwickl D (2006) Genetic algorithm approaches for the phylogenetic analysis of large biological sequence datasets under the maximum likelihood criterion—PhD thesis, University of Texas at Austin.

Chapter 2

Comparative osteology of the genus *Pachytriton* (Caudata: Salamandridae) from southeastern China and its aquatic specializations[6]

[6] Results presented in this chapter are published in Asian Herpetological Research (2012).

Abstract

Osteological evidence provides invaluable insights into patterns of amphibian biodiversity. In small montane streams of southeastern China, an endemic genus of salamanders (*Pachytriton*) displays remarkable aquatic specializations, many of which are reflected in skeletal morphology, but these specializations remain to be studied in an integrated perspective. Attempts to fully resolve the taxonomy within the genus also can benefit from knowledge of internal morphology. I present a detailed description of the adult skeleton of *P. brevipes*, *P. inexpectatus* and *P. archospotus* by analyzing both cleared-and-stained and radiographed specimens in a comparative framework. Compared to terrestrial and amphibious salamanders, the most distinctive osteological features of *Pachytriton* include a modified hyobranchial apparatus, a reduced frontosquamosal arch, and deep neural and haemal arches of the caudal vertebrae. The hyobranchial apparatus of *P. archospotus* is distinctly different from that of congeners and likely secondarily derived. Patterns of interspecific variation suggest that northeastern *P. inexpectatus* is more closely related to *P. brevipes* than it is to southwestern *P. inexpectatus*, thereby reinforcing results from earlier molecular phylogenetic analyses. I advocate assigning northeastern *P. inexpectatus* to *P. brevipes*[7].

[7] The northeastern *P. inexpectatus* is now recognized as a separate species and assigned the name *P. granulosus* by Nishikawa *et al.* (2011). The latter name is used in Chapter 3 and Chapter 4.

Introduction

With the growing application of DNA-sequence and other genetic data since the 1990s, osteological work has largely given way to molecular approaches in the study of amphibian biodiversity. Many influential works from the mid-20th century (e.g., Francis 1934; Tihen 1958; Hansen & Tanner 1958; Wake 1963; Özeti & Wake 1969) are still cited today, but few such works are produced anew by contemporary biologists. However, as an independent source of data, osteological characters can provide invaluable insights into evolutionary relationships of living taxa that are as important as those derived from nucleotide substitutions. Homology and homoplasy are directly associated with biological functions.

The family Salamandridae, the second most diverse salamander group, exhibits remarkable differentiation in morphology and life history. One such extreme is exemplified by the Chinese stout newts (*Pachytriton*), which are highly specialized to inhabit small montane streams. Morphological adaptations include the loss of keratinized skin, a heavily ossified tongue skeleton that facilitates underwater feeding, and a paddle-like tail for efficient swimming (Özeti & Wake 1969; Titus & Larson 1995). Molecular phylogenies have defined relationships between *Pachytriton* and other salamandrid genera (Zhang *et al.* 2008), but the taxonomy of species within *Pachytriton* remains a source of contention. It is widely accepted that this genus contains at least three species, *P. brevipes*, *P. inexpectatus* and *P. archospotus* (Fig. 2-1; Fei *et al.* 2006; Shen *et al.* 2008). *Pachytriton archospotus* previously was considered a population of *P. brevipes* due to the similar external morphology and coloration of the two forms (Shen *et al.* 2008).

Figure 2-1. Distribution of *Pachytriton brevipes* (blue solid line), *P. archospotus* (red dashed line) and *P. inexpectatus* (brown dashed line) in southeastern China. Note disjunct distribution of southwestern and northeastern *P. inexpectatus*[8]. Modified from Wu *et al.* (2010).

[8] Nishikawa *et al.* (2011) assigned northeastern *P. inexpectatus* to a separate species, *P. granulosus*. The new name is used in Chapter 3 and Chapter 4.

Indeed, *P. archospotus* has only recently been recognized as a distinct species based on osteological and molecular evidence (Shen *et al.* 2008; Wu *et al.* 2010).

Pachytriton inexpectatus has long been understood to comprise two disjunct populations (northeast vs. southwest) separated by several hundreds of kilometers (Zhao & Hu 1984; Fei *et al.* 1999; Fei *et al.* 2006). However, molecular phylogenies based on mitochondrial and nuclear data indicate that northeastern *P. inexpectatus* is nested within *P. brevipes*, whereas the southwestern population represents the name-bearing species (Wu *et al.* 2010). To further tease apart phylogenetic relationships among these *Pachytriton* species, I analyzed osteological variation among them. Skeletal morphology of *P. archospotus* (misidentified as *P. brevipes*) and *P. inexpectatus* have been described in Chinese by Shen & Shen (1990) and Fan & Tian (1999), but neither of these works is sufficiently detailed to provide the basis for effective interspecific comparisons. In this paper I present a comprehensive osteological study of four groups of *Pachytriton* (*P. brevipes*, *P. archospotus* and the two geographic populations of *P. inexpectatus*) to characterize how aquatic specializations have modified skeletal structures in this genus, to describe how characters vary among and within species, and to gain insight into interspecific phylogenetic relationships within *Pachytriton*.

Materials and Methods

Adult specimens were skinned, eviscerated, cleared and differentially stained for cartilage and bone (Klymkowsky & Hanken 1991). Both sexes were included to evaluate sexual dimorphism. Because body length is linearly correlated with age in many salamandrid species until maximum length is reached (e.g., Caetano & Leclair 1996; Lima *et al.* 2000;

Üzüm 2009), I chose similar-sized specimens (140–150 mm total length) to minimize differences in ossification due to age. The sample of *Pachytriton archospotus*, a rare species in collections, was limited to two large females (~190 mm total length). Skeletons were dissected and photographed by using a Leica MZ 12.5 stereomicroscope mounted with a JVC 3-CCD digital camera. For each specimen or view, a series of images were stacked in Auto-Montage (Synoptics Group) to produce a single high-resolution image with maximum depth of field. Illustrations were prepared in Adobe Photoshop CS 3 and Illustrator 4 (San Jose, CA, USA). Radiographs of additional specimens were prepared with a Thermo Kevex X-ray System (Thermo Scientific) and used for interspecific comparisons. Skeletal nomenclature follows Francis (1934), except for the hyobranchial apparatus (Özeti & Wake 1969) and the carpus and tarsus (Holmgren 1933; Shubin & Wake 2003). To test statistical significance among groups, two-sampled student's *t*-tests were performed in SPSS (ver. 13, Chicago, IL).

The following specimens were utilized: *P. brevipes*, 4 cleared-and-stained (Fujian province), 23 x-rayed (18 from Fujian province and 5 from Zhejiang province); *P. archospotus*, 2 cleared-and-stained (Hunan province, the type locality), 3 x-rayed (Hunan province, the type locality); southwestern *P. inexpectatus*, 4 cleared-and-stained (Guangxi province) 20 x-rayed (16 from Guangxi province and 4 from Guizhou province); northeastern *P. inexpectatus*, 4 cleared-and-stained (Zhejiang province), 22 x-rayed (19 from Zhejiang province and 3 from Anhui province). Cleared-and-stained specimens of *Salamandra*, *Taricha* and *Cynops* were used for comparisons. Museum vouchers are listed in the appendix.

Results

Skull

The skull of *Pachytriton* consists of two components: all cranial cartilages and bones that form within them (endochondral ossifications) and the dermal investing bones (dermal ossifications). The latter include the premaxilla, maxillae, nasals, frontals, prefrontals, parietals and squamosals on the dorsal side, and the parasphenoid, prevomers and pterygoids on the ventral side (Figs. 2-2–2-5).

Premaxilla. The single premaxilla comprises three regions: the tooth-bearing *pars dentalis*, which forms the anterior border of the upper jaw; the *pars palatina*, a posterior extension of the *pars dentalis* that forms the anterior part of the bony palate; and the dorsally ascending *pars frontalis*, which separates the paired nasals. The shapes and sizes of the first two regions are relatively conserved in the genus, but the shape and size of the *pars frontalis* are subject to substantial individual variation. The *pars dentalis* is a short, arched bar that extends laterally and forms the ventral border of the external naris. A perforation is present medially. The *pars dentalis* articulates with the anterior tip of the *pars dentalis* of each maxilla. An inconspicuous ridge marks the boundary between the *pars dentalis* and the *pars palatina*. The posterior edge of the *pars palatina* bears an acuminate projection that extends posteriorly between the paired prevomers. The *pars frontalis* ascends dorsally and forms the medial border of each external naris. It articulates with the nasal laterally and overlaps the frontal posteriorly. The frontal process expands in width and bifurcates posteriorly. The process is longest and most attenuate in *P. brevipes* and shortest and most robust in southwestern *P. inexpectatus*. Northeastern *P. inexpectatus* and *P. archospotus* are intermediate between the two extremes. A small

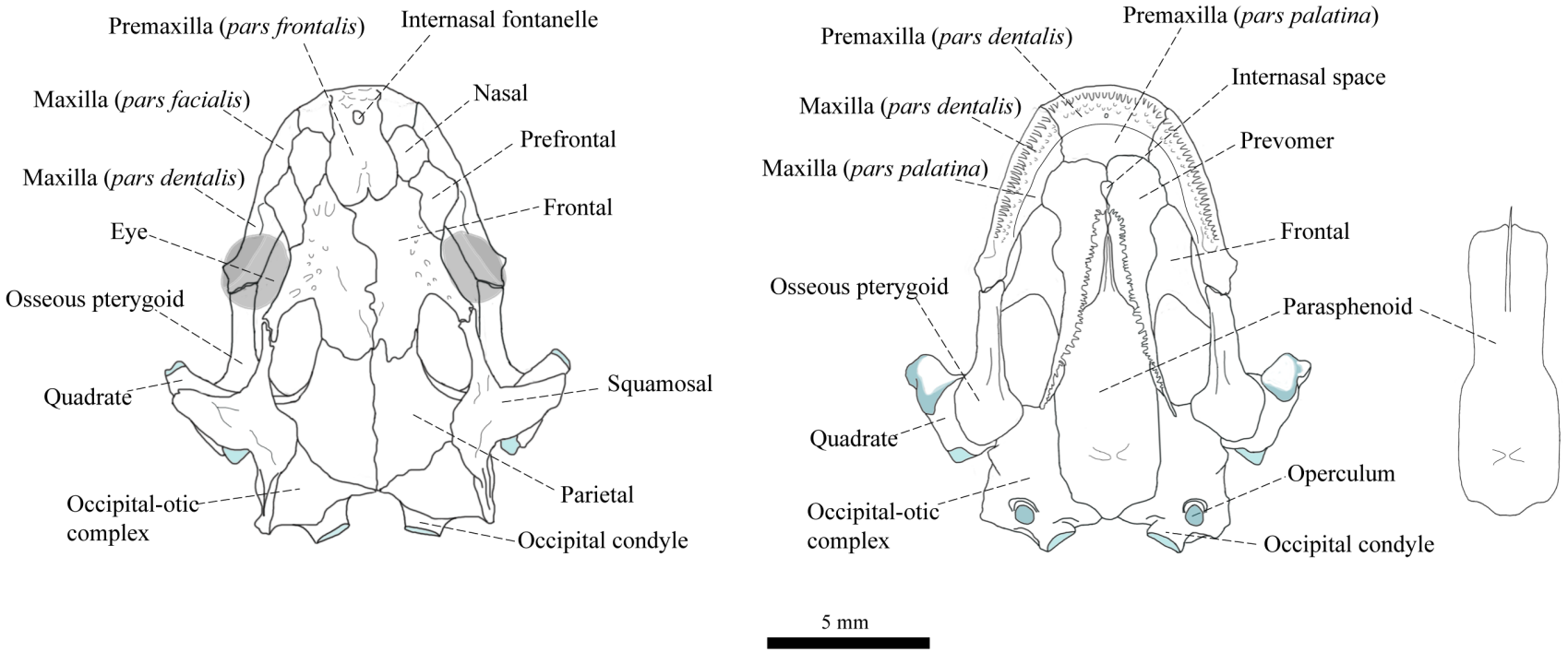

Pachytriton brevipes

Figure 2-2. The skull of *Pachytriton brevipes* (CIB 88208). Left: dorsal view; right: ventral view. The parasphenoid is shown with prevomers removed; the size of the medial spike varies among individuals. Blue shading indicates cartilage. Scale bar, 5 mm.

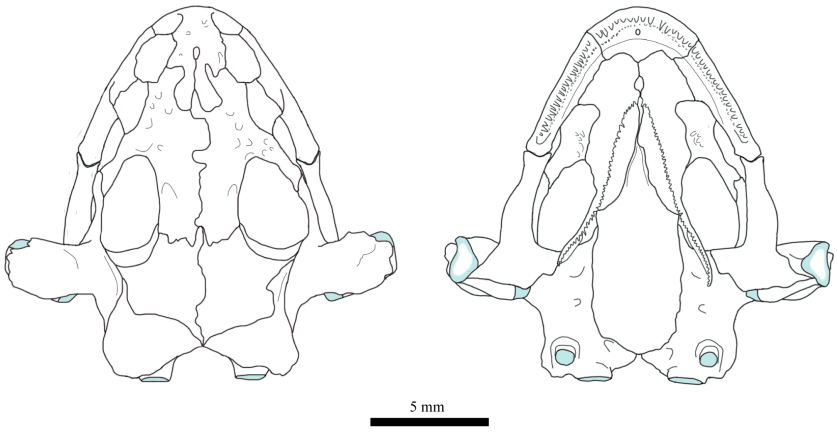

P. archospotus

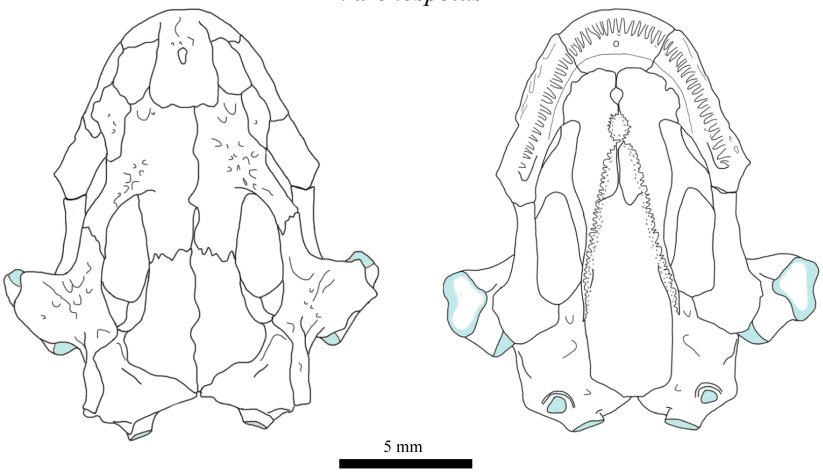

southwestern *P. inexpectatus*

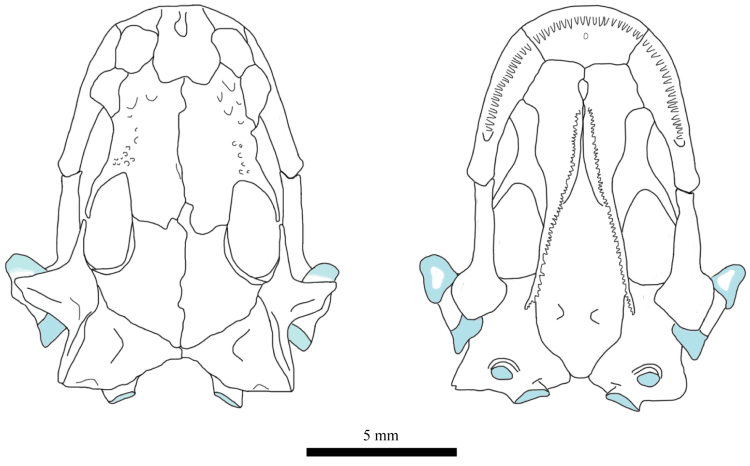

northeastern *P. inexpectatus*

Figure 2-3, 2-4, 2-5. The skull of *Pachytriton archospotus*, southwestern *P. inexpectatus* and northeastern *P. inexpectatus*.

internasal fontanelle is enclosed by the frontal process. The fontanelle is occasionally open posteriorly so that the frontal process appears deeply bifurcated.

Maxilla. Similar to the premaxilla, three regions can be recognized in the paired maxillae, namely, the *pars dentalis*, the *pars palatina* and the *pars facialis*. The tooth-bearing *pars dentalis*, which joins the *pars palatina* medially and *pars facialis* dorsally, is the main component of the maxilla. It articulates with the *pars dentalis* of the premaxilla anteriorly and extends posteriorly (but not beyond the orbit) to form the arch of the upper jaw. In adult specimens, the posterior tip of the *pars dentalis* articulates with the anteriorly pointed pterygoid bone in a nearly straight line. In juveniles, tips of the two bones closely approach one another and are joined by a ligament. The maxillary-pterygoid joint is unique to *Pachytriton* among Asian salamandrids (Wake & Özeti 1969; Titus & Larson 1995). The ventral surface of the *pars dentalis* is populated by numerous pedicellate teeth but the posterior portion remains toothless. The toothless region measures about one third of the length of the maxilla in northeastern *P. inexpectatus*, one quarter in *P. brevipes*, and only one fifth in southwestern *P. inexpectatus* and *P. archospotus*. Northeastern *P. inexpectatus* also has the most slender *pars dentalis* compared to the other three groups. While the posterior tip of the *pars dentalis* expands laterally in all groups, southwestern *P. inexpectatus* has dorsal extensions from the buccal and lingual sides of the posterior half of the bone. These extensions produce a deep dorsal groove, which has not been observed in other groups. The *pars palatina* is the medial extension of the *pars dentalis*; it forms the anterolateral portions of the palate as well as the lateral border of each internal naris. The *pars palatina* attenuates and terminates near the toothless region of the *pars dentalis*. The *pars facialis*

arises from the anterior tip of the *pars dentalis* and extends dorsally to reach the middle level of the orbit. This region is well developed into a large plate that measures half the length of the maxilla. It articulates with the nasal and overlaps the base of the prefrontal. The anterior margin of the *pars facialis* forms the lateral border of the external naris; the posterior margin forms the anteroventral border of the orbit. Perforations for nerves and blood vessels are abundant on the *pars facialis*.

Nasal. The nasals are paired bony plates that cover much of the dorsal surface of the cartilaginous nasal capsule. Each nasal is located above the anterior roof of the dorsal nasal fenestra and never extends beyond the posterior tip of the *pars frontalis* of the premaxilla. The nasal articulates with the *pars frontalis* medially, with the *pars facialis* of the maxilla laterally, and with the frontal and prefrontal bones posteriorly. The *pars frontalis* of the premaxilla always separates the two nasals. The shape of the nasal is subject to individual variation; it typically ranges from oval to rectangular, and sometimes the bone is pointed posteriorly. The margin of the nasal is relatively smooth in northeastern *P. inexpectatus*, but serrated in southwestern *P. inexpectatus*, *P. brevipes* and *P. archospotus*. The nasal contacts the prefrontal posterolaterally in all but two specimens. One specimen of northeastern *P. inexpectatus* (CIB 88152) has its left nasal separated from the prefrontal by the *pars facialis* of the maxilla, whereas in another specimen (CIB 88137) from the same group the right nasal is fused with the prefrontal.

Prefrontal. The small amorphous prefrontal is located immediately anterior to the orbit. Its shape varies ontogenetically but is usually quadrangular, except for some northeastern *P. inexpectatus*, in which it is triangular. It forms the anterodorsal rim of the orbit. The prefrontal is partially covered by the *pars facialis* of the maxilla laterally,

articulates with the nasal anteromedially, and overlies the anterior edge of the frontal medially.

Frontal. The paired frontal forms the anterior roof of the braincase. It is covered anteriorly by posterior edges of the *pars frontalis* of the premaxilla and of the nasal, and by the medial edge of the prefrontal. Posteriorly, the frontal overlies the anterior edge of the parietal. The commissure between left and right frontals is relatively straight in northeastern *P. inexpectatus* but strongly uneven in the other three groups. The lateral edge descends and meets the orbitosphenoid ventrally. A frontal process extends posterolaterally to form the dorsal rim of the orbit. When the frontal process connects with the squamosal process posteriorly, it forms a complete frontosquamosal arch. The complete arch is a synapomorphy of all true newts (Titus & Larson 1995).

Due to the phylogenetic importance of this feature, the morphology of the frontosquamosal arch in *Pachytriton* has been evaluated extensively. A complete and robust arch (i.e., the frontal and the squamosal process articulate firmly) is reported in *P. archospotus* and southwestern *P. inexpectatus* (Shen & Shen 1990; Fan & Tian 1999; Shen *et al.* 2008). Cai (1985) described an attenuate frontosquamosal arch in adult northeastern *P. inexpectatus* but a more robust arch in juveniles. On the contrary, Chan *et al*. (2001) suggest that the arch of *P. brevipes* and northeastern *P. inexpectatus* is rarely complete and attenuate if present at all. Chang & Boring (1935) find substantial variation in *P. brevipes* and northeastern *P. inexpectatus*, from an incomplete arch (the frontal and squamosal process are widely separated) to a well-formed, robust arch. My examination supports the claim of considerable variation both between and within groups. Most *P. archospotus* and southwestern *P. inexpectatus* possess a complete, relatively firm

frontosquamosal arch. Grooves and ridges may provide additional strength (Naylor 1978). However, lack of contact between the two processes is occasionally observed and can occur on either side. In the four cleared-and-stained *P. brevipes*, two specimens display a complete but slender frontosquamosal arch, whereas the arch is incomplete in the other two specimens. No direct frontal-squamosal contact is observed in any northeastern *P. inexpectatus* examined, although most specimens have a spine-like frontal process that closely approaches the squamosal process.

Parietal. The posterior braincase is roofed by the large, paired parietal. The posterior half of each bone expands laterally to form a wing-like structure that is located most posteriorly in southwestern *P. inexpectatus*. The wing position is similar in northeastern *P. inexpectatus*, *P. brevipes* and *P. archospotus*. The posterior tip of the parietal reaches the caudal end of the skull. A sagittal crest is prominent in southwestern *P. inexpectatus*, less evident in *P. brevipes* and *P. archospotus*, and indistinct in northeastern *P. inexpectatus*. The parietal underlies the posterior edge of the frontal anteriorly, overlies the anteromedial portion of the occipital-otic complex, articulates with the posterior part of the orbitosphenoid ventrally and may loosely contact the squamosal laterally. In *Pachytriton*, it provides a partial origin for the jaw-closing muscle (*levator mandibulae anterior*), which passes through the large fenestra formed by the frontosquamosal arch and inserts on the coronoid process of the prearticular in the mandible.

Squamosal. The paired squamosal overlies the quadrate and lies lateral to the occipital-otic complex. This splint-like structure is T-shaped, with the largest process pointed ventrally. Its anterior process articulates with the frontal process, or approaches the frontal process if the frontosquamosal arch is incomplete. Its posterior process firmly

articulates with the anterolateral portion of the occipital-otic complex and may contact the lateral side of the parietal wing. The ventral process, which overlies the quadrate, varies in shape and size among groups (Fig. 2-6). In southwestern *P. inexpectatus* and *P. archospotus*, the ventral process expands in width and covers much of dorsal surface of the quadrate. In comparison, northeastern *P. inexpectatus* and *P. brevipes* have a much narrower and pointed ventral process, which leaves the quadrate largely exposed dorsally. In the latter two groups, the ventral process is located next to a vertical crest on the dorsal surface of the quadrate. The entire squamosal is thickened and rugose in southwestern *P. inexpectatus* and *P. archospotus*, whereas it is relatively thin and smooth in northeastern *P. inexpectatus* and *P. brevipes*.

Orbitosphenoid. The vertically oriented orbitosphenoid is an endochondral ossification that forms the lateral side of the braincase. Its shape is nearly rectangular, with the anterior portion narrower than the posterior. Two foramina are entirely enclosed by bone. The larger opening, *optic fenestra*, is located one quarter of the distance from the caudal end of the orbitosphenoid. The smaller *foramen oculomotorium* is located posterodorsally to the *optic fenestra*. *Pachytriton* has a much smaller *optic fenestra* in comparison to those of some terrestrial and amphibious species of similar size (e.g., *Salamandra* and *Paramesotriton*), which correlates with its relatively small eyes. The orbitosphenoid contacts the nasal capsule anteriorly and the occipital-otic complex posteriorly, articulates with the ventral surface of the frontal and the parietal dorsally, and articulates with the parasphenoid ventrally.

Occipital-otic complex. The posterior region of the adult skull comprises a pair of large bones. Each forms via fusion of three distinct components: prootic, opisthotic and

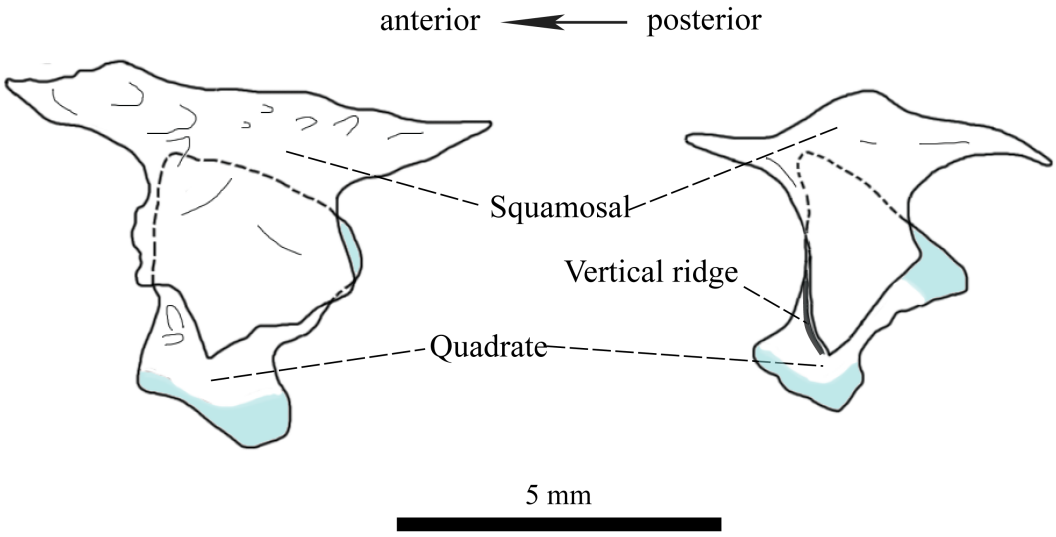

Figure 2-6. The squamosal and quadrate of southwestern *P. inexpectatus* and *P. archospotus* (left, CIB 88153) and northeastern *P. inexpectatus* and *P. brevipes* (right, CIB 88208) seen in left lateral view. Blue shading indicates cartilage. Scale bar, 5 mm.

exoccipital (Trueb 1993). The shape of the occipital-otic complex is often triangular or obliquely quadrangular in dorsal view. Left and right bones contact along the sagittal axis by a narrow commissure, the *tectum synoticum*. The dorsal surface of the occipital-otic complex, which encloses the membranous labyrinth of the auditory system, is depressed compared to its lateral margin. Three elevations outline the three semicircular canals, which are most prominent in northeastern *P. inexpectatus*. The dorsolateral margin contains a groove that accommodates the posterior process of the squamosal. The exoccipital portion of the occipital-otic complex encloses the *foramen magnum*. The occipital condyle arises as a cylindrical, bony extension lateroventral to the *foramen magnum*; its flat head is capped with cartilage. The occipital condyle and the odontoid facet on the lateral wall of the *foramen magnum* articulate with the condylar facet and odontoid process of the atlas. The operculum is located along the posteroventral surface of the occipital-otic complex, covering the *fenestra vestibule* with a fibrous membrane. This partially mineralized plate is oval in shape, with both its external and internal surfaces slightly convex. A small bundle of muscle (*musculus opercularis*) connects the operculum to the suprascapula of the pectoral girdle. A distinct and separate columella is not observed; this structure is reported as fused to the occipital-otic complex in adult *Pachytriton* and the stylus portion is absent (Dunn 1922). The occipital-otic complex articulates with the parietal anteriorly, with the squamosal dorsolaterally, and with the posterior margin of the parasphenoid ventrally. It also loosely contacts the posterior base of the pterygoid bone.

Suspensorium. The suspensory apparatus of the mandible is located at the lateral side of the occipital-otic complex and the ventral side of the squamosal. It consists of the

pterygoid and quadrate bones; the latter in addition has three processes (ascending, otic and basal) that articulate with the lateral wall of the occipital-otic complex in a tripod-like manner. The ascending process is the most anterior and the most slender. The otic process is located on the dorsal side of the suspensorium and completely overlain by the squamosal. The basal process, which is the largest of all three, is situated posteroventrally to the otic process and connects the obliquely oriented quadrate. The ossified quadrate forms a direct lateral continuation of the cartilaginous basal process and is nearly perpendicular to the sagittal axis of the skull. An elevated crest runs vertically on the dorsal surface of the quadrate in northeastern *P. inexpectatus* and *P. brevipes*, whereas the dorsal surface is flat or slightly depressed in southwestern *P. inexpectatus* and *P. archospotus*. The quadrate is overlain dorsally by the squamosal, covers the pterygoid dorsolaterally, and articulates anteroventrally with the articular of the mandible. The pterygoid of *Pachytriton* has a dorsal groove that accommodates a cartilaginous rod, which originates from the joint between the basal and ascending process and extends anteriorly into the *pars dentalis* of the maxilla. The pterygoid has an elongate anterior ramus and a laterally expanded posterior region, which yields a spoon-like profile. The pterygoid firmly contacts the *pars dentalis* of the maxilla anteriorly in most specimens; together, the two bones form the ventral border of the orbit. *Pachytriton archospotus* has a distinct pterygoid with the anterior ramus curved medially and large lateral and medial processes at the posterior region. In contrast, the ramus is relatively straight and the posterior region is more round in other groups. The pterygoid articulates with the occipital-otic complex dorsomedially, with the quadrate dorsolaterally and with the *pars dentalis* of the maxilla anteriorly.

Prevomer. The paired prevomer forms the dorsal and anterior roof of the oral cavity, as well as the posterior floor of the nasal capsule. Its anterior portion is a broad, toothless and dorsally convex plate that contacts the *pars palatina* of the maxilla laterally. Left and right prevomers enclose an internasal space medially. The middle-to-posterior portion bears small teeth on its medial edge. Left and right dental ridges form an inverse-V. The posterior tip of the prevomer flares laterally and does not contact the parasphenoid. The distance between the two tips is about one half the length of either dental ridge. Laterally, the prevomer forms the medial rim of the internal naris. Each prevomer also articulates with the *pars palatina* of the premaxilla anteriorly, with the *pars palatina* of the maxilla anterolaterally, and with the parasphenoid dorsally.

Parasphenoid. This is the largest single bone in the skull; it forms the posterior roof of the oral cavity and the floor of the braincase. It also provides support for the posterior portion of the nasal capsule. Previous studies report its shape as sword-like with an acute anterior end (Shen & Shen 1990; Fan & Tian 1999). However, after removal of the articulated prevomers the parasphenoid appears nearly rectangular (Fig. 2-2). Its anterior half is only slightly narrower than the posterior half. The dental ridge of the prevomer covers the lateral edge of parasphenoid, obscuring its shape. The parasphenoid is a broad and elongate plate. Its anterior tip is slightly bifurcated or trifurcated and underlies the cartilaginous *planum internasale*, which connects left and right nasal capsules ventrally. Its posterior end reaches the *foramen magnum*. A medial spike is present on the ventral surface; its size varies among individuals. The parasphenoid articulates with the orbitosphenoid dorsally, with the prevomers ventrally, and with the occipital-otic complex posterolaterally.

Mandible

The mandible of *Pachytriton* is a semicircular structure comprised of two rami that join at a median symphysis. Each ramus consists of the Meckel's cartilage, the replacing mento-Meckelian and articular bones, and two dermal investing bones, the dentary and the prearticular (Figs. 2-7, 2-8). Teeth are present on the anterior two thirds of each ramus. Individual variation is observed in the number of teeth and the shape of the prearticular. Otherwise, mandibular morphology is highly similar among groups.

Meckel's cartilage. Meckel's cartilage is the primary lower jaw skeleton in larvae and is retained in adult salamanders (Francis 1934). In adults it extends from the posterior tip of the mandibular ramus and terminates a short distance from the median symphysis, where cartilage has ossified to form a mento-Meckelian bone that is fused with the dentary. The anterior portion is enclosed by the dentary but the posterior tip is exposed dorsally.

Articular. The posterior tip of Meckel's cartilage ossifies as the articular bone, which articulates with the quadrate of the skull to form the mandibular joint. The shape of the articular resembles an inverted flask with the dorsal surface expanded. The articular contacts the prearticular medially and ventrally and contacts the dentary laterally.

Dentary. The dentary is the major bone of the mandibular ramus. Its anterior part forms a dorsomedial groove that accommodates numerous pleurodont teeth. The groove terminates anteriorly at a dentary process that is as high as or higher than the coronoid process of the prearticular posteromedially. The posterior part of the dentary resembles a vertically oriented thin blade. The length of the tooth row and the size of the dentary

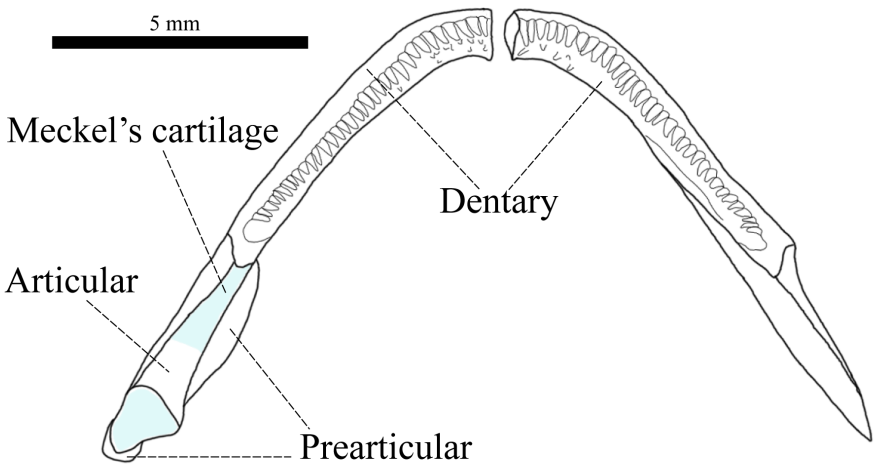

Figure 2-7. Mandible of *P. brevipes* (CIB 88208) in dorsal view. Meckel's cartilage and articular and prearticular bones are removed from the right side. Blue shading indicates cartilage. Scale bar, 5 mm.

Pachytriton brevipes

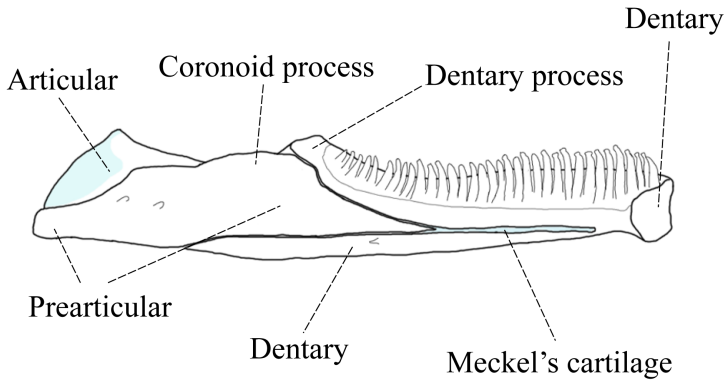

Pachytriton archospotus

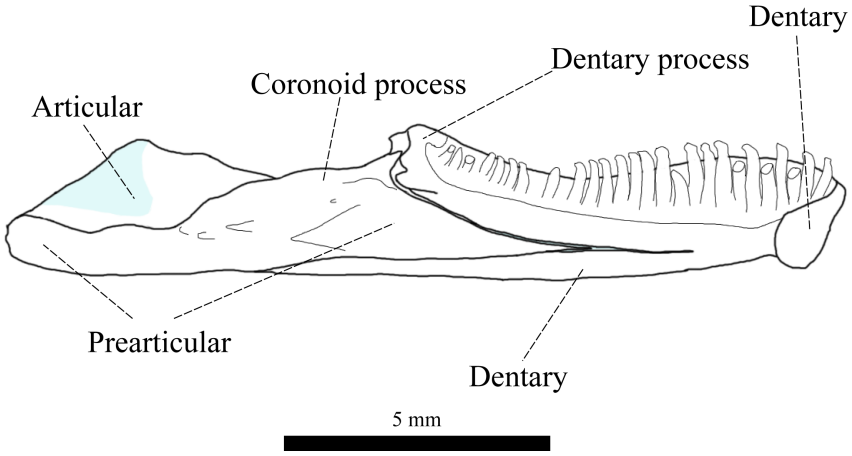

Figure 2-8. Mandible of *P. brevipes* (CIB 88208) and *P. archospotus* (CIB 95952) viewed from the lingual side. Blue shading indicates cartilage. Scale bar, 5 mm.

process are subject to individual variation. The dentary of *P. archospotus* is relatively straight, whereas that of the other three groups is more arched (Fig. 2-9).

Prearticular. The wedge-like prearticular is inserted on the lingual side of the dentary, forming the lingual border of the posterior half of the ramus. It extends beneath the ventral surface of the articular and thus supports the jaw articulation. A coronoid process arises on its dorsal surface and inflects lingually. The apex of the coronoid process is often lower than the apex of the dentary process anterolaterally. The inflection results in an expanded broad shelf on the dorsal surface of the prearticular, where the adductor muscle *levator mandibulae* inserts. Southwestern *P. inexpectatus* has a broader shelf than the other three groups, perhaps indicating a large muscle and thus more powerful jaw closure. The prearticular of *P. archospotus* extends more posterior to the jaw joint than that of other *Pachytriton* groups (Figs. 2-8, 2-9). Perforations on the lingual surface of the prearticular allow passage of nerves and blood vessels.

Hyobranchial apparatus

The hyobranchial apparatus constitutes the tongue skeleton. The apparatus consists of paired ceratohyals, a central basibranchial that bears a pair of radials, paired first and second ceratobranchials, and paired epibranchials (Fig. 2-10). The hyobranchial skeleton of *Pachytriton* is highly ossified, whereas those of other salamandrid genera are largely cartilaginous. Extensive ossification provides extra strength and rigidity to the apparatus, which facilitates suction feeding in water (Özeti & Wake 1969).

Ceratohyal. The paired ceratohyal is the largest element in the hyobranchial apparatus. Its anterior third is cartilaginous and laterally expanded into a spatula shape.

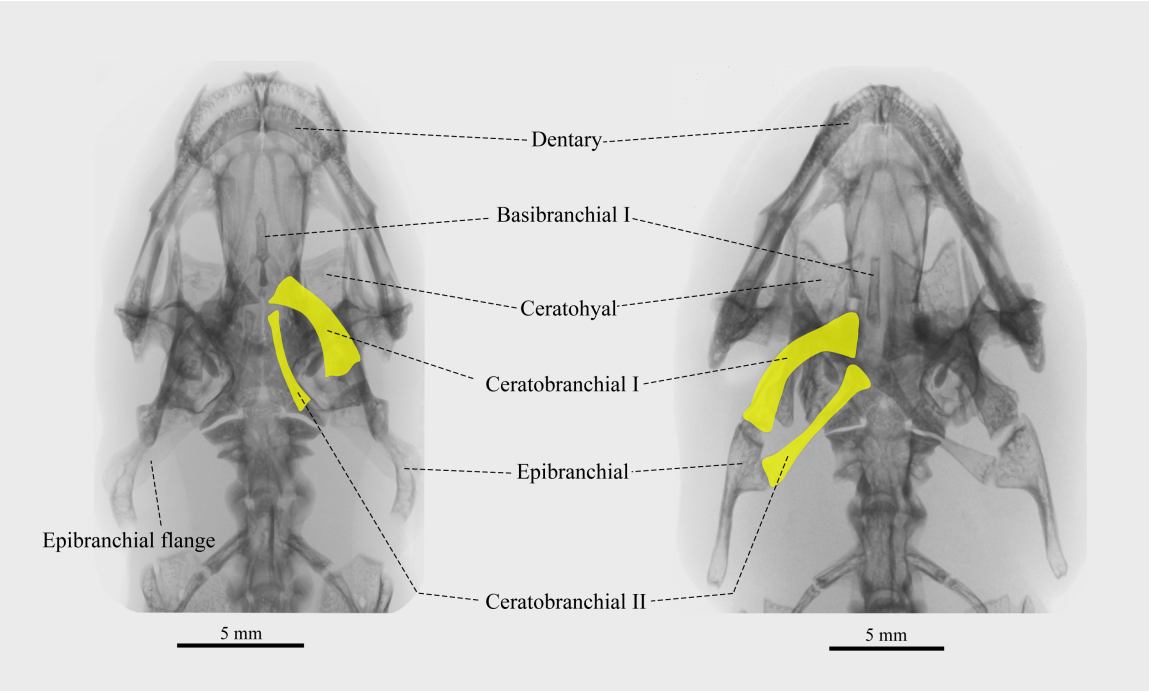

Figure 2-9. Relative position of the hyobranchial apparatus and skull in dorsal view. Posterior portions of the first and second ceratobranchials (yellow) are visible posterior to the skull in *P. archospotus* (right, CIB 95953) but not in other species (such as northeastern *P. inexpectatus*, left, CIB 88146). Scale bar, 5 mm.

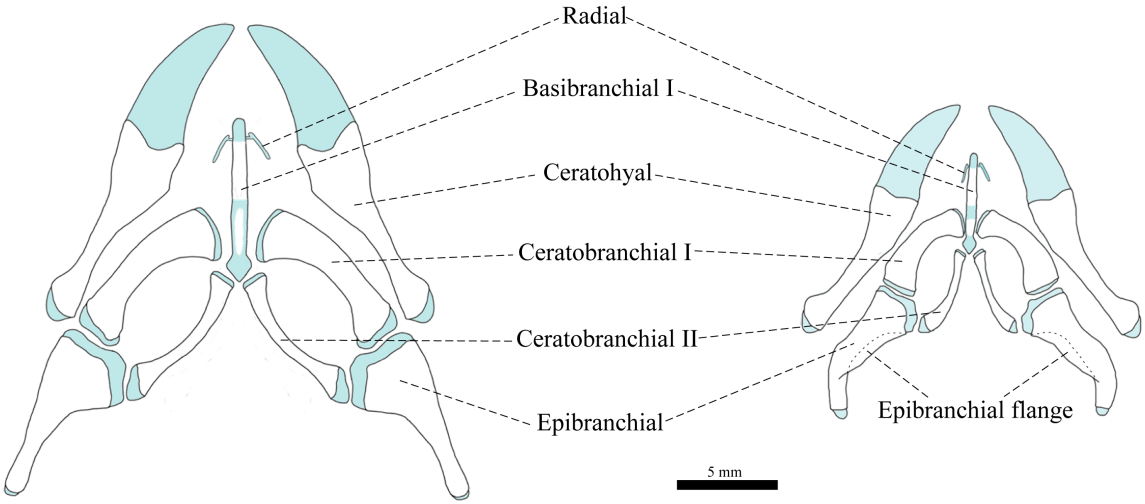

Figure 2-10. Hyobranchial apparatus of *P. archospotus* (left, CIB 95952) and other *Pachytriton* (represented by *P. brevipes*, right, CIB 88208) in ventral view. The interradial cartilage, which is found on the dorsal side of the first basibranchial, is not visible. Blue shading indicates cartilage. Scale bar, 5 mm.

The anterior tip inflects medially and closely approaches its counterpart from the opposite side. The posterior two-thirds are ossified and gradually attenuate into a rod. Individuals vary in the shape of the border between cartilaginous and ossified parts. The border is highly curved (S- or C-shaped) in larger and thus older salamanders, but relatively straight in smaller animals. The posterior portion of the ceratohyal flares dorsolaterally; its tip is expanded and capped with cartilage. In *P. archospotus* the ceratohyal is located more anteriorly than in other groups; the posterior tip barely reaches the joint between the first ceratobranchial and the epibranchial. In the other three groups the posterior tip extends caudally far beyond this joint.

Basibranchial I. The rod-like first basibranchial is the only basibranchial present in *Pachytriton*. In all specimens examined, the anterior tip remains cartilaginous, from which extends a pair of cartilaginous radials that point posterolaterally. An interradial cartilage bridges the two radials at their proximal ends dorsal to the first basibranchial. The posterior half of the first basibranchial is mostly cartilaginous and slightly flattened dorsoventrally, but its central portion is mineralized to variable extent. It articulates with the proximal ends of the first ceratobranchials. The posterior tip is diamond-shaped and articulates with the proximal ends of the second ceratobranchials. My observations differ from those of Özeti & Wake (1969), who report that the radials of *Pachytriton* point laterally and the entire basibranchial is ossified.

Ceratobranchial I. The paired first ceratobranchial in *Pachytriton* is a stout, well-ossified and strongly bowed bone. Both proximal and distal ends are capped with cartilage. The proximal end articulates with the ventral surface of the basibranchial; the distal end articulates with the proximal tip of the epibranchial. The first ceratobranchial

of *P. archospotus* is elongate; the distal tip may reach the atlas of the vertebral column and is visible posterior to the skull in radiographs (Fig. 2-9). In other *Pachytriton*, the first ceratobranchial is smaller and the distal tip does not exceed caudally beyond the occipital condyle.

Ceratobranchial II. The paired, rod-like second ceratobranchial is much more slender and slightly shorter than the first ceratobranchial and bows in an opposite direction from it. Both proximal and distal ends are capped with cartilage. The second ceratobranchial articulates with the posterior tip of the basibranchial proximally, and with the proximal tip of the epibranchial posterolaterally. The second ceratobranchial is much larger in *P. archospotus* than in the other three groups. Consequently, the distal tip of each second ceratobranchial of *P. archospotus* is also visible posterior to the skull in dorsal view (Fig. 2-9).

Epibranchial. The robust epibranchial is a solid, paired bone with both ends capped by cartilage. The proximal portion is expanded laterally to accommodate the distal ends of ceratobranchials I and II. The shape of the distal portion, which is sheathed by thick muscle, is subject to interspecific variation. In all groups except *P. archospotus*, the distal portion elongates, bows and flares dorsolaterally to wrap around the neck; it reaches the height of the upper limit of the quadrate. In contrast, *P. archospotus* has a straight epibranchial. This difference offers the most convincing morphological evidence to support *P. archospotus* as a separate species from *P. brevipes* (Shen & Shen 2008). Its rod-like distal portion does not wrap around the neck but instead is elevated and tapers caudally. *Pachytriton archospotus* also differs from other groups by the absence of a flange on the medial side of the epibranchial. Özeti & Wake (1969) hypothesize that the

function of the epibranchial flange is to strengthen the hyobranchial apparatus during aquatic feeding. Lack of this feature in *P. archospotus* may suggest modified feeding mechanics in this species.

Dentition

Teeth are borne on four bones of the skull: premaxilla, maxilla, dentary and prevomer. Tooth shapes, sizes and numbers are subject to ontogenetic and among-group variation. The teeth are pedicellate and similar to those of other amphibians; each consists of a pedicel and crown connected by fibrous tissue. Premaxillary, maxillary and dentary teeth are pleurodont and prevomerine teeth are acrodont. The following tooth counts are based on cleared-and-stained specimens, except for the premaxillary tooth count, which includes additional radiographed specimens.

Premaxillary teeth are elongated and saber-like. A chisel-like lingual cusp and an inconspicuous labial cusp constitute the crown. Eleven southwestern *P. inexpectatus* have 12–16 premaxillary teeth, mean 14.1, which are fewer than reported by Fan & Tian (1999): 14–18. Twelve northeastern *P. inexpectatus* have 17–21 teeth, mean 18.8; and fourteen *P. brevipes* have 13–18, mean 16.4. Five *P. archospotus* have 12–15 teeth, mean 13.8, which is more than reported by Shen & Shen (1990): around 11. Two-sampled *t*-tests indicate that southwestern *P. inexpectatus* and *P. archospotus* have the fewest premaxillary teeth ($P < 0.05$), but these two groups are not significantly different from each other ($P = 0.067$). Northeastern *P. inexpectatus* possess significantly more premaxillary teeth than any other group ($P < 0.01$).

The recurved maxillary teeth are similar to the premaxillary teeth. Teeth decrease in

size posteriorly and are more conical with a single cusp. There are total 33–55, mean 41.8, maxillary teeth in the four southwestern *P. inexpectatus*; 35–40, mean 37.0, in the four northeastern *P. inexpectatus*; 42–46, mean 43.5, in the four *P. brevipes*; and 29 and 32 teeth, mean 30.5, in the two *P. archospotus*. Tooth counts for southwestern *P. inexpectatus* and *P. archospotus* are consistent with those from Fan & Tian (1999) and Shen & Shen (1990). I did not perform statistical tests of these differences due to limited sample sizes.

Dentary teeth are longer than teeth on the upper jaw. The lingual cusp is recurved and the labial cusp is inconspicuous. Teeth decrease in size posteriorly and are more conical with a pointed cusp. There are total 50–62, mean 53.5, dentary teeth in the four southwestern *P. inexpectatus*; 53–66, mean 58.0, in the four northeastern *P. inexpectatus*; 55–70, mean 63.0, in the four *P. brevipes*; and 44 and 53 teeth, mean 48.5, in the two *P. archospotus*.

Prevomerine teeth, which are smaller than oral teeth, have a sharp, recurved and unicuspid tip. The teeth decrease in size posteriorly but to a lesser extent than do oral teeth. Their number varies greatly among individuals. There are total 84–91, mean 86.7, prevomerine teeth in the four southwestern *P. inexpectatus*; 74–88, mean 79.0, in the four northeastern *P. inexpectatus*; 74–82, mean 78.7, in the four *P. brevipes*; and 71 and 89 teeth, mean 80.0, in the two *P. archospotus*.

Vertebral column

The vertebral column of *Pachytriton* consists of a single cervical vertebra (the atlas), typically twelve trunk vertebrae, one sacrum and several caudal vertebrae. The number of

caudal vertebrae varies greatly among individuals and groups. All vertebrae are opisthocoelous. Ribs are typically borne on the trunk and sacral vertebrae.

Cervical vertebra. The cervical vertebra is hourglass-shaped in dorsal view with its anterior end wider than the posterior (Fig. 2-11). A well-developed odontoid process arises from the ventral side and extends into the *foramen magnum* of the skull. Lateral to the odontoid process are two cervical condylar facets that accommodate the condylar processes of the occiput. A lateral process is present posterior to the facet near the middle of the atlas. The centrum portion is limited to the posterior end of the vertebra, which is conical-shaped and opens posteriorly to accommodate the intervertebral cartilage of the first trunk vertebra. Dorsally, the atlas is covered by a broad neural arch, which bears an indistinct neural spine on its rugose dorsal surface. The neural arch is constricted at the middle and expands posteriorly. The disc-like postzygapophysis arises at the lateral side of the posterior margin and articulates with the prezygapophysis of the first trunk vertebra. All articulating surfaces are sheathed with cartilage. There are three major perforations laterally (Francis 1934). The anterior foramen is located just posterior to the condylar facet, which allows passage of the first spinal nerve. Posterodorsally, the second foramen allows passage of blood vessels. The third opening, on the lateroventral side of the centrum, conducts the second spinal nerve. The shape and size of the atlas are subject to ontogenetic and individual variation, but there is no obvious group-specific variation.

Trunk Vertebrae. Typically *Pachytriton* have 12 trunk vertebrae. The one exception I observed is a northeastern *P. inexpectatus*, which possesses one additional trunk vertebra. Chan *et al*. (2001) examine 15 specimens of *Pachytriton* and find one individual with thirteen trunk vertebrae as well. Each vertebra consists of two portions, a ventral centrum

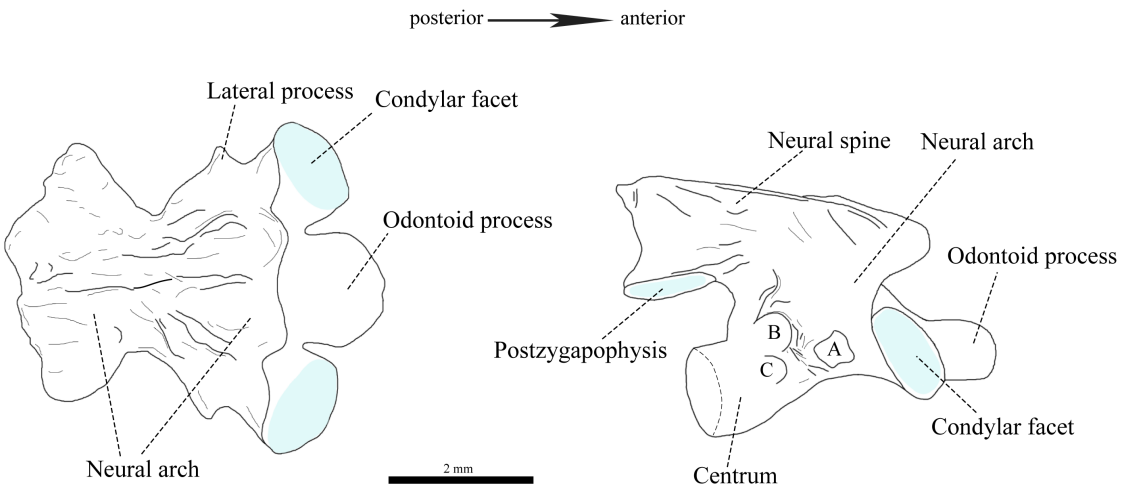

Figure 2-11. Atlas of *P. brevipes* (CIB 88208) in dorsal (left) and lateral (right) views. A: foramen for the first spinal nerve; B: foramen for blood vessels; C: foramen for the second spinal nerve. Blue shading indicates cartilage. Scale bar, 2 mm.

and a dorsal neural arch. The centrum is slightly shorter than the neural arch. One pair of ribs is borne on the transverse processes of the centrum. The shape and size of the vertebral column, as well as rib length, are subject to ontogenetic variation, but there is no group-specific variation. The following description is based on the eighth vertebra, which is taken as a representative of the entire trunk series (Fig. 2-12).

The trunk vertebrae are strongly opisthocoelous. The centrum bears an anterior intervertebral cartilage that is solidified in adults as a condyle, which fits into the hollow cavity of the previous vertebra. The transverse section of the centrum is rounded anteriorly and oval posteriorly, with its breadth wider than height. The ventral surface is almost flat and the central region is depressed to various extents with several fossae. The dorsal part of the vertebra is formed by the neural arch, which covers the neural canal below. The anterior opening of the neural canal is triangular and the posterior opening is rounded. A thin, plate-like neural spine arises on the dorsal surface of the neural arch. The anterior margin of the neural arch is notched and covered by the posterior margin of the previous vertebra. The wing-like prezygapophysis arises anterolaterally and bears a disc-like articulating facet dorsally. The posterior margin of the neural arch expands laterally to form the postzygapophysis, which bears a ventral articulating facet. The prezygapophysis extends slightly anterior to the intervertebral condyle, and the postzygapophysis extends well posterior to the centrum. The posteromedial portion of the neural arch is elevated and thickened. It provides the origin for the inter-spinal muscle that inserts on the dorsal surface of the neural arch of the vertebra next behind (Francis 1934).

Near the midpoint of the vertebra two transverse processes extend posterolaterally to

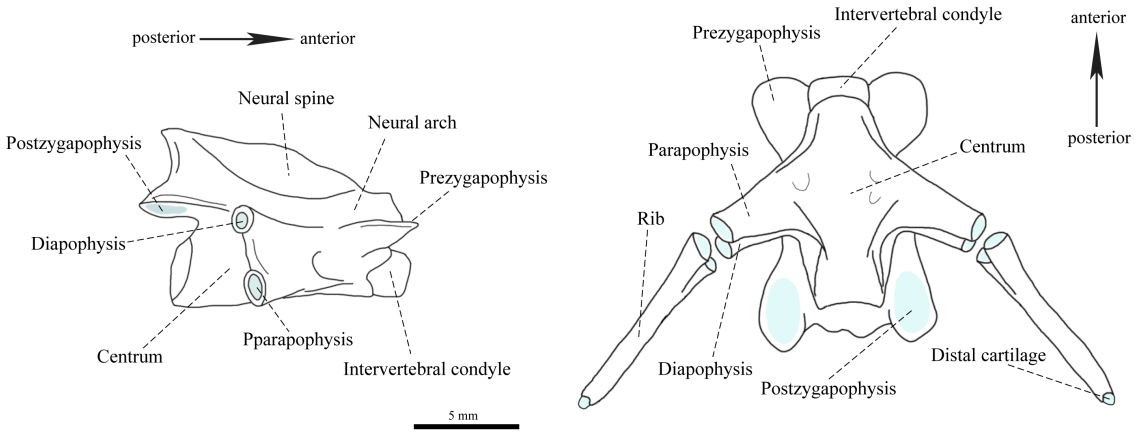

Figure 2-12. The eighth trunk vertebra and associated ribs of *P. brevipes* (CIB 88208) in lateral (left) and ventral (right) views. Blue shading indicates cartilage. Scale bar, 2 mm.

articulate with the rib. The diapophysis arises from the lateral side of the neural arch dorsally, and the parapophysis arises from the lateral side of the centrum ventrally. In all cleared-and-stained specimens, the parapophysis is slightly anteroventral to the diapophysis except for the first three trunk vertebrae, in which the former process is directly beneath the latter. The two transverse processes are of similar length and connected by a thin bony plate. Knob-like cartilages are borne on their distal tips, which support the two corresponding proximal heads of the rib. Ribs are longest in the middle region of the trunk and shorten into acuminate spines with fused proximal heads near the sacrum. The distal tip of the rib bears a small cartilage that is absent from the last two or three trunk vertebrae. In the terrestrial genus *Salamandra*, the distal cartilage on ribs of the first and second trunk vertebrae expands into a spatula-like structure, to which attach muscles from the scapula that suspend the trunk and therefore support the upper body (Francis 1934). In contrast, distal cartilages remain knob-like throughout the whole trunk series in aquatic *Pachytriton*. The first three-to-four ribs are bent downwards at about their middle or distal one-third, where a dorsal spine arises. Posteriorly along the vertebral column, the distal tip of the rib lacks a process but instead has a dorsal groove or fossa, which provides attachment for costal muscles. Perforations on the vertebra allow passage of spinal nerves and blood vessels.

Sacral Vertebra. The sacral vertebra resembles trunk vertebrae except for its modified ribs. Its centrum and neural arch exhibit no major difference from those of the most caudal trunk vertebra, but the diapophysis and parapophysis are much stouter and longer. Unlike trunk vertebrae, the distal tips of the two transverse processes are not attenuate. The rib is modified into a very robust spine, with the two proximal heads not

divergent from each other. The rib is oriented posterolaterally, but its distal one-third is curved forward and articulates anteriorly with the cartilaginous tip of the ilium of the pelvic girdle. A well-developed dorsal flange borne on the curved region increases muscle attachment surface area. A knob-like cartilage is present at the distal tip of the rib. Some specimens develop a bony process near the proximal end.

Caudal Vertebrae. The caudal vertebrae of *Pachytriton* are largely compressed laterally as an adaptation for swimming in permanent montane streams (Fig. 2-13). The first caudal vertebra resembles the anterior sacrum but bears no ribs. In rare cases, an acuminate appendage is attached to the first caudal vertebra. The transverse process arises near the midpoint of the vertebra and is not differentiated into diapophysis and parapophysis. The process diminishes posteriorly to a mere osseous thickening on the last one-third of the caudal series and is ultimately lost in the last three to five vertebrae. The caudal zygapophyses reduce from disc-like articulations of the trunk and sacral vertebrae to pointed contacts that are absent completely after the middle of the caudal series. The neural arch is similar to those of trunk and sacral elements. An elevated neural spine is borne on the dorsal surface of the neural arch; jointly, the two structures form a Y-shaped chevron in dorsal view. The haemal arch arises on the ventral surface of the second caudal vertebra, where it is restricted to the posterior ventral margin. Beginning with the third vertebra, the haemal arch completely covers the ventral surface of the centrum and allows the passage of caudal blood vessels. A prominent haemal spine is developed along the mid-ventral line, resembling the neural spine dorsally. The haemal arch and spine also form a Y-shaped chevron in ventral view. Caudal vertebral size decreases posteriorly. The last 5-to-7 vertebrae each consist of only a tiny centrum with no arch or spine.

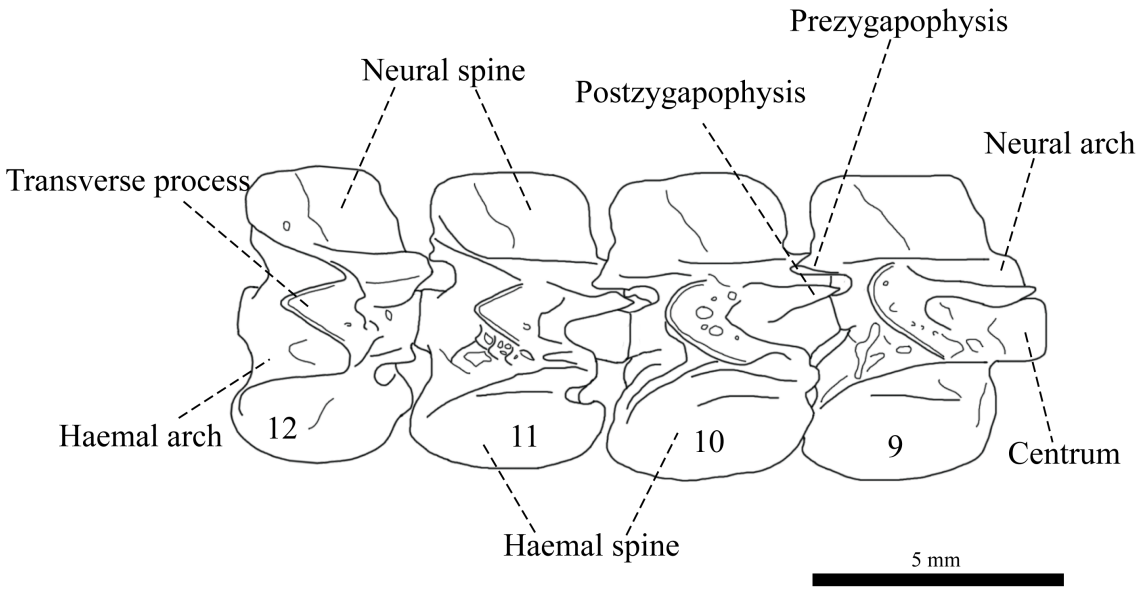

Figure 2-13. The ninth to twelfth caudal vertebrae of *P. archospotus* (CIB 95952) in right lateral view. Individual transverse processes are not differentiated into a diapophysis and parapophysis. The articulation between adjacent prezygapophyses and postzygapophyses is absent after the eleventh caudal vertebrae. Scale bar, 5 mm.

Caudal vertebral number is subject to individual and group-specific variation. Variation is least in southwestern *P. inexpectatus*, which has 28 to 31 caudal vertebrae, mean 29.4 (n = 19). In contrast, the number is most variable in *P. brevipes*, where it ranges from 27 to 34, mean 30.5 (n = 17). Northeastern *P. inexpectatus* has 29 to 34 caudal vertebrae, mean 31.4 (n = 15). My sample of *P. archospotus* comprises only five specimens, which have 27 to 31 caudal vertebrae, mean 28.4. These data are consistent with those of Fan & Tian (1999) for southwestern *P. inexpectatus* but not with those of Shen & Shen (1990) for *P. archospotus*, who reported only 21 and 23 caudal vertebrae in two specimens. Two-sampled *t*-tests indicate that southwestern *P. inexpectatus* and *P. archospotus* have significantly fewer caudal vertebrae than northeastern *P. inexpectatus* and *P. brevipes* ($P < 0.005$ for all tests). However, the former two groups do not differ significantly from each other ($P = 0.289$), nor do the latter two groups ($P = 0.113$).

Pectoral girdle

As is typical for salamanders, each half of the pectoral girdle consists of the scapula, procoracoid and coracoid (Fig. 2-14). All three components converge to the glenoid cavity, which articulates with the proximal head of the humerus. Most of the pectoral girdle remains cartilaginous in adults except for the ossified region that surrounds the glenoid cavity. The extent of ossification and how left and right coracoids overlap are subject to individual variation. No group-specific difference is apparent.

The rounded or triangular glenoid cavity is bordered by the scapula laterally, by the procoracoid anteriorly and by the coracoid medially. The scapula arises dorsally from the glenoid region and expands laterally, attaining the greatest width at the connection with

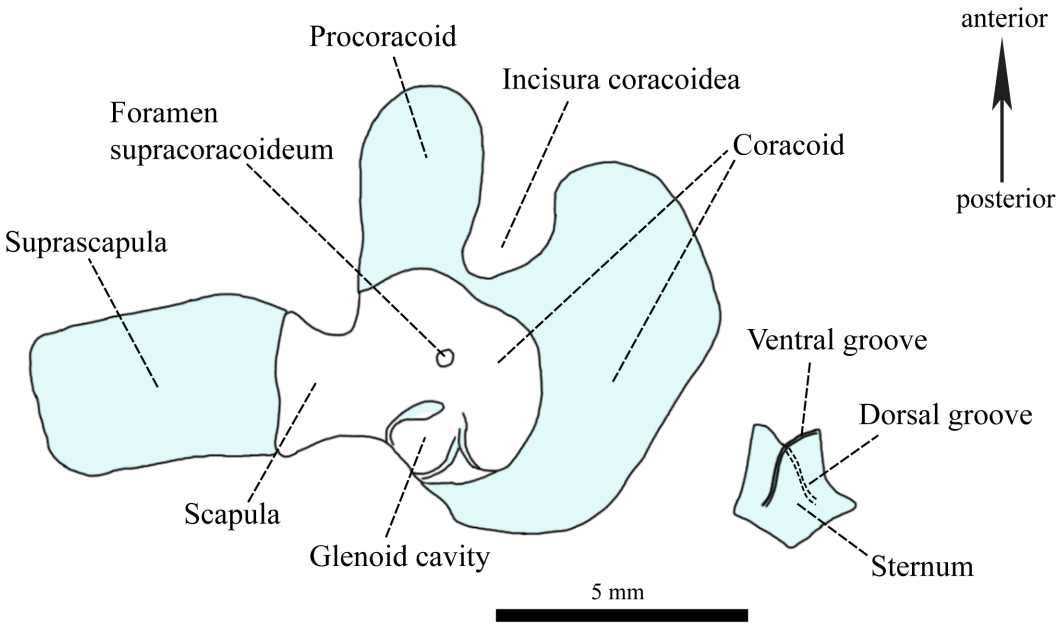

Figure 2-14. The right pectoral girdle (left) and sternum (right) of *P. brevipes* (CIB 88208) in ventral view. Blue shading indicates cartilage. Scale bar, 5 mm.

the suprascapula, which is the cartilaginous extension of the scapula. The spatulate suprascapula is inflected at its proximal one-third and attaches to the lateral side of the trunk through muscles and connective tissues. On the ventral side, the cartilaginous procoracoid extends rostrally and expands laterally; its distal end may reach as far as the occipital condyles. The procoracoid is separated from the coracoid by a deep, U-shaped notch, the *incisura coracoidea*. A large opening, *foramen supracoracoideum*, is completely enclosed in bone and conducts nerves and blood vessels (Francis 1934). The largest component of the pectoral girdle is the coracoid, which includes a bony part that extends medially from the glenoid region and a large sector-shaped distal cartilage that overlaps medially with its bilateral counterpart. In some specimens the right coracoid overlies the left, whereas others have the opposite condition. Both arrangements occur at about equal frequency. The extent of overlap also differs among specimens, varying from half the width of the cartilage to its entire width. The sternum is a thickened rhomboid cartilage at the ventral midline. It has two grooves that accommodate posteromedial edges of the cartilaginous coracoid. One groove is located on the dorsal surface and the other one on the ventral surface, which gives the sternum a notched anterior tip.

Forelimb

The forelimb of *Pachytriton* is similar to that of other tetrapods, which consists of the humerus (Fig. 2-15), the radius and ulna (Fig. 2-16), and the carpus, metacarpals and phalanges (Fig. 2-16). Epiphyses of long bones and all articulating surfaces are cartilaginous.

Humerus. The humerus is a single straight element. Its proximal head expands

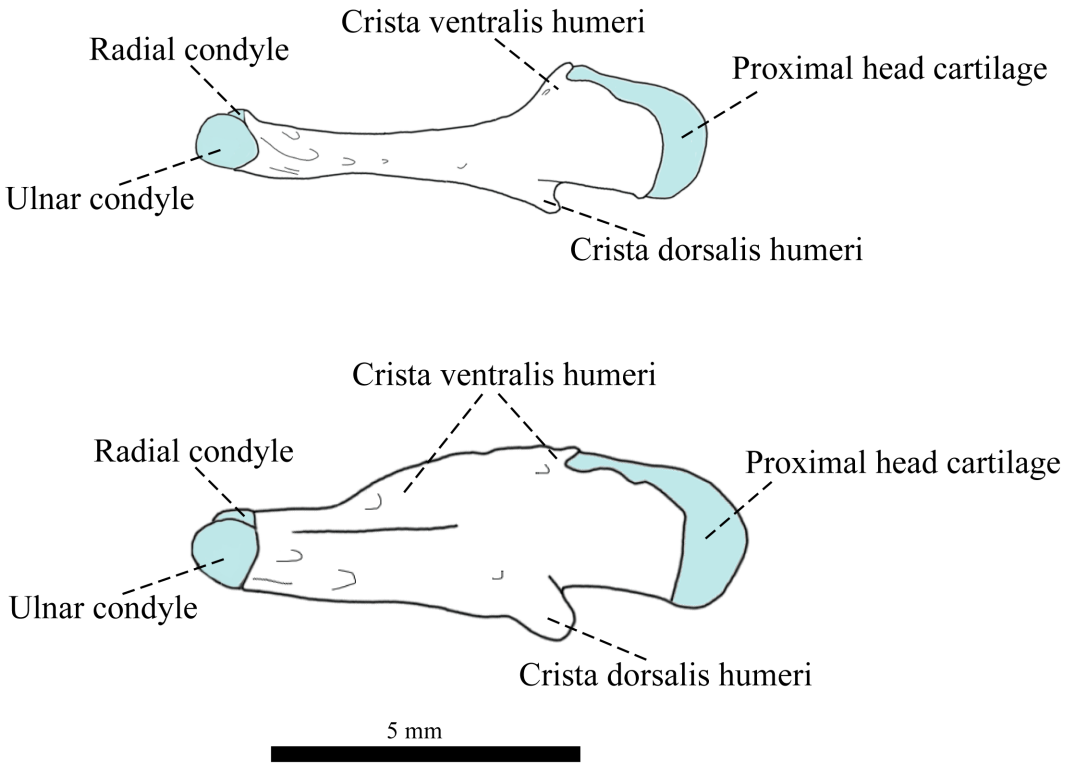

Figure 2-15. The right humerus of northeastern *P. inexpectatus* and *P. brevipes* (upper, CIB 88208) and southwestern *P. inexpectatus* and *P. archospotus* (lower, CIB 88160) in ventral view. Blue shading indicates cartilage. Scale bar, 5 mm.

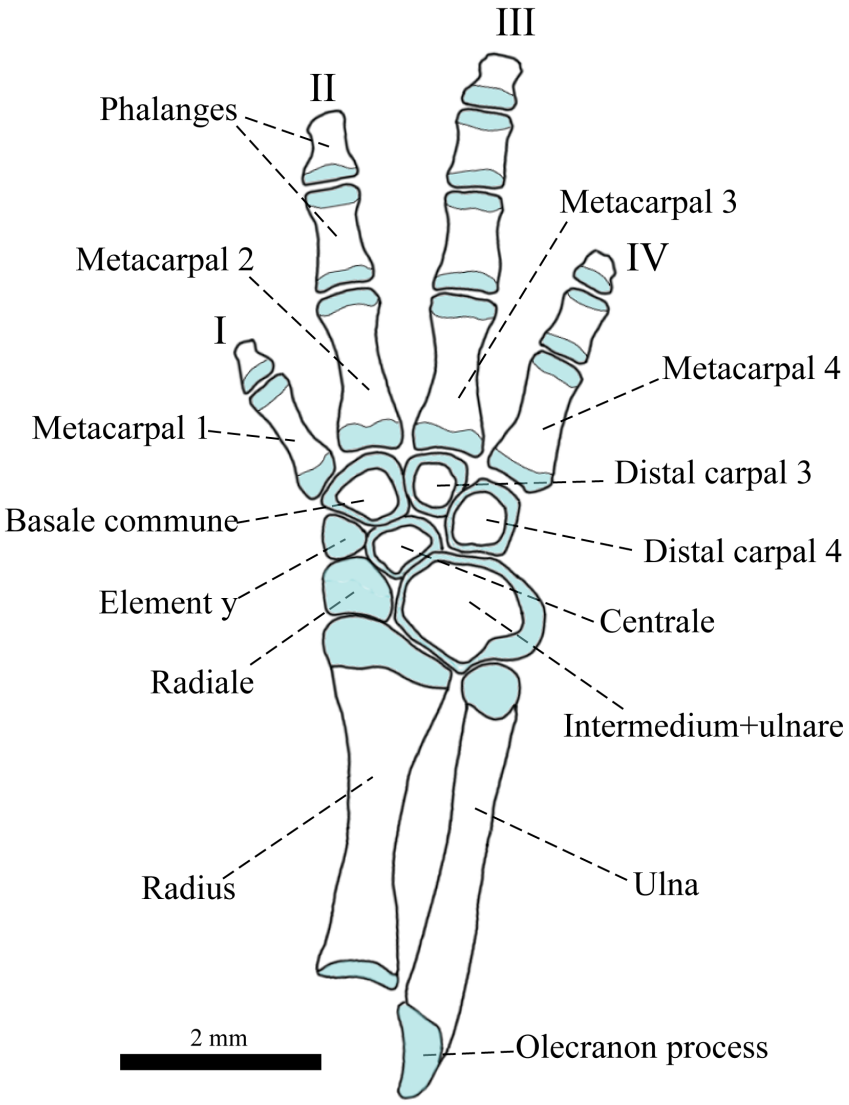

Figure 2-16. Right forelimb of northeastern *P. inexpectatus* (CIB 88152) in dorsal view. I–IV: digits I–IV. Blue shading indicates cartilage. Scale bar, 2 mm.

anteroposteriorly and is capped with hemispherical cartilage that fits into the glenoid cavity of the pectoral girdle. The cartilage extends distally to a prominent crest, the *crista ventralis humeri*, on the anteroventral surface of the shaft. On the opposite side, the *crista dorsalis humeri* arises as a smaller and more pointed crest. Both crests serve as insertions for locomotor muscles. The distal head of the humerus rotates 90° as it expands dorsoventrally and is equipped with two distinct cartilaginous condyles. The preaxial radial condyle is much larger than the postaxial ulnar condyle. Group-specific variation is observed in the size of the dorsal and ventral crests. Southwestern *P. inexpectatus* and *P. archospotus* develop a massive *crista ventralis humeri* that extends to the distal end of the humerus. In contrast, in northeastern *P. inexpectatus* and *P. brevipes* the ventral crest is confined to the proximal one-third of the shaft. The dorsal crest of southwestern *P. inexpectatus* and *P. archospotus* is also much more prominent than that of northeastern *P. inexpectatus* and *P. brevipes*.

Radius. The radius is a long, straight bone with expanded ends. The cartilaginous epiphysis on the proximal end is bowl-shaped, which creates a concavity that receives the radial condyle of the humerus. The epiphysis on the distal end is asymmetrical with the preaxial portion elongated, which creates an oblique articulation with the radiale and the amalgamated intermedium+ulnare.

Ulna. The ulna is slightly bowed, with a shaft longer than the radius. A horseshoe-shaped cartilage at the proximal end forms the olecranon process, which articulates with both radial and ulnar condyles of the humerus. The distal end bears only a small knob of cartilage that articulates with the amalgamated intermedium+ulnare.

Manus. Proximodistally, the *manus* is composed of the carpus, metacarpals and

phalanges. The carpus comprises seven elements: the proximal radiale and the amalgamated intermedium+ulnare; a single central; the preaxial element y (Holmgren 1933; Shubin & Wake 2003); and three basal carpals. The element y is designated as the prepollex by Francis (1934) and Duellman & Trueb (1994) and as the centrale 1 by Schaeffer (1941) and Wake (1963). The carpus is cartilaginous in juveniles but ossifies gradually in older animals. All articulating surfaces remain cartilaginous. Except for obvious deformities, all four *Pachytriton* groups share the same *manus* morphology.

The largest element in the carpus is the amalgamated intermedium+ulnare. Shubin & Wake (2003) make a distinction between amalgamation and fusion, reserving the former term for cartilages that fail to separate during embryonic development and the latter term for initially independent cartilaginous condensations that subsequently merge. In salamanders, the intermedium and ulnare are connected in early ontogenetic stages (Blanco & Alberch 1992; Wake & Shubin 1998). Therefore, the union of these two elements should be regarded as amalgamation. In *Pachytriton*, the intermedium+ulnare is always the first element to begin ossification. The intermedium+ulnare is oval in shape and bordered by cartilage, which is thicker at the postaxial margin. It articulates with the ulna and radius proximally, with the centrale and the distal carpal 4 distally, and slightly with the radiale preaxially. The quadrangular radiale is a small element, only one-third the size of the intermedium+ulnare. It is the penultimate carpal element to ossify, always slightly earlier than the neighboring element y. The radiale articulates with the radius proximally, with the intermedium+ulnare and the centrale postaxially, and with the element y preaxially. In many adult *Pachytriton*, the radiale and the element y are the only completely cartilaginous elements. The triangular element y, which is about half the

size of the radiale, loosely contacts the centrale and articulates extensively with the *basale commune* postaxially. There is no direct contact between the element y and the metacarpal 1, thus the former does not support the first digit. The small, irregular-shaped centrale is located in the center of the carpus. In rare cases, one or two extra centralia are present (Chang & Boring 1935). Distally, the *basale commune* is the largest basal carpal; it represents the amalgamated distal carpals 1 and 2. This unit is quadrangular to pentagonal in shape and supports metacarpals 1 and 2 distally. It articulates with the element y preaxially, with the centrale proximally, and with distal carpal 3 postaxially. The triangular or round distal carpal 3 is the smallest basal carpal. It supports metacarpal 3 and articulates extensively with the *basale commune* and distal carpal 4. It articulates loosely with the centrale. The round distal carpal 4 supports metacarpal 4. It articulates with the centrale and distal carpal 3 preaxially and with the intermedium+ulnare proximally. A variant carpal morphology is found in one northeastern *P. inexpectatus*, which has amalgamated distal carpals 3 and 4 in the right hand.

Four metacarpals are present in *Pachytriton*. The first one is the shortest; metacarpals 3, 4 and 5 are of about equal length. All metacarpals are dumbbell-shaped and capped with cartilage at both ends. Proximally, both metacarpals 1 and 2 are supported by the *basale commune* and metacarpals 3 and 4 are supported by distal carpals 3 and 4, respectively. Phalanges are also dumbbell-shaped except for the terminal ones, which are triangular with an expanded distal tip. The phalangeal formula of *Pachytriton* is 1-2-3-2; digits, in order of decreasing length, are: 3 > 2 > 4 >1. One *P. brevipes* (CIB 88186) exhibits extra phalanges in the left hand (phalangeal formula 2-3-3-2) and the entire left carpus is cartilaginous.

Pelvic girdle

The pelvic girdle consists of three components: ilium, pubo-ischium plate and ypsiloid cartilage (Fig. 2-17). The rod-like ilium points dorsally from the acetabulum with its proximal end expanded anteroposteriorly. The distal one-fourth remains cartilaginous and tapers to a pointed tip, which attaches to the curved tip of the sacral rib posteriorly by fibrous connective tissues. The pubis and ischium are fused to form the rectangular pubo-ischium plate. The anterior portion of the plate is the cartilaginous pubis, which is thickened at its anterolateral margin and forms an indistinct prepubic process. A large perforation at the center of each pubis, the obturator foramen, allows passage of the obturator nerve (Francis 1934). The posterior portion, the ischium, is ossified except at the anterolateral margin and the midline symphysis. Each ischium bears a posteriorly pointed spine with a cartilaginous tip. The acetabulum is formed by the proximal end of the ilium dorsally, by the lateral margin of the ischium posteriorly, and by the lateral margin of the pubis anteriorly. The acetabulum receives the large cartilaginous head of the femur. The ypsiloid cartilage is located along the midline, immediately anterior to the pubo-ischium plate, but there is no direct articulation between the two structures. Instead, the cartilage connects to the plate via a short connective tissue. The two tips of the ypsiloid cartilage are usually longer than its stem. All four groups of *Pachytriton* share the same pelvic girdle morphology. The extent of ossification at the pubo-ischium plate varies individually.

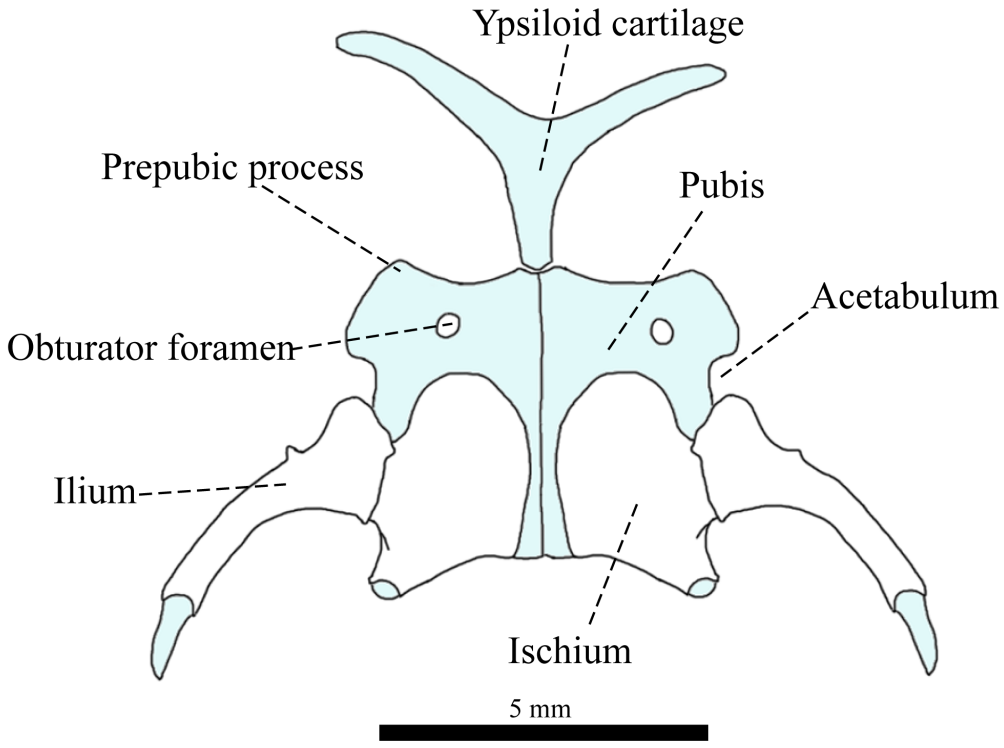

Figure 2-17. Pelvic girdle of *P. brevipes* (CIB 88208) in dorsal view. Blue shading indicates cartilage. Scale bar, 5 mm.

Hind limb

The hind limb skeleton of *Pachytriton* comprises the femur (Fig. 2-18), the tibia and fibula (Fig. 2-19), and the tarsus, metatarsals and phalanges (Fig. 2-19). Epiphyses of long bones and all articulating surfaces are cartilaginous.

Femur. The femur is the longest bone in the hind limb. The shaft constricts in the middle. Its proximal end bears a large cartilaginous condyle that fits into the acetabulum of the pelvic girdle. Depressions are present on both preaxial and postaxial surfaces of the condyle. Ligaments that insert on depressions attach the condyle to the pubis and ilium. The trochanter crest arises on the ventral surface of the proximal one-third of the shaft; it provides the insertion for the ventral caudal muscle (*musculus caudali-femoralis*), which flexes the tail or retracts the femur (Francis 1934). The tip of the crest remains cartilaginous. Cartilaginous tibial and fibular condyles arise on the distal end of the shaft. Groups vary in the size of the trochanter crest, which is spine-like and rapidly merges into the shaft surface in northeastern *P. inexpectatus* and *P. brevipes*. In southwestern *P. inexpectatus*, a second crest arises as an extension of the trochanter crest and extends to the distal end of the femur. This second crest is also present, but less distinct, in *P. archospotus*. Therefore, the femur is slender in northeastern *P. inexpectatus* and *P. brevipes* but very stout in the other two groups.

Tibia. The tibia is a straight bone that is dilated at both ends. In transverse section, the proximal end is a flat oval and the distal end is circular. The shaft constricts near the midpoint. A prominent, proximally pointed tibial spine arises on the dorsal surface; its length varies among specimens. In some the spine extends beyond the proximal end of the shaft, but in others the spine is much shorter. The tibia articulates proximally with the

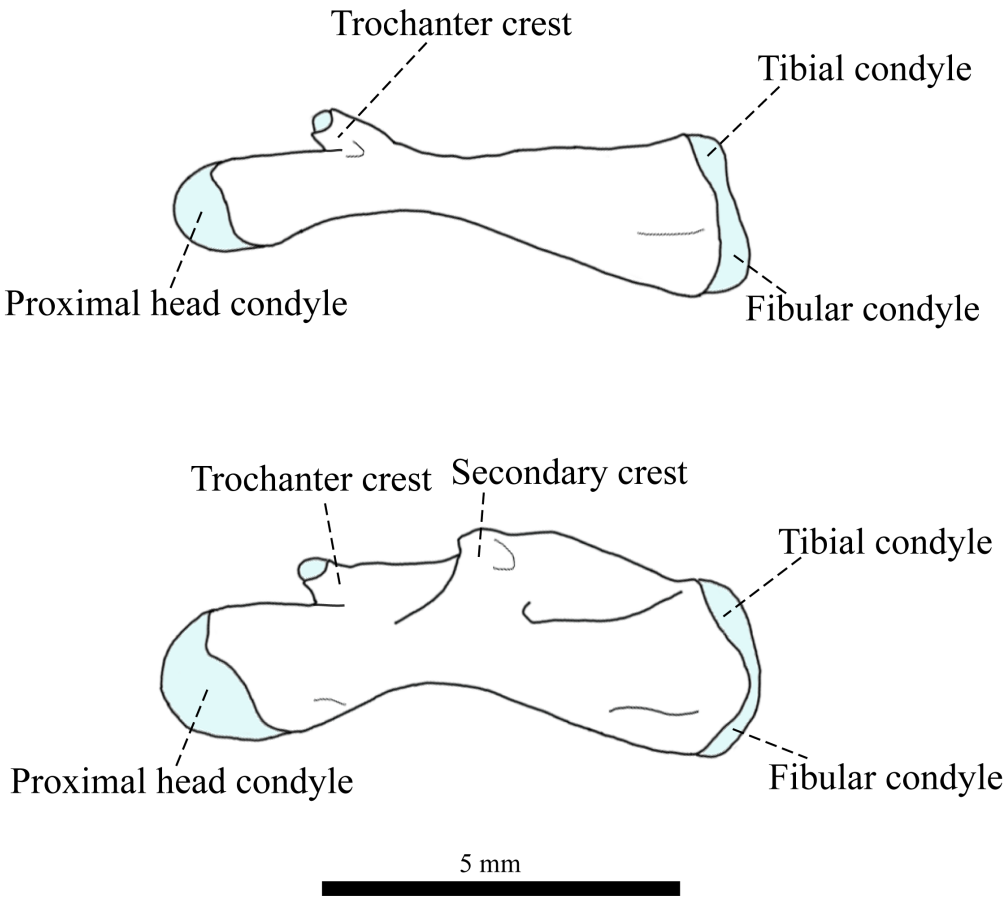

Figure 2-18. Right femur of northeastern *P. inexpectatus* and *P. brevipes* (upper, CIB 88208) and southwestern *P. inexpectatus* (lower, CIB 88160) in anterodorsal view. The femur of *P. archospotus*, while similar to that of southwestern *P. inexpectatus*, has a less prominent secondary crest. Blue shading indicates cartilage. Scale bar, 5 mm.

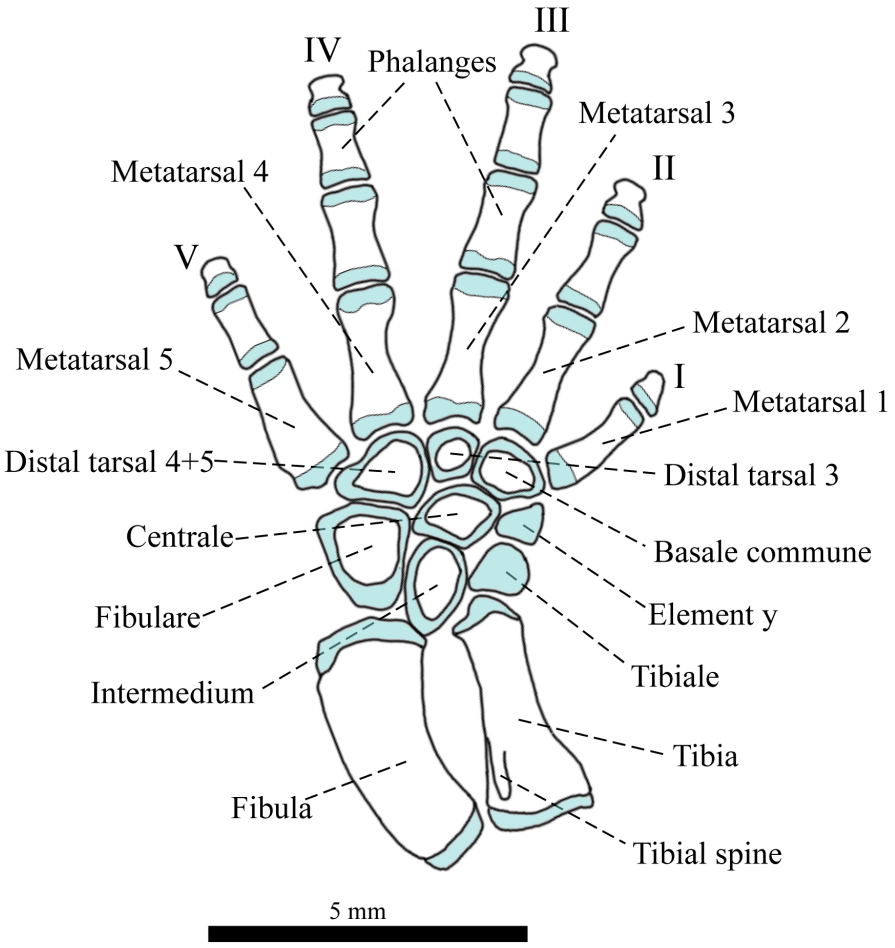

Figure 2-19. Left hind limb of southwestern *P. inexpectatus* (CIB 88160) in dorsal view. I–V: digits I–V. Blue shading indicates cartilage. Scale bar, 5 mm.

femur and distally with the tibiale and intermedium.

Fibula. The fibula is the same length as the tibia, but much wider. The slightly bowed fibula is dorsoventrally compressed with a concave dorsal surface, which yields a relative thin shaft. The fibula articulates proximally with the femur and distally with the fibulare and intermedium.

Pes. Much resembling the *manus*, the *pes* consists of the tarsus, metatarsals and phalanges. The tarsus further comprises eight elements: tibiale, intermedium and fibulare in the proximal row; one centrally located centrale; one preaxial element y (Holmgren 1933; Shubin & Wake 2003); and three basal tarsals. In adults the tibiale and element y are frequently cartilaginous but other elements are ossified in the center. All *Pachytriton* groups share the same *pes* morphology, except for obvious deformities observed in individual specimens.

The triangular-or-round fibulare is the largest element in the tarsus. Unlike the ulnare of the *manus* that has amalgamated with the intermedium, the fibulare is separate from but articulates extensively with the intermedium. It also articulates extensively with the amalgamated distal tarsals 4 and 5. It only loosely contacts the centrale. The oval intermedium is slightly smaller than the fibulare and is wedged between the distal ends of the fibula and tibia. The intermedium articulates preaxially with the tibiale and distally with the centrale. The irregularly shaped tibiale is only half the size of the intermedium. Similar to the radiale in the *manus*, the tibiale is the penultimate element to be ossified in the tarsus, slightly earlier than the element y (prehallux of Francis [1934] and Duellman & Trueb [1994]). The triangular element y articulates postaxially with the centrale and distally with the *basale commune* of the tarsus. The centrale is located in the center of the

tarsus and is about half the size of the fibulare. This sector-shaped element articulates with all other tarsal elements. In the distal row, the first two basal tarsals are amalgamated into the oval *basale commune*, which is larger than distal tarsal 3 but smaller than amalgamated distal tarsal 4+5. The *basale commune* articulates proximally with the centrale and element y and postaxially with distal tarsal 3, and supports metatarsals 1 and 2 distally. The rounded distal tarsal 3 is only half the size of the *basale commune* and supports metatarsal 3. The distal tarsal 4+5 of *Pachytriton* is a single amalgamated element that is slightly larger than the centrale. It supports both metatarsals 4 and 5. One northeastern *P. inexpectatus* (CIB 88137, Fig. 2-20) is unique in having separate distal tarsals 4 and 5 (in this case, tarsal 5 is much smaller than tarsal 4), which resembles the ancestral state in Paleozoic temnospondyls, *Salamandra* and *Taricha* (Francis 1934; Shubin *et al.* 1995). Another atavistic condition is observed in one *P. brevipes* (MVZ 204299, Fig. 2-20), which has a small bone that is surrounded by distal tarsal 4+5, centrale, fibulare and intermedium. This extra bone represents the m element of Schmalhausen (1917). Chang & Boring (1935) describe a *P. brevipes* that has the intermedium, centrale and element y all fused to the tibiale.

Metatarsals resemble metacarpals of the *manus*. All five dumbbell-shaped bones are capped with cartilage at each end. The first and fifth metatarsals are much shorter than metatarsals 2–4, which are of similar length. Distally, each metatarsal supports 1–3 phalanges, which are successively shorter towards the toe tip. Each phalanx is also dumbbell-shaped except for the terminal one, which is triangular and has an expanded distal tip. The phalangeal formula of *Pachytriton* is 1-2-3-3-2; digits, in order of decreasing length, are: 3 > 4 > 2 > 5 > 1. Rare cases of toe loss and polydactyly are

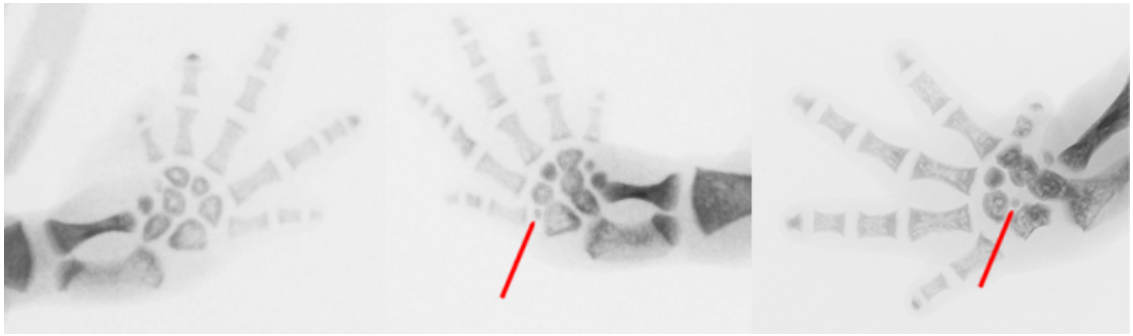

Figure 2-20. Left: right hind limb of CIB 88137, representing the typical condition of *Pachytriton*; middle: left hind limb of CIB 88137, the red arrow points to a separate distal tarsal 5; right: left hind limb of MVZ 204299, the red arrow points to an extra small bone.

described by Chang & Boring (1935).

Discussion

Aquatic specializations of Pachytriton

As adults, *Pachytriton* are permanently aquatic, inhabiting small montane streams (Pope 1931; Özeti & Wake 1969; Titus & Larson 1995). However, molecular phylogenies suggest that this genus descended from an amphibious ancestor and evolved special adaptations for its obligate aquatic lifestyle (Zhang *et al.* 2008). Among the most remarkable specializations is its heavily ossified hyobranchial apparatus. Basibranchial and second ceratobranchial elements typically remain cartilaginous in terrestrial salamanders (Özeti & Wake 1969), but they are solid bones in *Pachytriton*. Cartilage retained in the ceratohyal also is more reduced than in any other salamandrid species (Özeti & Wake 1969). Posterior components, which include the first ceratobranchial, the osseous portion of the ceratohyal and the epibranchial, are all laterally expanded, a configuration that provides extra rigidity to resist mechanical distortion during "gape and suck" feeding (Özeti & Wake 1969). During feeding, one group of muscles anchors the anterior part of the apparatus while a second group of muscles pulls the posterior part forward; this causes rapid depression of the throat and generates a negative pressure for suction. Extreme ossification and robustness of the tongue skeleton in *Pachytriton* enables rapid expansion of the oral cavity in these salamanders, which are much more efficient at prey capture than are amphibious salamanders (Miller & Larsen 1989). All *Pachytriton* except *P. archospotus* have a strongly bowed epibranchial, which flares dorsolaterally and wraps around the neck with the distal tip extending further posteriorly.

In contrast, the epibranchial is relatively short and straight in terrestrial or amphibious genera (Özeti & Wake 1969). This modification allows the epibranchial to be pulled further downward and forward, thereby increasing both the volume of the oral cavity and the negative pressure generated. The posterior extension of the epibranchial also extends the length of the sheathing muscle (*subarcualis rectus* I) yielding a stronger pulling force. Finally, all *Pachytriton* except *P. archospotus* possess a unique epibranchial flange on the medial side, which provides additional rigidity. These specializations of the hyobranchial apparatus are crucial for prey capture in montane streams.

Two synapomorphies are shared by the "true newts" (Salamandridae: Pleurodinae): keratinized skin and a frontosquamosal arch (Titus & Larson 1995). However, even though *Pachytriton* belongs to this clade, it has lost the first feature and exhibits reduction of the second one. Both specializations of *Pachytriton* may be due to its permanently aquatic habitat. Constant immersion in water relieves *Pachytriton* from the risk of evaporative water loss, which in terrestrial and amphibious newts is resisted by bound phospholipids and free fats that are linked to keratin side chains in the epidermis (Spearman 1968). The skin of *Pachytriton* is very smooth and has abundant capillary vessels, which facilitate underwater gas exchange (Xu 2007). In contrast, the granular skin of terrestrial and amphibious newts absorbs water more efficiently from the substrate through capillarity (Toledo & Jared 1993). In true newts, the frontosquamosal arch may act as a defensive mechanism that adds strength to the skull and protects the retracted eyeball during encounters with predators (Naylor 1978). This arch is attenuate or incomplete in *P. brevipes* and northeastern *P. inexpectatus* and relatively firm in *P. archospotus* and southwestern *P. inexpectatus*. In comparison, the closely related,

amphibious *Paramesotriton* has a much stouter frontosquamosal arch (Chang & Boring 1935; Chan *et al.* 2001). Arch reduction in *Pachytriton* may be associated with the absence of predators in shallow montane streams.

The locomotor system of *Pachytriton* is specialized for an aquatic habitat as well. In terrestrial salamanders such as the genus *Salamandra*, ribs of the first two trunk vertebrae bear large spatulate distal cartilages, to which insert muscles that originate from the scapula of the pectoral girdle (Francis 1934). Consequently, the anterior body is suspended above the ground by the pectoral girdle. In contrast, distal cartilages of the first two ribs in *Pachytriton* are knob-like. This reduction suggests that there may be less muscle attached from the scapula, and thereby less support for the axial skeleton by the pectoral girdle. Furthermore, the limbs of *Pachytriton* are short and gracile in comparison to its stout body; terrestrial locomotion is correspondingly cumbersome (Wu, unpublished). However, *Pachytriton* is an efficient swimmer. Its powerful, paddle-like tail is supported by caudal vertebrae with prominent neural and haemal spines. These maintain their size posteriorly until the terminal one-fifth of the tail, whereas other vertebral components (e.g., transverse processes, zygapophyses) gradually reduce in size towards the tip. The length of caudal spines may even increase slightly near the middle of the tail. In comparison, caudal spines in the pond-dwelling *Cynops orientalis* taper gradually. The laterally compressed tail skeleton of *Pachytriton* is wrapped by thick muscles, which enable the salamander to chase fast-swimming prey and avoid being washed downstream.

Hyobranchial apparatus of P. archospotus

For most of the time since the genus was first described in 1876, *Pachytriton* comprised just two named species, which clearly differ in external coloration: the spotted *P. brevipes* (Sauvage 1876) and the unspotted, uniformly dark brown *P. inexpectatus* (Unterstein 1930). A recent study, however, revealed unique phenotypic features in a geographic segment of spotted *Pachytriton*, which on that basis was described as a new species, *P. archospotus* (Shen *et al.* 2008). Subsequent molecular phylogenetic analyses confirm the validity of *P. archospotus* as a distinct species (Wu *et al.* 2010).

The most reliable characteristic that easily distinguishes *P. archospotus* from congeners is the morphology of the hyobranchial apparatus. In *P. archospotus*, the ceratohyal is placed more anteriorly than it is in other *Pachytriton* groups. First and second ceratobranchials also are greatly enlarged such that their distal ends, including their articulations with the epibranchial, are visible posterior to the skull in dorsal view. Unlike the strongly bowed and flared epibranchial that is characteristic of other *Pachytriton*, the epibranchial of *P. archospotus* is straight and rod-like, resembling that of many species of *Paramesotriton* and *Cynops* (Özeti & Wake 1969). Furthermore, *P. archospotus* lacks the distinct epibranchial flange that is unique to *Pachytriton* among all other salamandrids. One hypothesis that can explain this distribution of characters is that *P. archospotus* is the most basal species in the genus and its hyobranchial apparatus retains the ancestral condition. However, neither nuclear nor mitochondrial sequence data support this hypothesis; *P. archospotus* is likely the sister species to the group *P. brevipes*+northeastern *P. inexpectatus* (Wu *et al.* 2010). Instead, the first divergence within *Pachytriton* occurs between southwestern *P. inexpectatus* and the common

ancestor of *P. archospotus*, *P. brevipes* and northeastern *P. inexpectatus* (Wu *et al.* 2010). The most parsimonious explanation of hyobranchial variation among species of *Pachytriton* is that the typical *Pachytriton* hyobranchial apparatus evolved once in the common ancestor of the genus and is retained in all but *P. archospotus*, which evolved specializations that resemble those in *Cynops* and *Paramesotriton*. This resemblance, however, is superficial. The apparatus is much stouter and more laterally expanded in *P. archospotus*, for example, and the extraordinary enlargement of ceratobranchials I and II is not seen in any other Asian salamandrid. The derived hyobranchial anatomy in *P. archospotus* may indicate the evolution of a modified feeding habit in this species.

***Relationship between northeastern* P. inexpectatus *and* P. brevipes**

As currently understood, *Pachytriton inexpectatus* has a disjunct geographic distribution: two widely separated populations are located on either side of the range *P. brevipes* (Zhao & Hu 1984; Fei *et al.* 1999; Fei *et al.* 2006). Salamanders from both populations share the same external coloration, which at one time was the primary character used to diagnose species in the genus (Fei *et al.* 2006). However, based on recent molecular phylogenetic analyses, the shared color pattern is the product of homoplastic evolution and the northeastern population is instead nested within *P. brevipes* (Wu *et al.* 2010). Several osteological characters discussed above exhibit among-group variation, and in each case northeastern *P. inexpectatus* is more similar to *P. brevipes* than it is to southwestern *P. inexpectatus*. For example, southwestern *P. inexpectatus* develops dorsal extension on the buccal and lingual sides of the *pars dentalis* of the maxilla, but this distinct feature is absent in both northeastern *P. inexpectatus* and *P. brevipes*. Conversely,

in both northeastern *P. inexpectatus* and *P. brevipes* the squamosal has a narrow ventral process, which is located next to a vertical ridge on the dorsal surface of the quadrate. In southwestern *P. inexpectatus*, the ventral process instead is broad and covers the flat dorsal surface of the quadrate. The frontosquamosal arch is attenuate or incomplete in northeastern *P. inexpectatus* and *P. brevipes* but relatively firm in southwestern *P. inexpectatus*. The humerus of northeastern *P. inexpectatus* and *P. brevipes* is a slender, rod-like bone, but in southwestern *P. inexpectatus* the humerus is laterally dilated due to its massive dorsal and ventral humeral crests. Likewise, the trochanter crest on the femur of the former two groups is much smaller and shorter than that of southwestern *P. inexpectatus*, which develops a second crest that extends to the distal tip of the femur. The mean number of caudal vertebrae shows no statistical difference between northeastern *P. inexpectatus* and *P. brevipes*, whereas southwestern *P. inexpectatus* has significantly fewer caudal vertebrae. In sum, osteological comparisons corroborate the phylogenetic affinity between northeastern *P. inexpectatus* and *P. brevipes*. Given that northeastern *P. inexpectatus* is nested within *P. brevipes* in molecular phylogenies (Wu *et al.* 2010), I assign northeastern *P. inexpectatus* to *P. brevipes*, which eliminates paraphyly of the former species and restore monophyly of the latter species. The southwestern population should be regarded as the nominal *P. inexpectatus*.

References

Blanco MJ, Alberch P (1992) Caenogenesis, developmental variability, and evolution in the carpus and tarsus of the marbled newt, *Triturus marmoratus*. Evolution, 46, 677–687.

Caetano MH, Leclair R Jr. (1996) Growth and population structure of red-spotted newts

(*Notophthalmus viridescens*) in permanent lakes of the Laurentian shield, Quebec. Copeia, 1996, 866–874.

Cai CM (1985) A survey of tailed amphibians of Zhejiang, with description of a new species of *Hynobius*. Acta Herpetol Sinica, 4, 109–114.

Chan LM, Zamudio KR, Wake DB (2001) Relationships of the salamandrid genera *Paramesotriton*, *Pachytriton*, and *Cynops* based on mitochondrial DNA sequences. Copeia, 2001, 997–1009

Chang TK, Boring AM (1935) Studies in variation among the Chinese Amphibia. I. Salamandridae. Peking Natural History Bulletin, 9, 327-360.

Duellman WE, Trueb L (1994) Biology of Amphibians. Baltimore, USA: Johns Hopkins University Press.

Dunn ER (1922) The sound-transmitting apparatus of salamanders and the phylogeny of the Caudata. The American Naturalist, 56, 418–427.

Fan S, Tian Y (1999) The osteology of *Pachytriton labiatus*. Journal of Qiannan Teacher College, 19, 35–41.

Fei L, Hu S, Ye C, Huang Y (2006) Fauna Sinica, Amphibia Vol. 1. Beijing, China: Science Press.

Fei L, Ye C, Huang Y, Liu M (1999) Atlas of amphibians of China. Zhengzhou, China: Henan Science and Technical Press.

Francis EBT (1934) The Anatomy of the Salamander. Oxford, UK: Clarendon Press.

Hansen AM, Tanner WW (1958) A comparative osteological study of certain species belonging to the genus *Bolitoglossa* (Amphibia). Great Basin Naturalist, 18, 85–100.

Holmgren N (1933) On the origin of the tetrapod limb. Acta Zoologica, 14, 185–295.

Klymkowsky MW, Hanken J (1991) Whole-mount staining of *Xenopus* and other vertebrates. Methods of Cell Biology, 36, 419–441.

Lima V, Arntzen JW, Ferrand NM (2000) Age structure and growth pattern in two populations of the golden-striped salamander *Chioglossa lusitanica* (Caudata, Salamandridae). Amphibia-Reptilia, 22, 55–68.

Miller BT, Larsen JH Jr. (1989) Feeding performance in aquatic postmetamorphic newts (Urodela: Salamandridae): Are bidirectional flow systems necessarily inefficient? Canadian Journal of Zoology, 67, 2414–2421.

Naylor BG (1978) The frontosquamosal arch in newts as a defense against predators. Canadian Journal of Zoology, 56, 2211–2216.

Nishikawa K, Jiang J, Matsui M, Mo YM (2011) Unmasking *Pachytriton labiatus* (Amphibia: Urodela: Salamandridae), with description of a new species of *Pachytriton* from Guangxi, China. Zoological Science, 28, 453–461.

Özeti N, Wake DB (1969) The morphology and evolution of the tongue and associated structures in salamanders and newts (family Salamandridae). Copeia, 1969, 91–123.

Pope CH (1931) Notes on amphibians from Fukien, Hainan, and other parts of China. Bulletin of the American Museum of Natural History, 61, 397–611.

Reed HD (1920) The morphology of the sound-transmitting apparatus in caudate amphibians and its phylogenetic significance. Journal of Morphology, 33, 326–387.

Sauvage HE (1876) Sur quelques Batraciens de la Chine. L'Institut, Journal universel des Sciences et des Sociétés savantes, (n. s.), 4, 274–275.

Schaeffer B (1941) The morphology and evolution of the tarsus in amphibians and reptiles. Bulletin of the American Museum of Natural History, 78, 395–472.

Shen S, Shen Y (1990) Anatomy of the skeletal system of *Pachytriton brevipes* (Amphibia: Salamandridae). 53–59. In Zhao E. (Ed.), From water onto land. Beijing, China: Chinese Forestry Press.

Shen Y, Shen D, Mo X (2008) A new species of salamander *Pachytriton archospotus* from Hunan Province, China (Amphibia, Salamandridae). Acta Zoologica Sinica, 54, 645–652.

Spearman RIC (1968) Epidermal keratinization in the salamander and a comparison with other amphibia. Journal of Morphology, 125, 129–144.

Tihen JA (1958) Comments on the osteology and phylogeny of ambystomatid salamanders. Bulletin of the Florida State Museum Biological Sciences, 3, 1–50.

Titus TA, Larson A (1995) A molecular phylogenetic perspective on the evolutionary radiation of the salamander family Salamandridae. Systematic Biology, 44, 125–151.

Toledo RC, Jared C (1993) Cutaneous adaptations to water balance in amphibians. Comparative Biochemistry and Physiology Part A: Physiology, 105, 593–608.

Trueb L (1993) Patterns in cranial diversity among the Lissamphibia. 255–343. In Hanken J., Hall B. K. (Eds.), The vertebrate skull: patterns of structural and systematic diversity, Vol. 2. Chicago, USA: University of Chicago Press.

Unterstein W (1930) Beiträge zur Lurch und Kriechiterfauna Kwangsi's: II Schwanzlurche. Sitzungsbericht Gesellschaft Naturforschender Freunde Berlin, 2, 313–315.

Üzüm N (2009) A skeletochronological study of age, growth and longevity in a population of the Caucasian salamander, *Mertensiella caucasica* (Waga 1876) (Caudata: Salamandridae) from Turkey. North-Western Journal of Zoology, 5, 74–84.

Wake DB (1963) Comparative osteology of the plethodontid salamander genus *Aneides*. Journal of Morphology, 113, 77–118.

Wake DB, Özeti N (1969) Evolutionary relationships in the family Salamandridae. Copeia, 1969, 124–137.

Wake DB, Shubin N (1998) Limb development in the Pacific giant salamanders, *Dicamptodon* (Amphibia, Caudata, Dicamptodontidae). Canadian Journal of Zoology, 76, 2058–2066.

Wu Y, Wang Y, Jiang K, Chen X, Hanken J (2010) Homoplastic evolution of external coloration in Asian stout newts (*Pachytriton*) inferred from molecular phylogeny. Zoologica Scripta, 39, 9–22.

Xu J (2007) Histological observation on skin of *Pachytriton labiatus*. Sichuan Journal of Zoology, 26, 400–401.

Zhang P, Papenfuss TJ, Wake MH, Qu L, Wake DB (2008) Phylogeny and biogeography of the family Salamandridae (Amphibia: Caudata) inferred from complete mitochondrial genomes. Molecular Phylogenetics and Evolution, 49, 586–597.

Zhao E, Hu Q (1984) Studies on Chinese tailed amphibians. Chengdu, China: Sichuan Scientific and Technical Publishing House.

Appendix

Cleared-and-stained specimens

Pachytriton brevipes CIB 88186 ♀, 88191 ♂, 88207 ♀, 88208 ♂
Pachytriton archospotus CIB 95951 ♀, 95952 ♀
Southwestern *Pachytriton inexpectatus* CIB 88153 ♂, 88157 ♀, 88160 ♀, 88173 ♂
Northeastern *Pachytriton inexpectatus* CIB 88137 ♀, 88146 ♂, 88152 ♀, 88155 ♂
Salamandra salamandra MCZ 8048, 99122
Taricha granulosa MCZ 1207, 125980

Radiographed specimens

Pachytriton brevipes CIB 88187, 88188, 88192, 88193, 88194, 88195, 88196, 88197, 88199, 88200, 88201, 88203, 88204, 88205, 88221, 95965, 95972, 95973, 95975, 95978; MCZ 204107 204108; MVZ 204299
Pachytriton archospotus CIB 95949, 95950, 95953
Southwestern *Pachytriton inexpectatus* CIB 88134, 88147, 88148, 88156, 88158, 88161, 88162, 88163, 88164, 88165, 88166, 88170, 88178, 88180, 88182, 95944, 95945, 95946, 95947, 96948
Northeastern *Pachytriton inexpectatus* CIB 88135, 88136, 88138, 88139, 88143, 88144, 88145, 88149, 88150, 88151, 88154, 88159, 88169, 88179, 88181, 95912, 95913, 95914; CAS 194298 194299 194300
Paramesotriton hongkongensis MCZ 109447, 116047, 116048
Paramesotriton longliensis CIB 97884, 97885
Cynops wolterstorffi MCZ 1786, 8149, 8156, 9623
Cynops orphicus MVZ 22471, 22472, 22503

Chapter 3

Significance of pre-Quaternary climatic change for montane species diversity: insights from Chinese salamanders (Salamandridae: *Pachytriton*)[9]

[9] Results presented in this chapter are published in Molecular Phylogenetics and Evolution (2013).

Abstract

Despite extensive focus on the genetic legacy of Pleistocene glaciation, impacts of earlier climatic change on biodiversity are poorly understood. Because amphibians are highly sensitive to variations in precipitation and temperature, I use a genus of Chinese montane salamanders (Salamandridae: *Pachytriton*) to study paleoclimatic change in East Asia, which experienced intensification of its monsoon circulation in the late Miocene associated with subsequent Pliocene warming. Using both nuclear and mitochondrial DNA sequences, I reconstruct the species tree under a coalescent model and demonstrate that all major lineages originated before the Quaternary. Initial speciation within the genus occurred after the summer monsoon entered a stage of substantial intensification. Heavy summer precipitation established temporary water connectivity through overflows between adjacent stream systems, which may facilitate geographic range expansion by aquatic species such as *Pachytriton*. Species were formed in allopatry likely through vicariant isolation during or after range expansion. To evaluate the influence of Pliocene warming on these cold-adapted salamanders, I construct a novel temperature buffer-zone model, which suggests widespread physiological stress or even extinction during the warming period. A significant deceleration of species accumulation rate is consistent with Pliocene range contraction, which affected *P. granulosus* and *P. archospotus* the most because they lack large temperature buffer zones. In contrast, demographic growth occurred in species for which refugia persist. The buffer-zone model reveals the Huangshan Mountain as a potential climatic refugium, which is similar to that found for other East Asian organisms. My approach can incorporate future climatic data to evaluate the potential impact of ongoing global warming on montane species (particularly

amphibians) and to predict possible population declines.

Introduction

Compared to the extensively studied Quaternary climatic fluctuations and associated genetic legacy on extant organisms (reviewed in Hewitt 2000), the impacts of more ancient environmental changes as far back as the Pliocene and late Miocene, which witnessed remarkable shifts in global climate and continental ecosystems (Cerling *et al.* 1997; Zachos *et al.* 2001), are poorly known. Yet, those early climatic transitions may have had crucial roles in promoting diversification within radiations of Cenozoic organisms (Kozak *et al.* 2006; Vieites *et al.* 2007; Lo Presti & Oberprieler 2009; Zheng *et al.* 2009; Dasmahapatra *et al.* 2010; Miralles & Carranza 2010; Patel *et al.* 2011).

During the Quaternary glacial period, East Asia was largely not glaciated due to dry winters (Hewitt 2000; Li *et al.* 2004). Species from this region may not have experienced the extreme demographic fluctuations that characterize biota from glaciated areas. Old gene lineages are more likely to be preserved, which allows us to study the evolutionary forces that acted upon organismal diversity before the glacial period. Studies have demonstrated that glacial climatic oscillations are too recent to explain some of the deep genetic divergences observed today (Dasmahapatra *et al.* 2010; Miralles & Carranza 2010; Patel *et al.* 2011). East Asia experienced a distinctive climatic history since the late Miocene, which is characterized by development of the unique East Asian monsoon system accompanied by the accelerating uplift of the Tibetan Plateau (An *et al.* 2006; Harris 2006). Seasonality increased, with most precipitation occurring in summer (An *et al.* 2001). The monsoon is strongly associated with East Asian terrestrial ecosystem turnover (Jia *et al.* 2003). On the other hand, East Asia was affected by global warming in the Pliocene (Zachos *et al.* 2001; Ravelo *et al.* 2004; Salzmann *et al.* 2011). This warm

and wet period contrasts with the otherwise prevailing trend towards global cooling that existed since the late Miocene, and it could have devastated cold-adapted organisms in ways similar to current global warming (Pounds *et al.* 2006; Milanovich *et al.* 2010). Because these climatic shifts greatly altered precipitation patterns and environmental temperatures, I might expect to find signals in extant East Asian amphibians, whose life history and species richness are governed by precipitation and temperature (Buckley & Jetz 2007). Nevertheless, few phylogeographic studies have focused on East Asia, and our knowledge of the genetic consequences of historical climatic change in this region remains sparse.

The stout newts (*Pachytriton*, also known as paddle-tailed newts) from southeastern China are an ideal system with which to investigate organismal response to historical climatic change. Earlier studies suggest that *Pachytriton* diverged from its sister genus *Laotriton* as early as the middle Miocene (Zhang *et al.* 2008b; Vieites *et al.* 2009). Such long-term persistence is essential to be able to capture climatic signatures over the last 10 million years (Ma). Species in this genus are restricted to montane habitats at high elevations (i.e., on sky islands), which were uplifted by major orogenies before the middle Eocene (Guo 1998). Therefore, the phylogeographic pattern in *Pachytriton* evolved too recently to be explained by mountain orogeny. However, ranges of individual populations likely expanded and contracted along elevational gradients that changed as the result of climatic fluctuations, in a manner similar to that recorded in North American montane salamanders (Shepard & Burbrink 2008). Salamanders generally have low dispersal ability and exhibit philopatry; thus, they are more sensitive than are endotherms to changes in precipitation and temperature (Buckley & Jetz 2007; Vieites *et al.* 2009).

Adult *Pachytriton* permanently live in small, shallow and clean montane streams (usually 1–3 m wide) and have morphological and osteological specializations associated with their aquatic habitat (Özeti & Wake 1969; Zhao *et al.* 1994; Fei *et al.* 2006; Wu *et al.* 2012a). They are adapted to live in cold water, and a small increase of ambient temperature may be fatal (Zhao *et al.* 1994).

In this paper, I use *Pachytriton* to understand the likely impact of late-Miocene monsoon intensification and Pliocene warming on montane species diversity in East Asia. First, I evaluate the hypothesis that the substantial intensification of the East Asian summer monsoon in the late Miocene (7–10 Ma) triggered range expansion in *Pachytriton*, which subsequently promoted initial speciation in the genus. By sampling throughout the known geographic range of *Pachytriton*, I employ a coalescent method to generate a species tree along with divergence times and test whether speciation occurred after monsoon intensification. During the monsoon season, I have encountered *Pachytriton* in temporary waterways after heavy rains or in puddles with signs of a recent flood (unpublished personal observations). Given that this genus is the most aquatic in the family Salamandridae (Özeti & Wake 1969; Titus & Larson 1995), floods that connect neighboring stream systems could facilitate colonization of new habitats and lead to range expansion. Recent studies suggest a critical role for range expansion in promoting speciation (Moyle *et al.* 2009; Van Bocxlaer *et al.* 2010). Speciation could occur followed by vicariance that reduces gene flow across a barrier formed after expansion. Second, I follow the rationale of ecological niche-modeling to examine likely physiological constraints on *Pachytriton* and the extent to which Pliocene warming (3–5 Ma) may have affected their survival. Because these salamanders are sensitive to high

temperatures and restricted to specific montane habitats, they may experience range contraction toward higher elevations or even habitat collapse under a climatic warming scenario (Wake & Vredenburg 2008; Wake 2009; Wake 2012). Third, I reconstruct historical demography using a multi-locus coalescent model to assess how population size may have fluctuated under different climatic conditions. I predict no population growth in species that were most stressed by Pliocene warming and stable demographic growth in species for which areas of suitable habitat persisted. Fourth, I test the tempo of diversification in the genus against a null model of constant rate of lineage accumulation. A detrimental impact of Pliocene warming would favor rate deceleration over constancy.

Material and methods

Taxon sampling and sequence preparation

I conducted extensive fieldwork throughout southeastern China and acquired specimens and tissues from 6 of the 8 species in *Pachytriton*[10]: 4 populations of *P. archospotus*, 6 populations of *P. brevipes*, 7 populations of *P. granulosus*, 1 population of *P. feii*, 5 populations of *P. inexpectatus* and 1 population of *P. xanthospilos* (Fig. 3-1; Table 3-1). Samples of the recently described *P. moi* from Guangxi province and *P. changi* (described from two salamanders obtained from a Japanese pet store with unknown origin) were unavailable for this study.

Total genomic DNA was extracted from ethanol-preserved liver or muscle tissue by using a QIAGEN DNeasy Blood and Tissue Kit (Valencia, CA, USA). I amplified from all specimens two mitochondrial fragments (*ND2* and the *cytb* with flanking tRNAs, each

[10] *Pachytriton granulosus* (northeastern *P. inexpectatus* in Chapters 1 and 2), *P. feii*, and *P. xanthospilos* are recently recognized as separate species in the genus.

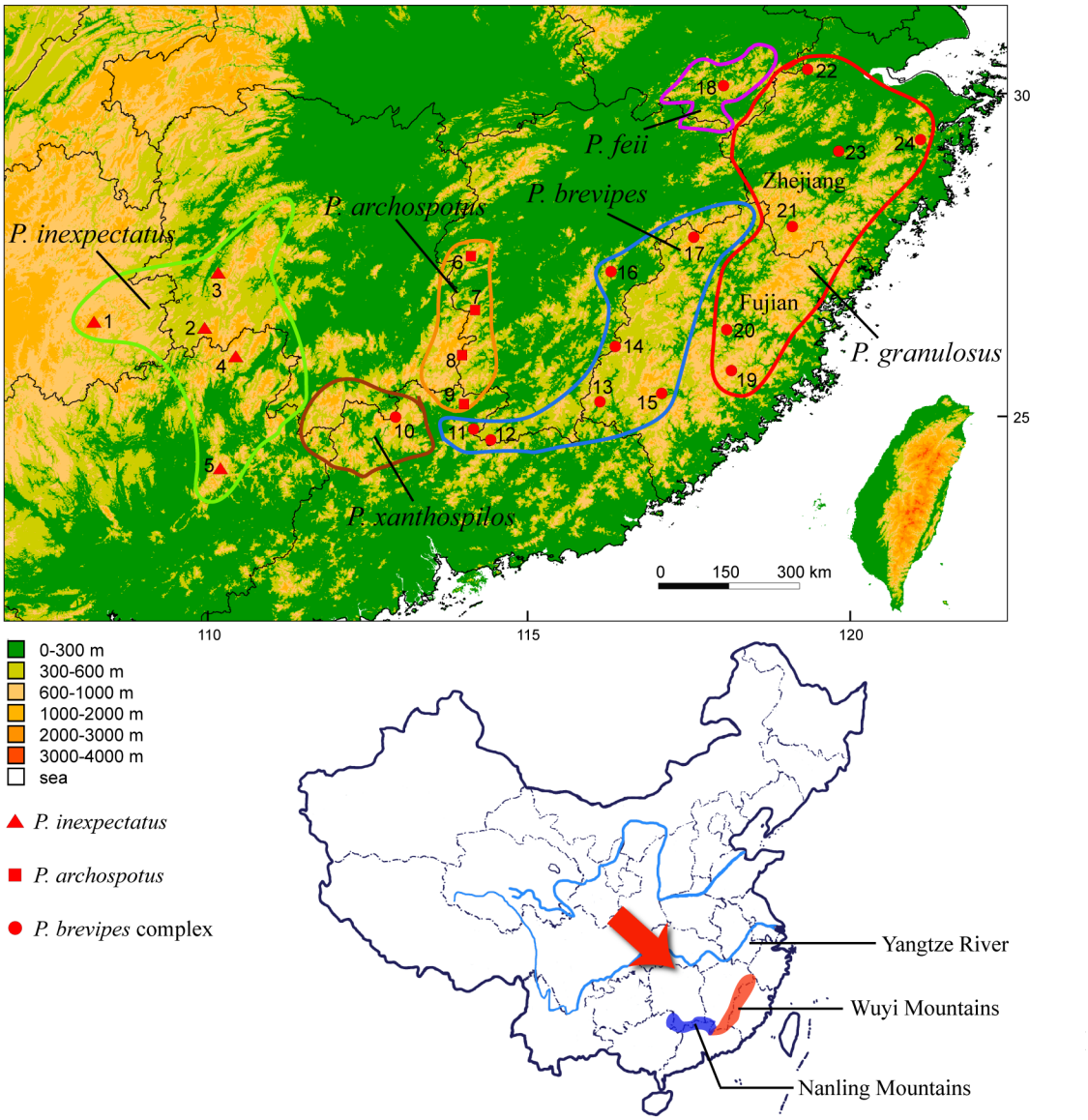

Figure 3-1. Top: Geographic distribution of the genus *Pachytriton* in southeastern China and sampling localities (Table 3-1). Several new species have been recognized after 2010 in additional to the three species (*P. archospotus*, *P. brevipes*, and *P. inexpectatus*) discussed in chapters 1 and 2. Bottom: Country map showing the focal study region (red arrow) and location of the Nanling and Wuyi mountain ranges.

Table 3-1. Sampled populations used in the study.

ID	Sampling Locality	Musuem No.	Genebank Accession No.			
	Pachytriton archospotus		*ND2*	*cytb*	*RAG-1*	*NCRT*
6	Wugongshan, Pingxiang Co. Jiangxi	CIB97913	JX907837	JX907934	JX907969	JX907881
		CIB97914	JX907838	JX907935	JX907970	JX907882
		CIB97915	JX907839	JX907936	JX907971	JX907883
7	Jianggangshan, Jiangxi	CIB97907	JX907840	JX907937	JX907972	JX907884
		CIB97908	JX907841	JX907938	JX907973	JX907885
		CIB97909	JX907842	JX907939	JX907974	JX907886
8	Qiyunshan, Guidong Co., Hunan	CIB95950	GQ303629	GQ303666	GQ303707	JX907879
		CIB95949	GQ303630	GQ303667	GQ303708	JX907880
		CIB95953	GQ303628	GQ303665	GQ303706	JX907878
9	Guanyindong, Shixing Co., Guangdong	CIB97863	JX237731	JX237751	JX907968	JX907877
	Pachytriton brevipes					
11	Chebaling, Shixing Co., Guangdong	CIB97857	JX907850	JX907948	JX907983	JX907911
		CIB97858	JX907851	JX907949	JX907984	JX907912
		CIB97859	JX907852	JX907950	JX907985	JX907913
12	Jiulianshan, Qunan Co., Jiangxi	N/A	DQ517796	N/A	N/A	N/A
13	Liangyeshan, Wuping Co., Fujian	CIB97939	JX907856	JX907954	JX907989	JX907917
		CIB97940	JX907857	JX907955	JX907990	JX907918
		CIB97946	JX907858	JX907956	JX907991	JX907919
14	Jigongdong, Ninghua Co., Fujian	CIB97929	JX907859	JX907957	JX907992	JX907920
		CIB97930	JX907860	JX907958	JX907993	JX907921
		CIB97934	JX907861	JX907959	JX907994	JX907922
15	Tiangongshan, Longyan city, Fujian	CIB97889	JX907853	JX907951	JX907986	JX907914
		CIB97890	JX907854	JX907952	JX907987	JX907915
		CIB97891	JX907855	JX907953	JX907988	JX907916
16	Junfengshan, Nanfeng Co., Jiangxi	CIB95930	GQ303627	GQ303664	GQ303705	JX907904
		CIB95926	GQ303626	GQ303663	GQ303704	JX907902
		CIB95928	JX907846	JX907944	JX907979	JX907903
17	Wuyishan, Wuyishan city, Fujian	CIB88188	GQ303617	GQ303654	GQ303695	JX907907
		CIB88194	GQ303616	GQ303653	GQ303694	JX907906
		CIB88221	GQ303615	GQ303652	GQ303693	JX907905
	Pachytriton feii					
18	Huangshan, Huangshan city, Anhui	CIB95914	JX907847	JX907945	JX907980	JX907908
		CIB95913	JX907848	JX907946	JX907981	JX907909
		CIB95912	JX907849	JX907947	JX907982	JX907910

Table 3-1 (continued)

ID	Sampling Locality	Musuem No.	Genebank Accession No.			
	Pachytriton granulosus					
19	Daiyunshan, Dehua Co., Fujian	MVZ231167	DQ517797	JX907940	JX907975	JX907887
20	Meixian, Youxi Co., Fujian	CIB88185	GQ303622	GQ303659	GQ303700	JX907898
		CIB88207	GQ303620	GQ303657	GQ303698	JX907896
		CIB88189	GQ303621	GQ303658	GQ303699	JX907897
21	Longquanshan, Longquan city, Zhejiang	CIB95963	JX907843	JX907941	JX907976	JX907899
		CIB95964	JX907844	JX907942	JX907977	JX907900
		CIB95960	JX907845	JX907943	JX907978	JX907901
22	Tianmushan, Zaoxi Co., Zhejiang	CIB88145	GQ303606	GQ303643	GQ303684	JX907888
		CIB88152	GQ303608	GQ303645	GQ303686	JX907890
		CIB88137	GQ303607	GQ303644	GQ303685	JX907889
23	Lipu, Jinhua city, Zhejiang	CIB95997	GQ303624	GQ303661	GQ303702	JX907894
		CIB95996	GQ303625	GQ303662	GQ303703	JX907895
24	Tiantaishan, Ninghai Co., Zhejiang	CIB88143	GQ303610	GQ303647	GQ303688	JX907891
		CIB88169	GQ303612	GQ303649	GQ303690	JX907893
		CIB88161	GQ303611	GQ303648	GQ303689	JX907892
	Pachytriton inexpectatus					
1	Leigongshan, Leishan, Guizhou	CIB88148	GQ303600	GQ303637	GQ303678	JX907866
		CIB88170	GQ303601	GQ303638	GQ303679	JX907867
		CIB88147	GQ303599	GQ303636	GQ303677	JX907865
2	Linkou, Tongdao Dong, Hunan	CIB95931	JX907831	JX907928	JX907962	JX907871
		CIB95935	JX907832	JX907929	JX907963	JX907872
		CIB95933	JX907833	JX907930	JX907964	JX907873
3	Xuefengshan, Hongjiang city, Hunan	CIB95940	JX907834	JX907931	JX907965	JX907874
		CIB95938	JX907835	JX907932	JX907966	JX907875
		CIB95941	JX907836	JX907933	JX907967	JX907876
4	Mao'ershan, Xin'an Co. Guangxi	CIB88182	GQ303594	GQ303631	GQ303672	JX907862
		CIB88158	GQ303596	GQ303633	GQ303674	JX907863
		CIB88156	GQ303597	GQ303634	GQ303675	JX907864
5	Dayaoshan, Jinxiu Co. Guangxi	CIB88165	GQ303602	GQ303639	GQ303680	JX907868
		CIB95947	JX907830	JX907926	JX907960	JX907869
		CIB95946	GU980583	JX907927	JX907961	JX907870
	Pachytriton xanthospilos					
10	Mangshan, Yizhang Co., Hunan	CIB97900	JX237740	JX237760	JX907995	JX907923
		CIB97901	JX237741	JX237761	JX907996	JX907924
		CIB97903	JX237743	JX237763	JX907997	JX907925

with ~1200 base pairs, bp) and two nuclear fragments that cover the 3' end of the *RAG-1* (~1200 bp), as well as a non-coding region of the tyrosinase gene (*NCRT*, 600 bp). The first three markers are widely used in phylogenetic studies; *NCRT* is used for the first time and developed following the anonymous-loci development method described in Espregueira Themudo *et al.* (2009). The *NCRT* fragment was amplified using the forward primer TYR-F (5'AGC GGT AGA CCT GTG GCT TC 3') and reverse primer TYR-R (5' TGC ACA CTG ATG GGG TTG GT 3'). Other PCR primers and thermal cycle protocols are the same as Wu *et al.* (2010). Nucleotide sequences were manually aligned in Se-Al 2.0 (Rambaut 1995). Sequences are deposited in GenBank (Table 3-1).

Individual gene-trees estimation

I inferred separate gene genealogies from *RAG-1*, *NCRT* and the concatenated mitochondrial DNA (mtDNA). I utilized the Bayesian criterion in MrBayes 3.1.2 (Huelsenbeck & Ronquist 2001) and the maximum-likelihood (ML) criterion in RAxMLv7.4.3 (Stamatakis 2006). The concatenated mtDNA was partitioned by codon positions, but nuclear DNAs were not partitioned due to limited variable sites. Substitution models in Bayesian inference were determined by the Akaike Information Criterion (AIC) in MRMODELTEST 2.2 (Nylander 2004). Bayesian Markov Chain Monte Carlo (MCMC) was run for 10-million generations sampled every 100 generations. In the ML analysis, the GTRGAMMA model was used for each gene partition, and 1000 nonparametric bootstrap replicates were performed to calculate node support.

Species-tree and divergence-time estimation

It is a common practice to assume that a species phylogeny equals a single-gene genealogy (including trees derived from gene concatenation). However, a gene tree represents only one realization of the stochastic process embedded inside the species tree (Ho & Shapiro 2011). Discrepancies between species trees and gene trees can arise if lineage sorting is incomplete among recently diverged species (Pamilo & Nei 1988). Therefore, I used a multispecies coalescent model to estimate the species tree based on multi-locus data under the Star BEAST (*BEAST) option implemented in BEAST v1.6.1 (Drummond & Rambaut 2007; Heled & Drummond 2010). This approach outperforms gene-concatenation methods in both species-tree topology inference and speciation-time estimation (Heled & Drummond 2010). Sequence data were tri-partitioned into mtDNA, *RAG-1* and *NCRT*. Substitution models were unlinked across partitions and determined by AIC in MRMODELTEST 2.2 (Nylander 2004). Star BEAST does not require outgroup taxa (Heled & Drummond 2010). The root of the species tree and speciation times were estimated through an uncorrelated relaxed-clock model, in which evolutionary rate in each branch is drawn independently from a lognormal distribution. This relaxed-clock model performs well with both clocklike and non-clocklike data (Drummond *et al.* 2006). Due to the paucity of the fossil record for East Asian salamandrids, I imported calibration dates from Zhang *et al.* (2008), who propose two sets of divergence times within Salamandridae based on mitogenomic data. The younger set is more compatible with independent biogeographic evidence and congruent with corresponding dates from another study that uses both mitochondrial and nuclear genes with different fossil calibrations (Roelants *et al.* 2007). This set of divergence times likely

approximates the true ages of salamandrids and is consistent across data types (mtDNA vs. nuclear DNA). Following Zhang *et al.* (2008), I constrained the age of the genus *Pachytriton* between 3.9 and 18.3 Ma with a uniform prior distribution. This interval includes the oldest estimate for the split between *Pachytriton* and its sister genus *Laotriton* as well as the youngest divergence time within *Pachytriton*. A second calibration prior was placed at the split between *P. granulosus* and *P. xanthospilos* at 7.5 Ma (Zhang *et al.* 2008b) with a normal-distributed 95% confidence interval (CI) between 3.9 and 11.2 Ma. Bayesian MCMC was performed for 100-million generations with a sample frequency at every 1000 generations. Burn-in period was determined by Tracer 1.4 (Rambaut & Drummond 2007). Node ages were calculated as mean node heights from the maximum clade credibility tree summarized from the posterior distribution trees, which were displayed with DensiTree (Bouckaert 2010).

Influence of Pliocene warming

It is difficult to assess the impact of Pliocene warming on montane-adapted *Pachytriton* when relevant physiological data do not exist. By assuming that physiological constraints are reflected in habitat selection, which also is the key assumption of the ecological niche-modeling approaches (Kozak *et al.* 2008), I can use environmental temperature at a population's lowest elevational limit as a proxy for its maximum heat tolerance. Because there is only one collecting locality on each mountain and no historical collection data available, standard ecological niche-modeling approaches (e.g., Maxent) cannot be applied to obtain a mountain-specific response to climatic change. Given that I know only the temperature increase during Pliocene warming and have no information on

quantitative precipitation change, my evaluation of the impact is limited to temperature-related variables. Although temperature and precipitation are coupled in driving amphibian diversity, changes in either constraint influence the distributional limit of amphibians (Buckley & Jetz 2007).

When global temperature rises, the elevational limits of montane salamanders are pushed upwards and eventually there may no longer be suitable habitat, and the population, or even species, goes extinct (Wake & Vredenburg 2008; Wake 2009; Wake 2012). Montane salamanders are less likely to acclimate because small increases in temperature can induce significant metabolic depression (Bernardo & Spotila 2006). In southeastern China, summer and winter temperatures of the late Miocene are about equal to present values (Utescher *et al.* 2011). The subsequent Pliocene, however, witnessed a global warming of 2–5 °C (Novacek 1999; Ravelo *et al.* 2004; Salzmann *et al.* 2011). This provides a comparable scenario to the current path of climatic warming projected to the end of the 21st century (IPCC 2007; Salzmann *et al.* 2009). Therefore, I proposed a temperature buffer zone for *Pachytriton*, calculated as the contemporary temperature difference between the top of the mountain (the theoretical refugium) and the population's lowest distributional limit. If the buffer zone does not or only slightly exceeds the 2–5 °C window, suitable environmental conditions would not exist locally during the Pliocene warming period. *Pachytriton* at this local area would have declined or even been extirpated. I used seven climatic variables to calculate seven buffer zones that address different aspects of the environmental temperature: annual mean temperature (AMT), maximum temperature of the warmest month, minimum temperature of the coldest month, and mean temperatures of warmest, coldest, wettest and driest quarters.

My method assumes that the ancestral *Pachytriton* were adapted to a cool climate, which is consistent with the reconstruction of climatic envelopes of Salamandridae through geological time (Vieites *et al.* 2009).

All sampled *Pachytriton* were collected in cold, montane streams. The exact lowest distributional limit of most samples is unknown. However, in many cases the lowest collecting locality should be close to the limit because I collected from downstream to upstream. Consequently the same locality was treated as the upper bound of the lowest distribution, which yields a conservative (minimum) estimate of the buffer zone. I also sampled five random localities 200 m lower than the lowest collecting locality, and used those localities, where *Pachytriton* are absent based on previous fieldwork, as the lower bound of the lowest distribution limit. The arithmetic mean of temperatures from the five absence locations was used to yield a more liberal (maximum) estimate of the temperature buffer zone. In each case there are at most minimal differences in either stream availability or forest composition between occurrence and absence locations. No other aquatic organism has been recorded to compete with or prey on *Pachytriton*. Thus, environmental temperature difference is likely the primary factor that determines the occurrence and absence of *Pachytriton* at these sites.

Temperature variables for East Asia were obtained from the WorldClim contemporary database (Hijmans *et al.* 2005) at 30 arc-seconds resolution (~1 km^2). Country-level elevational data at the same resolution were downloaded from the DIVA-GIS website (http://www.diva-gis.org/). Both data sets were imported into the geographic analysis program DIVA-GIS 7.1.7. For each of the 24 sampling locations, values of the seven temperature variables were extracted at the mountain top, the

collecting site and the five corresponding absence locations (110 absence locations in total). The temperature buffer zone for each population was established as the temperature difference between the mountain top and the lower and upper bound of the lowest distribution and was compared to the 2–5 °C temperature increment of the Pliocene.

Historical demographic analyses

To estimate population-size dynamics through geological time, I reconstructed Extended Bayesian Skyline Plots (EBSPs, Heled & Drummond 2008) implemented in BEAST v1.6.1 for four species for which I sampled more than one locality: *P. archospotus*, *P. brevipes*, *P. granulosus* and *P. inexpectatus*. This coalescent-based, non-parametric Bayesian MCMC algorithm incorporates multi-locus data to reduce estimate errors associated with single genes (e.g., traditional Bayesian Skyline Plots) and increases the power to detect demographic dynamics (Ho & Shapiro 2011). Sequence partitions, substitution models and the clock model were the same as those used in the species-tree analysis. Divergence time was converted from number of substitutions to millions of years by inputting the geometric mean of substitution rates of genes. Population growth was depicted as piecewise linear, allowing population size to change continuously through the genealogical history (Heled & Drummond 2008). Bayesian MCMC was performed for 50-million generations with a sampling frequency of every 1000 generations. The first 10% of the sample was discarded as burn-in. Skyline plots were visualized using EXCEL. I further used non-genealogical summary statistics including Tajima's D (Tajima 1989) and Fu and Li's D* (Fu & Li 1993) to detect historical

population-size change. Assuming neutral alleles, a significantly negative value indicates recent demographic growth, whereas a significantly positive value indicates a very recent bottleneck event. Summary statistics were calculated in DNAsp v5 (Librado & Rozas 2009); associated confidence intervals were estimated through 1000 coalescent simulations.

Tempo of diversification

If Pliocene warming had a detrimental impact on *Pachytriton*, I expect to find a slowdown of lineage accumulation after initial speciation in the genus. I tested a deviation from the null model of constant diversification rate using the constant-rate (CR) test and the gamma statistic (γ) by Pybus & Harvey (2000). Negative values of γ imply a deceleration of diversification rate on a given chronogram. The null model can be rejected at the 95% significance level when $\gamma < -1.645$ (Pybus & Harvey 2000). Because I included 6 of 8 described species in the genus, incomplete sampling at the species level should have little effect on γ estimation (Pybus & Harvey 2000; Cusimano & Renner 2010). However, to account for new species yet to be discovered, I performed a Monte Carlo constant-rate (MCCR) test by simulating 100 phylogenies under the constant-rate model (pure-birth process) with a full sampling of total 10 and 20 species assumed in *Pachytriton*, respectively. Phylogenies were randomly pruned to retain 6 species to reflect the actual sampling. The observed γ was compared to the distribution of gamma values estimated from those pruned trees. If the observed value is statistically different from the null distribution, the constant-rate model will be rejected given incomplete taxon sampling (Pybus & Harvey 2000). Both CR test and MCCR test were conducted using

the LASER package in R.

Results

Gene-tree estimation

No premature stop codon or insertion-deletion is detected in the protein-coding regions of *ND2*, *cytb* or *RAG-1*. A single insertion-deletion is present in the *NCRT* fragment, which exhibits moderate interspecific variation in salamandrids comparable to the level observed in *RAG-1*. Individual gene trees reveal different relationships among species of *Pachytriton* (Fig. 3-2). Tree topologies are almost identical from Bayesian and the ML analyses. The mtDNA and *NCRT* gene trees are congruent with each other and with the result from Wu *et al.* (2010, 2012b) in recovering *P. inexpectatus* as the sister taxon to a clade comprising the rest of the sampled species. In contrast, the *RAG-1* data recognize a sister-taxon relationship between *P. inexpectatus* and *P. archospotus*. All sampled species of *Pachytriton* are monophyletic with strong support in the mitochondrial gene tree, but populations of *P. brevipes*, *P. feii*, *P. granulosus* and *P. xanthospilos* are admixed in the two independent nuclear gene trees. The latter three species were once considered conspecific populations of *P. brevipes* (Fei *et al.* 2006), and were recently elevated to full species based on mtDNA data (Nishikawa *et al.* 2011; Wu *et al.* 2012b). Notably, the mtDNA gene tree estimates that the most recent common ancestors (MRCA) of sampled populations of *P. archospotus* and *P. granulosus* date only to the end of the Pliocene, although both species likely originated before the Pliocene. Because gene trees overestimate divergence times (Edwards & Beerli 2000), diversification within each of these species likely is even more recent.

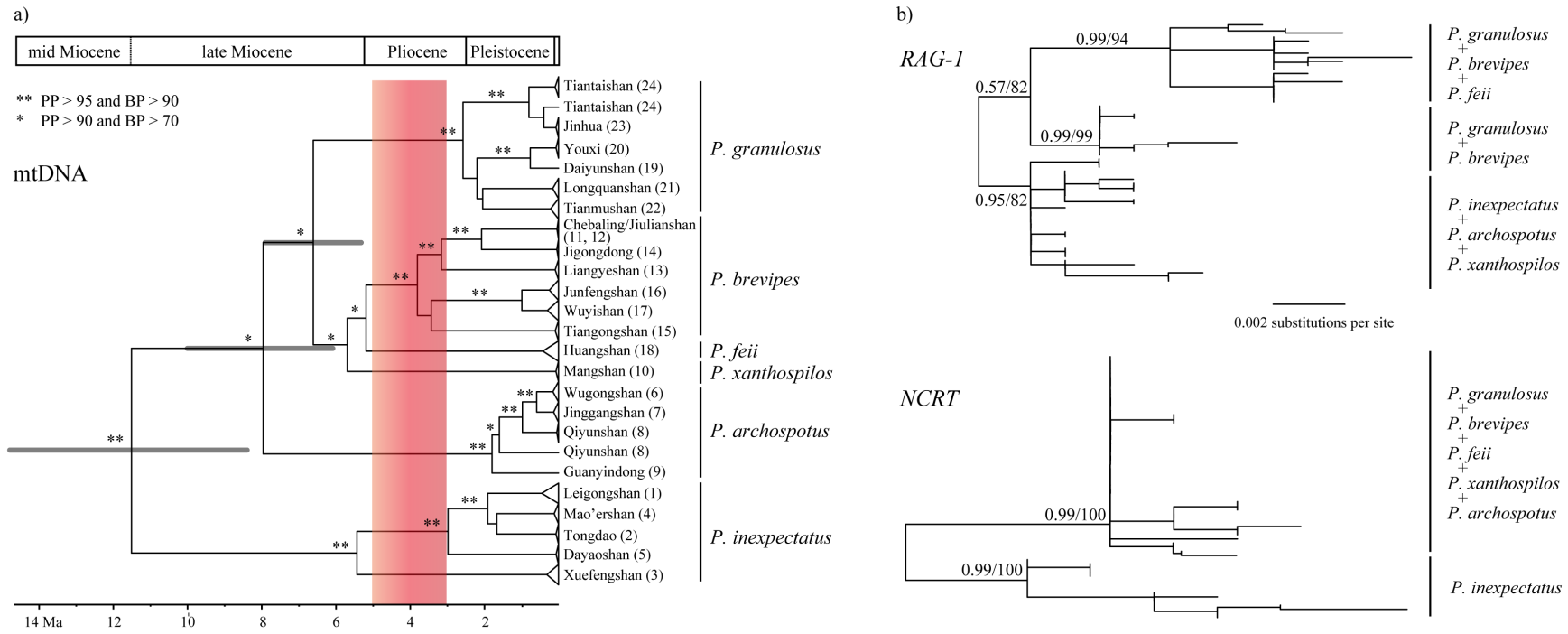

Figure 3-2. (a) Bayesian mtDNA gene tree and (b) ML nuclear gene trees. The mtDNA gene tree is scaled with geological times; nuclear gene trees are scaled with substitution unit. Numbers at the tips of the mtDNA tree correspond to sampling localities. Grey bars represent 95% HPD of the node age. The red vertical column indicates the warm Pliocene. Numbers and asterisks on branches are Bayesian posterior probabilities and ML bootstrap values.

Species-tree estimation

Consistent with mtDNA and *NCRT* gene trees, the multi-locus species tree resolves the basal split between *P. inexpectatus* and other sampled species (Fig. 3-3). *Pachytriton archospotus* forms the sister taxon to a clade comprising *P. brevipes*, *P. feii*, *P. granulosus* and *P. xanthospilos*. This topology is favored by 90.9% of the 75,000 post-burn-in MCMC trees. However, relationships among the latter four species cannot be resolved with high node support. Given their admixture pattern in nuclear gene trees, the four species are most appropriately treated as comprising a species complex (*P. brevipes* complex), which requires further studies of species delimitation. Only 6.4% of the MCMC trees suggest that *P. inexpectatus* and *P. archospotus* are sister species, and the remaining 2.7% of the trees group *P. inexpectatus* with the *P. brevipes* complex. The first speciation event in *Pachytriton* occurred in the late Miocene, 9.4 Ma (95% CI: 6.1–12.9 Ma). Subsequent divergence between *P. archospotus* and the *P. brevipes* complex dates to 6.8 Ma (95% CI: 4.5–9.1 Ma). Both speciation events largely overlap the period when the East Asian summer monsoon underwent a significant intensification at 7–10 Ma. Star BEAST also estimates a mitochondrial substitution rate of 7.7×10^{-9} per site per year (95% Highest Posterior Density, HPD: 5.9×10^{-9}–9.9×10^{-9}), which corresponds to a sequence divergence of 1.54% between taxa per million years of separation.

Impact of Pliocene warming

Temperature buffer zones were derived from temperature variables for each of 24 populations. Considerable variation in the size of buffer zones occurs among species and localities (Fig. 3-4). Because the only available Pliocene temperature data are estimated

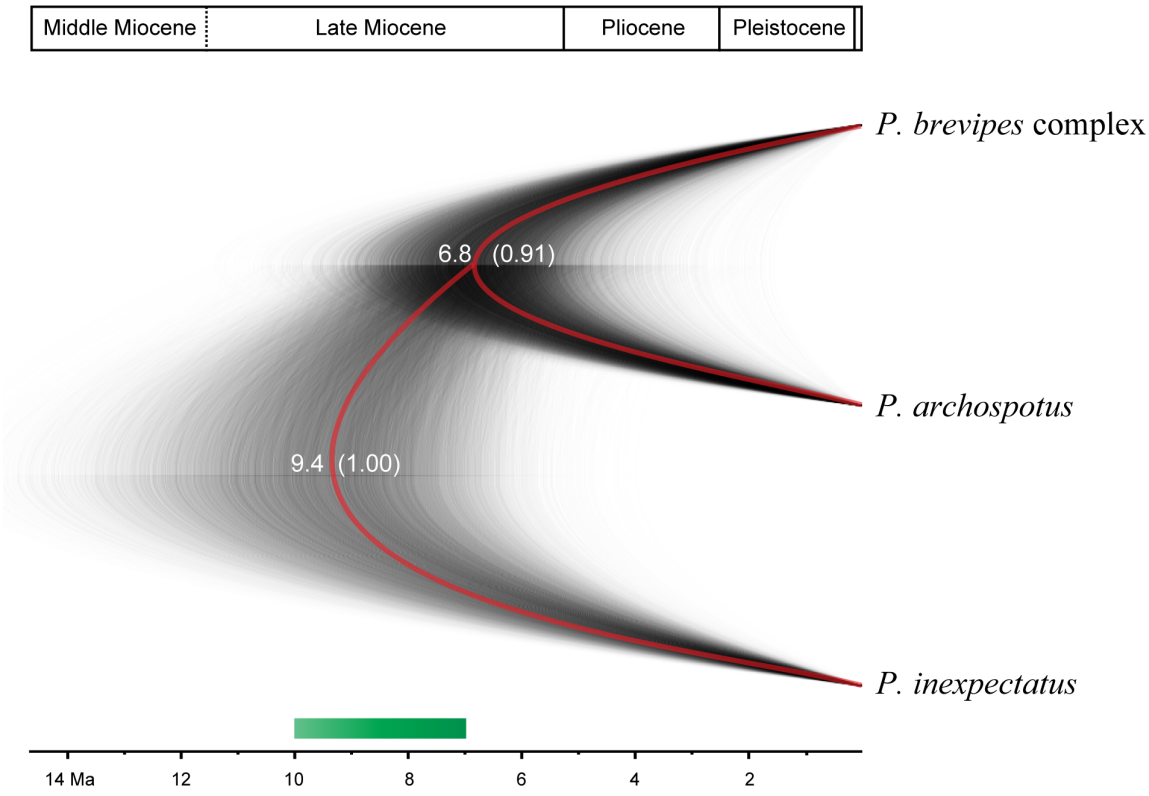

Figure 3-3. Species tree of *Pachytriton* inferred from two nuclear and two mitochondrial loci. This topology is supported by 90.9% of the 75,000 total post-burn-in MCMC trees, each of which is displayed by a thin black line. The consensus tree is shown in red. Nodes are marked by divergence times with Bayesian posterior probabilities of branch support in parentheses. The green horizontal bar indicates the start of substantial Asian summer monsoon intensification.

Figure 3-4. (a) Left: schematic depiction of the temperature buffer zone on a mountain, with a salamander species' distribution shaded orange. Right: conservative (red bar) and more liberal (red bar plus the whisker) estimates of the temperature buffer zone inferred from known collecting localities and absence points. (b) Temperature buffer zones estimated for 24 populations of *Pachytriton*. The horizontal axis corresponds to sampling sites (populations): *P. inexpectatus* light green, *P. archospotus* orange, *P. xanthospilos* brown, *P. brevipes* blue, *P. feii* purple, and *P. granulosus* red. Lowest distributions are known for sites 8 and 10 (Xu *et al.* 2002; Shen *et al.* 2008), so their bars represent the actual buffer zones. T, type locality. Dashed lines represent the 2–5 °C increment of global temperature in the Pliocene. If the buffer zone does not or only slightly exceeds this increment, *Pachytriton* at this local area could have declined or even been extirpated during the Pliocene warming period.

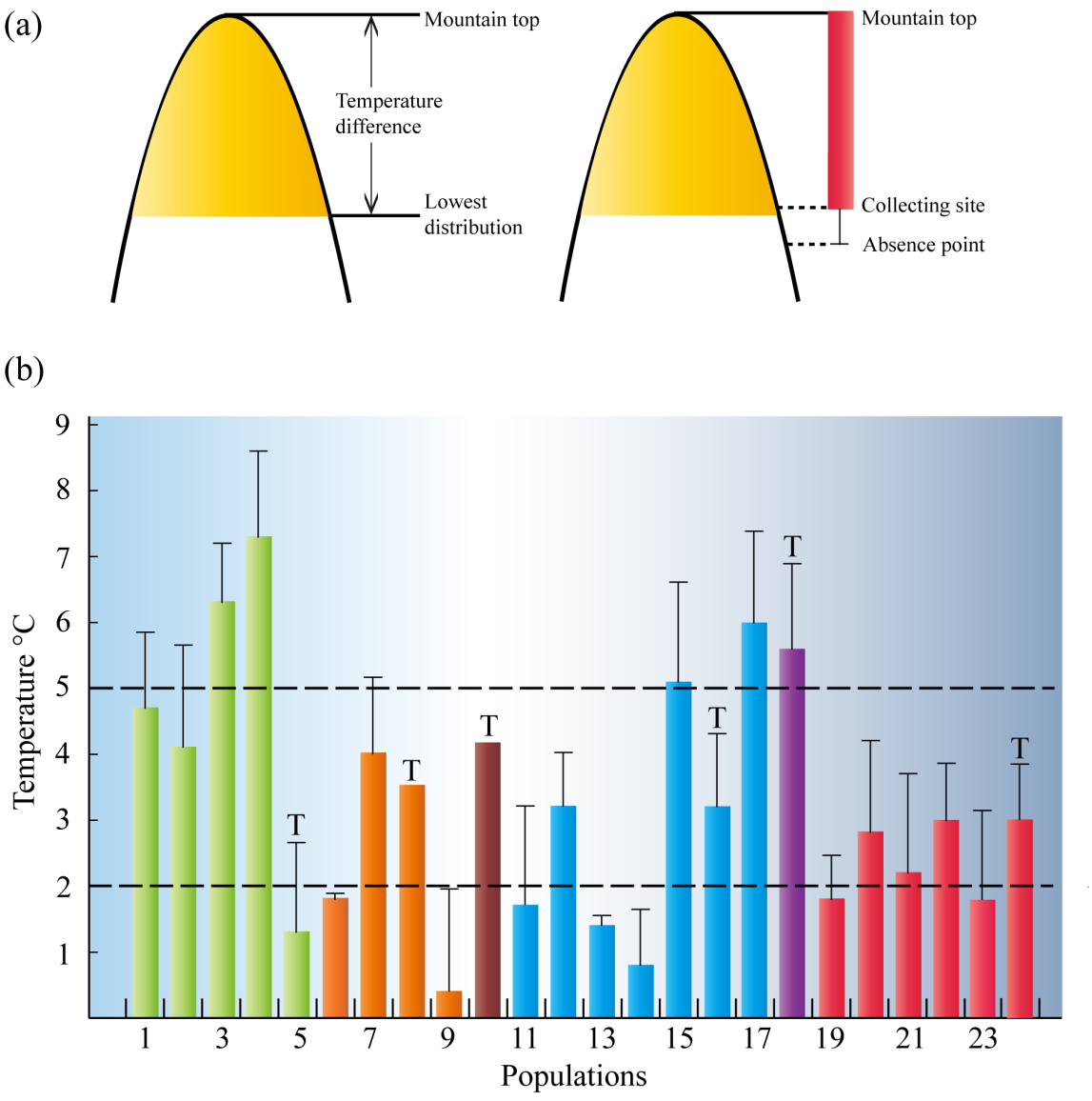

Figure 3-4 (continued)

using mean annual temperatures (Novacek 1999; Ravelo *et al.* 2004; Salzmann *et al.* 2011), I focus on temperature buffer zones derived from AMT. The other six temperature variables yield a very similar trend of variation (Fig. 3-5). When collecting localities are treated as the lowest elevational limits, buffer zones of eight populations are below the 2-degree threshold, which is likely the minimal global temperature increase in the Pliocene. These populations were physiologically stressed and likely declined during the warming period. When temperature buffer zones are calculated more liberally by inferring the lowest elevational limits from absence localities, two thirds of the populations still have buffer zones narrower than 5 °C. Buffer zones derived from temperature variables measuring winter conditions (the coldest and driest times) all infer a more severe and widespread decline compared to estimates from AMT, whereas those derived from measurements of summer conditions (the warmest and wettest times) show less stress. Regardless of which temperature variable is used, conservative estimates, which are closer to true values than liberal estimates, reveal that none of the mountains sampled from the known distribution of *P. archospotus* and *P. granulosus* provides adequate temperature buffer zones. Similarly, *P. xanthospilos* from the eastern Nanling Mountain Range and *P. brevipes* from the middle-to-southern portion of the Wuyi Mountain Range are at high risk. Except for *P. feii*, all species from their respective type localities could be threatened by global warming. On the other hand, I identify several high mountains that are capable of buffering large temperature changes. These include Xuefengshan (site 3) and Mao'ershan (site 4) for *P. inexpectatus*, Tiangongshan (site 15) and Wuyishan (site 17, at the northern end of the Wuyi Mountain Range) for *P. brevipes*, and Huangshan (site 18) for *P. feii.*

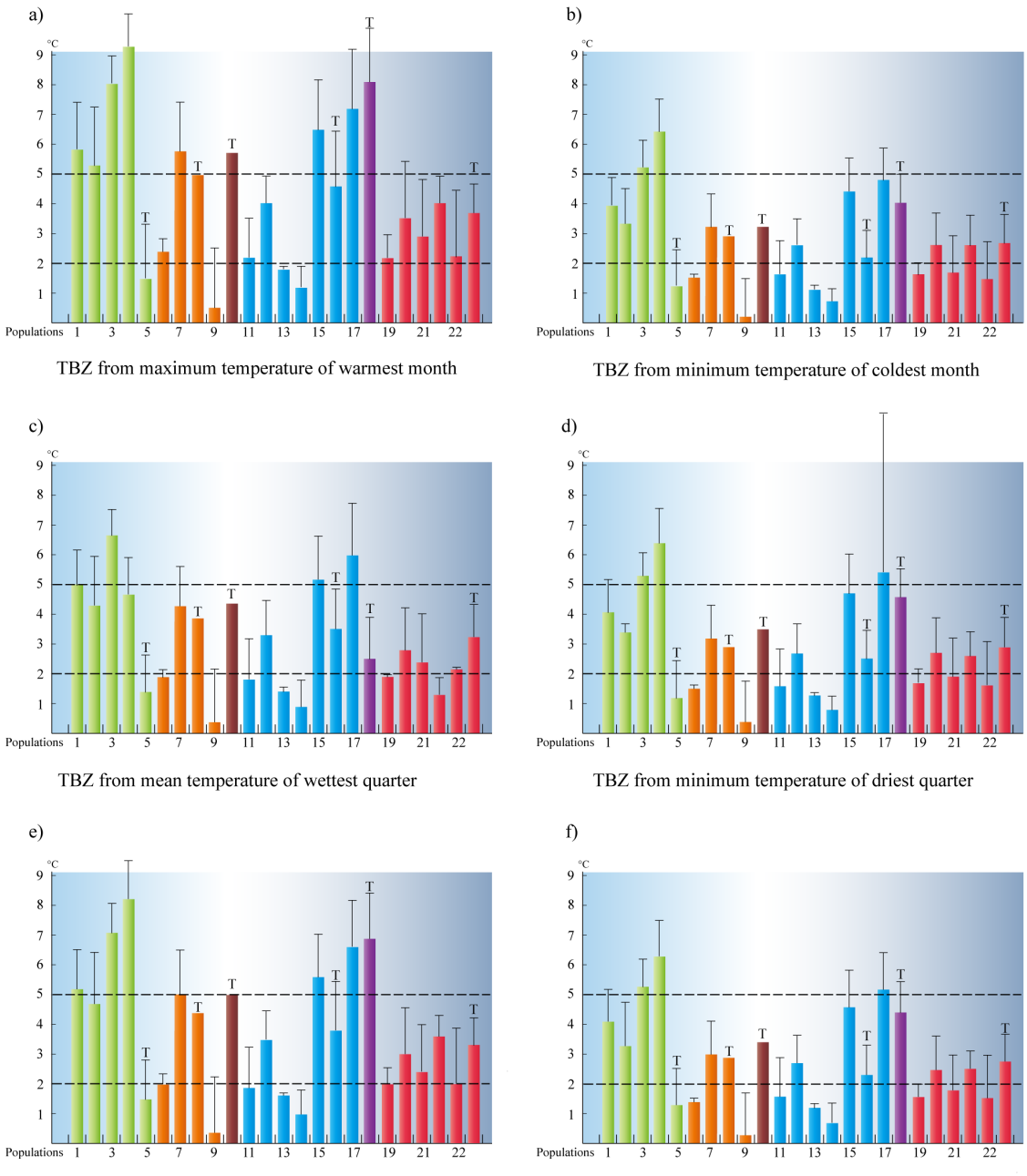

Figure 3-5. Temperature buffer zones estimated based on summer and winter conditions.

Historical demography

The coalescent-based EBSPs reveal distinct demographic history among species (Fig. 3-6). *Pachytriton inexpectatus* and *P. brevipes* share a gradual demographic growth from 5 Ma until 1 Ma, when population size started to decrease rapidly. In contrast, population sizes of *P. archospotus* and *P. granulosus* remained low from 5 to 3 Ma. Weak growth occurred in *P. archospotus* after 2 Ma and in *P. granulosus* after 3 Ma. Non-genealogical summary statistics, including Tajima's D and Fu and Li's D*, fail to reject the null model of a stable population demography for all four species (Table 3-2). However, compared to EBSPs, which directly quantify demography from gene genealogies (Ho & Shapiro 2011), these summary statistics do not take tree structure into account and thus are not based on all available information (Pybus *et al.* 2000).

Tempo of diversification

Because the species tree did not resolve relationships within the *P. brevipes* complex, I performed the CR test on the fully resolved mtDNA chronogram, which is co-estimated with the species tree and pruned to leave one individual per species. The gamma statistic ($\gamma = -1.662807$) significantly rejects the null model of a constant diversification rate in favor of a deceleration in the accumulation of lineages in *Pachytriton*. When assuming a total of 10 or 20 extant species in the genus (i.e., 4 or 14 species more than I included; the latter of which is unlikely given my extensive sampling), the observed γ value is still significantly smaller than the null distribution generated by Monte Carlo simulations assuming a constant rate ($P = 0.039$ and $P = 0.049$, respectively). This confirms that the slowdown of the rate of lineage accumulation is not an artifact.

Table 3-2. Fu and Li's D* and Tajima's D for four species of *Pachytriton*.

Taxa	Locus	Fu and Li's D*	Tajima's D
	mtDNA	-0.24950	-0.46840
Pachytiton archospotus	*RAG-1*	-0.02396	-0.43027
	NCRT	1.02623	1.33722
	mtDNA	1.48629	0.38235
Pachytriton brevipes	*RAG-1*	-0.52690	-0.11272
	NCRT	0.33154	-0.17682
	mtDNA	1.10411	0.68887
Pachytriton granulosus	*RAG-1*	-0.43062	-0.35603
	NCRT	-1.87275	-1.49051
	mtDNA	1.35641	0.62504
Pachytriton inexpectatus	*RAG-1*	-0.49800	-0.98497
	NCRT	-0.18788	0.28029

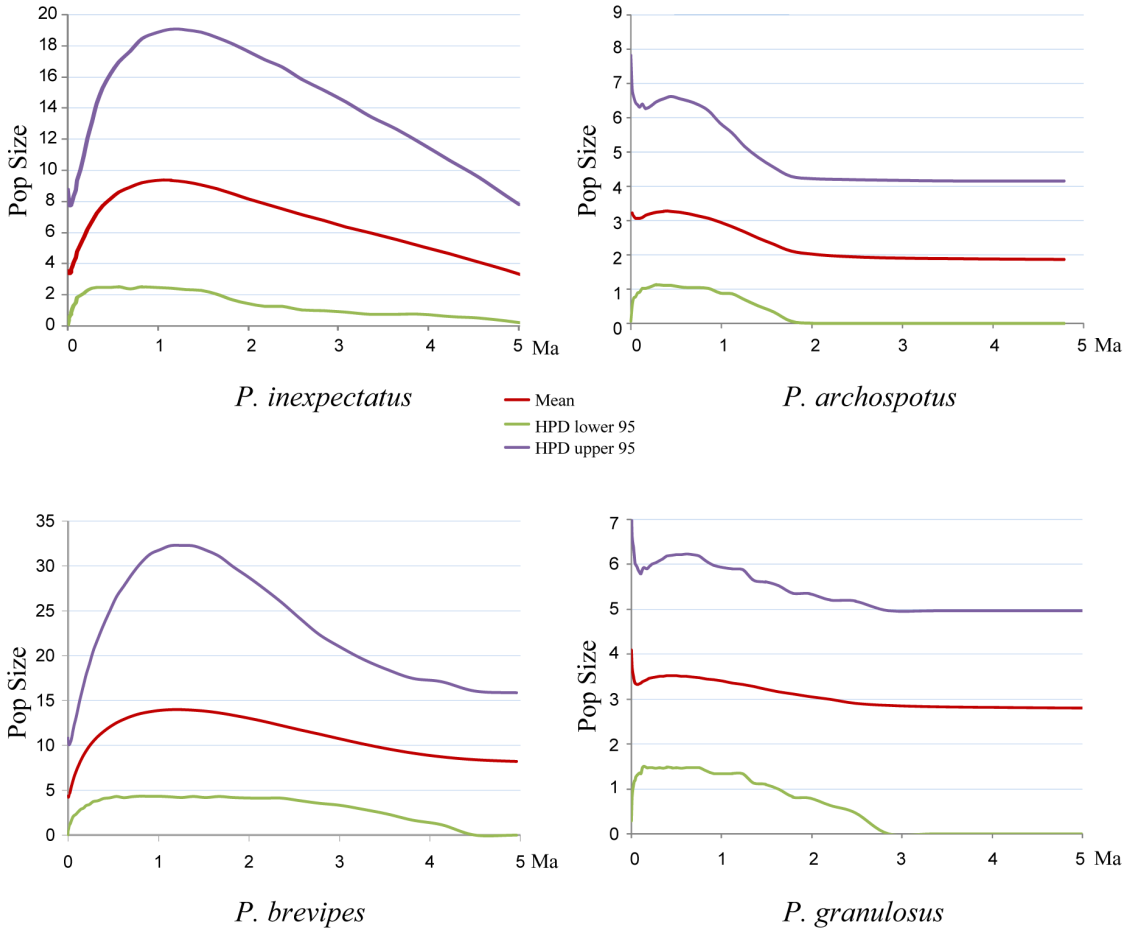

Figure 3-6. Extended Bayesian Skyline Plots (EBSPs) showing demographic dynamics through geologic time. The central red line measures the mean value of the product of effective population size and generation time in millions of years ($N_e \times \tau$); the upper blue line and lower green line represent the 95% HPD.

Discussion

Analyses of conspecific populations may reveal significant geographic structure and variation within a species, whereas interspecific comparisons advance understanding of historical processes that generate regional biodiversity (Bermingham & Moritz 1998). My study provides a unique perspective from which to analyze the significance of pre-Quaternary climate change for East Asian organisms by incorporating both population-level and species-level components. The results suggest a potentially critical role of monsoon activity and global warming in shaping the genetic diversity and distributional pattern in *Pachytriton*.

Summer monsoon and initial speciation in Pachytriton

Onset and intensification of Asian monsoons has been one of the most important factors in global climatic change since the middle Miocene (Clemens *et al.* 1996; Ravelo *et al.* 2004). However, the likely impact on organismal diversity has rarely been assessed in a phylogenetic context. The multi-locus coalescent model indicates that all three major lineages of *Pachytriton* originated well before the Quaternary glacial period, and initial speciation occurred around a critical period in the development of the East Asian monsoon system. These divergence times are reasonable because the mitochondrial substitution rate, which is co-estimated with the species tree, is very similar to rates of *ND2* or *cytb* in other salamanders and frogs (Weisrock *et al.* 2001; Crawford 2003; Mueller 2006). When summer monsoons underwent substantial intensification, precipitation increased due to strengthened circulation (An *et al.* 2006). This climatic shift is regarded as an environmental response to the rapid uplift of much of the Tibetan

Plateau as it approached its present elevation during the same time period (Harrison *et al.* 1992; An *et al.* 2001). In southern China, the summer monsoon begins in May, peaks in June and extends to late August (Qiang & Yang 2008). The monsoon season corresponds to the breeding season of *Pachytriton* (Fei *et al.* 2006). Rainfall increases dramatically compared to the non-monsoon period and accounts for most of the annual precipitation (Qiang & Yang 2008). Downpours are especially prevalent in mountainous regions, flooding streams that *Pachytriton* inhabit. Overflows form temporary waterways that connect neighboring stream systems, thereby providing opportunities for aquatic organisms such as *Pachytriton* to disperse across otherwise separated habitats that are hundreds of meters apart. After summer monsoonal rains, I have found salamanders in temporary waterways caused by stream flooding as well as in small catchments fed by overflows (unpublished personal observations). This after-rain dispersal mechanism has been proposed for North American aquatic salamanders after lab experiments, which demonstrate much higher dispersal ability when salamanders are submerged in water compared to when they are exposed on dry land (Schalk & Luhring 2010).

Given that contemporary species distributions are generally non-overlapping in *Pachytriton*, speciation most likely occurred in allopatry, which is the predominant mode of animal diversification (Mayr 1963; Barraclough & Vogler 2000). Recent studies reveal that range expansion associated with subsequent vicariance may accelerate speciation rate (Moyle *et al.* 2009; Van Bocxlaer *et al.* 2010). Yet, direct factors that reduce gene flow within formerly continuous populations vary among regions and taxa. It is possible that weakening of the summer monsoon led to vicariant isolation in *Pachytriton*. The strength of summer monsoonal circulation exhibits considerable variability and cyclicity over both

short and long terms, from tens to thousands of years (An *et al.* 2001; Cosford *et al.* 2008). When the summer monsoon enters its weakened stage, connectivity among streams is lost due to the lack of stream flooding. Without sufficient gene flow to maintain a common gene pool, populations undergo differentiation and eventually speciation.

On the other hand, colonization of unoccupied streams could promote local adaptation within new habitats, which may facilitate phenotypic diversification and ultimately speciation. One potential example in *Pachytriton* is evolution of the unusual hyobranchial skeleton in *P. archospotus*. Ceratobranchial bones in this species are greatly enlarged, which causes a reconfiguration of the posterior hyobranchial skeleton (Wu *et al.* 2012a). The epibranchial bones are straight and rod-like in *P. archospotus* but strongly bowed and dorsolaterally flared in other species (Shen *et al.* 2008). The medial epibranchial flange, a feature unique to *Pachytriton* among salamandrids (Özeti & Wake 1969), also is absent from *P. archospotus* (Wu *et al.* 2012a). Given the inferred species tree, these characters of *P. archospotus* are likely autapomorphies. The hyobranchial skeleton of *Pachytriton* is specialized for underwater suction feeding (Özeti & Wake 1969). Reconfiguration of the skeleton in *P. archospotus* implies a modified feeding habit in this species, which in turn may reflect novel prey availability (Bouton *et al.* 1999).

Global warming and temperature buffer zones

Modeling *Pachytriton*'s response to a warming climate predicts that many extant populations are at high risk for future decline if environmental temperature should again rise to levels seen in the Pliocene. Populations that occur in mountains of low elevations

and are not heat-tolerant are the most likely to be stressed. Furthermore, the model assumes that over time salamander populations retreat to the very top of the mountain to escape environmental warming. In reality, stringent habitat requirements often preclude *Pachytriton* from occupying mountain tops where suitable streams and broadleaf-forest are absent. The actual sizes of buffer zones thus are equal to or smaller than my predictions, indicating an even more severe impact. The eastern Nanling Mountain Range and the middle-to-southern portion of the Wuyi Mountain Range, which generally do not exceed 1300 m in elevation, may not provide sufficiently cool habitat for *Pachytriton* as global temperatures rise. Even high mountains may not offer refuge. If salamanders that occur on high mountains are found only at high elevations, the resulting temperature buffer zone is still narrow. This phenomenon occurs in those populations for which a small conservative estimate is associated with a large liberal estimate (e.g., Fig. 3-4, sites 9 and 21). For *P. archospotus* and *P. granulosus*, the highest mountains within their geographic range reach 2000 m above sea level, but corresponding collecting sites are over 1000 m. Because all high mountains have been sampled for these two species, it is unlikely that any large temperature buffer zone remains to be discovered. *Pachytriton xanthospilos* also lacks a large buffer zone at its type locality, but the western Nanling Mountains remain to be surveyed adequately.

I identify several mountains capable of buffering large temperature increases for populations of *P. inexpectatus*, *P. brevipes* and *P. feii* that occur there. Among those mountains, Huangshan (site 18), the type locality of *P. feii*, is located at the lower reaches of the Yangtze River, a region that has been proposed as a Pleistocene refugium for eastern Asian conifers, frogs and non-migratory birds based on patterns of intraspecific

genetic variation (Gao *et al.* 2007; Zhang *et al.* 2008a; Li *et al.* 2009). Huangshan is characterized by a heterogeneous topography with numerous high peaks interspersed among low valleys, where refugia may have been abundant and supported habitats with relatively stable microclimates when the global climate underwent major changes (Qian & Ricklefs 2000; Li *et al.* 2009; Song *et al.* 2009). Moreover, nucleotide diversity is highest in the Huangshan population of the Chinese giant salamander and the sharp-snouted pitviper (Murphy *et al.* 2000; Huang *et al.* 2007), which further suggests preservation of old gene lineages in this region. Huangshan may have served as a refugium for eastern Asian species during both warming and cooling periods over geologic time.

The novel buffer-zone modeling approach provides a unique opportunity to understand the temperature constraints of *Pachytriton* populations and their possible response to climatic change in the absence of physiological data. This approach is particularly useful when there is very limited occurrence data (even as few as one observation per locality). By combining knowledge of geographic distribution with the global climate database, I establish a mountain-based model that can be projected back to the Pliocene warming period. This model intuitively identifies locations that are potential climatic refugia. Most importantly, my approach can incorporate future climatic models to reveal the association between global warming and worldwide amphibian declines. Particularly, precipitation-related variables should be incorporated along with temperature to derive more accurate projections. According to the Fourth Assessment Report of the Intergovernmental Panel on Climate Change, global temperature is likely to rise 1.1–6.4 °C by the year 2100 relative to 1980 levels if greenhouse gas emissions are

not reduced (IPCC 2007). *Pachytriton*, as well as other cold-adapted montane amphibians, may be forced to higher and higher elevations and ultimately vanish in some locations. Species with elevational ranges but essentially no latitudinal or longitudinal ranges are at highest risk of extinction (Wake 2012).

My model can be made more precise by incorporation of finer-scale climatic and elevational data. The resolution of data currently available (30 arc-seconds, ~1 km^2) is still coarse for analyses that involve temperature gradients on mountains. I also assume species-climate equilibrium by treating absence localities as unsuitable habitats and predictors of maximum temperature tolerance (Nogués-Bravo 2009). Instead of using a correlative model, implementation of mechanistic niche models may differentiate the relative roles of physiological tolerance and biotic constraints (interspecific competition, predation and anthropogenic activity) in determining a population's lowest distribution (Gifford & Kozak 2012). Using actual water temperature instead of air temperature may also improve model precision. However, a large number of samples (24 populations in my analysis) help to reduce noise and to reveal shared trends among populations and species.

Molecular evidence for Pliocene warming

Phylogenetic analyses based on DNA sequences are consistent with the buffer-zone model regarding a detrimental impact of Pliocene warming on *Pachytriton*. The CR and MCCR tests significantly reject a model of constant diversification rate over time and suggest a slowdown of lineage accumulation in the genus. My conclusion is not affected by incomplete taxon sampling at the species level. Furthermore, although the mtDNA

chronogram indicates that both *P. archospotus* and *P. granulosus* may extend back as early as the late Miocene, lineage accumulation within these two species occurred only after the end of the warming period. In contrast, I find much earlier intraspecific divergences in *P. brevipes*, which is younger than both *P. archospotus* and *P. granulosus*. The contrasting coalescent patterns are congruent with the hypothesis that extinction terminated early branches and that all surviving populations have a recent origin (Harvey & Rambaut 1998). Consistently, large-temperature buffer zones are identified for *P. brevipes* but not for *P. archospotus* or *P. granulosus*. This result is not an artifact of including only slightly genetically differentiated populations from the latter two species. Instead, all localities were chosen without *a priori* knowledge of their genetic affinity and are evenly distributed across the corresponding geographic range. Due to limited availability of samples of *P. feii* and *P. xanthospilos* (one population each), it is unclear whether the pattern of early origin contrasting with recent divergence occurs in either species. The EBSPs indicate that demographic growth occurred in *P. archospotus* and *P. granulosus* only after the warming period, whereas *P. brevipes* and P. *inexpectatus* continuously increased in population size from 5 Ma until 1 Ma. Multiple climatic refugia identified for *P. brevipes* and *P. inexpectatus* (e.g., Mao'ershan, Xuefengshan, Wuyishan, and Tiangongshan) may account for the overall population growth, even though some local populations with narrow buffer zones may have declined.

Conclusions

Molecular phylogenetic analyses that incorporate two nuclear and two mitochondrial DNA sequences, combined with climatic and geographic data, highlight the potential

significance of historical monsoonal activities in promoting speciation in aquatic salamanders through range expansion followed by vicariance. Comparative phylogeographic analyses can test whether the same processes have affected other East Asian montane organisms with stringent water requirements. Evaluation of the impact of Pliocene warming by estimating temperature buffer zones represents an effective approach that can be applied to other studies of how environmental changes, including those that involve temperature or precipitation, affect montane species, both in the past and in the future. Such studies serve a pivotal conservation purpose in light of the threat posed by future global temperature change to a majority of the world's species (Hansen *et al.* 2006), and especially montane amphibians (Stuart *et al.* 2004; Wake & Vredenburg 2008; Rovito *et al.* 2009; Wake 2009; Wake 2012).

References

An Z, Kutzbach JE, Prell WL, Porter SC (2001) Evolution of Asian monsoons and phased uplift of the Himalayan Tibetan plateau since Late Miocene times. Nature, 411, 62–66.

An Z, Zhang P, Wang E, Wang S, Qiang X, Li L, Song Y, Chang H, Liu X, Zhou W, Liu W, Cao J, Li X, She J, Liu Y, Ai L (2006) Changes of the monsoon-arid environment in China and growth of the Tibetan Plateau since the Miocene. Quaternary Sciences, 26, 678–693.

Barraclough TG, Vogler AP (2000) Detecting the geographical pattern of speciation from species-level phylogenies. The American Naturalist, 155, 419–434.

Bermingham E, Moritz C (1998) Comparative phylogeography: concepts and applications. Molecular Ecology, 7, 367–369.

Bernardo J, Spotila JR (2006) Physiological constraints on organismal response to global

warming: mechanistic insights from clinally varying populations and implications for assessing endangerment. Biology Letters, 2, 135–139.

Bouckaert RR (2010) DensiTree: making sense of sets of phylogenetic trees. Bioinformatics, 26, 1372–1373.

Bouton N, Witte F, Van Alphen JJM, Schenk A, Seehausen O (1999) Local adaptations in populations of rock-dwelling haplochromines (Pisces: Cichlidae) from southern Lake Victoria. Proceedings of the Royal Society of London B, 266, 355–360.

Buckley LB, Jetz W (2007) Environmental and historical constraints on global patterns of amphibian richness. Proceedings of the Royal Society B: Biological Sciences, 274, 1167–1173.

Cerling TE, Harris JM, MacFadden BJ, Leakey MG, Quade J, Eisenmann V, Ehleringer JR (1997) Global vegetation change through the Miocene/Pliocene boundary. Nature, 389, 153–158.

Clemens SC, Murray DW, Prell WL (1996) Nonstationary phase of the Plio-Pleistocene Asian monsoon. Science, 274, 943–948.

Cosford J, Qing H, Eglington B, Mattey D, Yuan D, Zhang M, Cheng H (2008) East Asian monsoon variability since the Mid-Holocene recorded in a high-resolution, absolute-dated aragonite speleothem from eastern China. Earth and Planetary Science Letters, 275, 296–307.

Crawford AJ (2003) Huge populations and old species of Costa Rican and Panamanian dirt frogs inferred from mitochondrial and nuclear gene sequences. Molecular Ecology, 12, 2525–2540.

Cusimano N, Renner SS (2010) Slowdowns in diversification rates from real phylogenies may not be real. Systematic Biology, 59, 458–464.

Dasmahapatra KK, Lamas G, Simpson F, Mallet J (2010) The anatomy of a 'suture zone' in Amazonian butterflies: a coalescent-based test for vicariant geographic divergence and speciation. Molecular Ecology, 19, 4283–4301.

Drummond AJ, Ho SYW, Phillips MJ, Rambaut A (2006) Relaxed phylogenetics and dating with confidence. PLoS Biology, 4, e88.

Drummond AJ, Rambaut A (2007) BEAST: Bayesian evolutionary analysis by sampling trees. BMC Evolutionary Biology, 7, 214.

Edwards SV, Beerli P (2000) Perspective: gene divergence, population divergence, and the variance in coalescence time in phylogeographic studies. Evolution, 54, 1839–1854.

Espregueira Themudo G, Babik W, Arntzen JW (2009) A combination of techniques proves useful in the development of nuclear markers in the newt genus *Triturus*. Molecular Ecology Notes, 9, 1060–1162.

Fei L, Hu S, Ye C, Huang Y (2006) Fauna Sinica, Amphibia Vol. 1. Science Press, Beijing.

Fu YX, Li WH (1993) Statistical tests of neutrality of mutations. Genetics, 133, 693–709.

Gao LM, Möller M, Zhang X-M, Hollingsworth ML, Liu J, Mill RR, Gibby M, Li D-Z (2007) High variation and strong phylogeographic pattern among cpDNA haplotypes in *Taxus wallichiana* (Taxaceae) in China and North Vietnam. Molecular Ecology, 16, 4684–4698.

Gifford ME, Kozak KH (2011) Islands in the sky or squeezed at the top? Ecological causes of elevational range limits in montane salamanders. Ecography, 35, 193–203.

Guo F (1998) Meso-Cenozoic Nanhua (South China) orogenic belt: subaerial tridirectional orogeny. Acta Geologica Sinica, 72, 22–33.

Hansen J, Sato M, Ruedy R, Lo K, Lea DW, Medina-Elizade M (2006) Global temperature change. Proceedings of the National Academy of Sciences of the United States of America, 103, 14288–14293.

Harris N (2006) The elevation history of the Tibetan Plateau and its implications for the Asian monsoon. Palaeogeography, Palaeoclimatology, Palaeoecology, 241, 4–15.

Harrison TM, Copeland P, Kidd WSF, Yin A (1992) Raising Tibet. Science, 255, 1663–1670.

Harvey PH, Rambaut A (1998) Phylogenetic extinction rates and comparative methodology. Proceedings of the Royal Society B: Biological Sciences, 265, 1691–1696.

Heled J, Drummond AJ (2008) Bayesian inference of population size history from multiple loci. BMC Evolutionary Biology, 8, 289.

Heled J, Drummond AJ (2010) Bayesian inference of species trees from multilocus data. Molecular Biology and Evolution, 27, 570–580.

Hewitt G (2000) The genetic legacy of the Quaternary ice ages. Nature, 405, 907–913.

Hijmans RJ, Cameron SE, Parra JL, Jones PG, Jarvis A (2005) Very high resolution interpolated climate surfaces for global land areas. International Journal of Climatology, 25, 1965–1978.

Ho SYW, Shapiro B (2011) Skyline-plot methods for estimating demographic history from nucleotide sequences. Molecular Ecology Resources, 11, 423–434.

Huang S, He S, Peng Z, Zhao K, Zhao E (2007) Molecular phylogeography of endangered sharp-snouted pitviper (*Deinagkistrodon acutus*; Reptilia, Viperidae) in Mainland China. Molecular Phylogenetics and Evolution, 44, 942–952.

Huelsenbeck JP, Ronquist F (2001) MRBAYES: Bayesian inference of phylogenetic trees. Bioinformatics 17, 754–755.

IPCC (2007) Climate Change 2007: The Physical Science Basis. Contribution of Working Group I to the Fourth Assessment. Report of the Intergovernmental Panel on Climate Change. In: Solomon, S., Qin, D., Manning, M., Chen, Z., Marquis, M., Averyt, K.B., Tignor M., Miller H.L. (Eds.), Report of the Intergovernmental Panel on Climate Change. Cambridge University Press, Cambridge and New York.

Jia GD, Peng PA, Zhao QH, Jian ZM (2003) Changes in terrestrial ecosystem since 30 Ma in East Asia: stable isotope evidence from black carbon in the South China Sea. Geology, 31, 1093–1096.

Kozak KH, Graham CH, Wiens JJ (2008) Integrating GIS-based environmental data into evolutionary biology. Trends in Ecology and Evolution, 23, 141–148.

Kozak KH, Weisrock DW, Larson A (2006) Rapid lineage accumulation in a non-adaptive radiation: phylogenetic analysis of diversification rates in eastern North American woodland salamanders (Plethodontidae: *Plethodon*). Proceedings of the Royal Society B: Biological Sciences, 273, 539–546.

Li J, Shu Q, Zhou S, Zhao Z, Zhang J (2004) Review and prospects of Quaternary glaciation research in China. Journal of Glaciology and Geocryology, 26, 235–243.

Li SH, Yeung CKL, Feinstein J, Han LX, Manh HL, Wang CX, Ding P (2009) Sailing through the Late Pleistocene: unusual historical demography of an East Asian endemic, the Chinese Hwamei (*Leucodioptron canorum canorum*), during the last glacial period. Molecular Ecology, 18, 622–633.

Librado P, Rozas J (2009) DnaSP v5: A software for comprehensive analysis of DNA polymorphism data. Bioinformatics, 25, 1451–1452.

Lo Presti RM, Oberprieler C (2009) Evolutionary history, biogeography and eco-climatological differentiation of the genus *Anthemis* L. (Compositae, Anthemideae) in the circum-Mediterranean area. Journal of Biogeography, 36, 1313–1332.

Mayr E (1963) Animal Species and Evolution. Cambridge, MA: Harvard University Press.

Milanovich JR, Peterman WE, Nibbelink NP, Maerz JC (2010) Projected loss of a salamander diversity hotspot as a consequence of projected global climate change. PLoS One, 5, e12189.

Miralles A, Carranza S (2010) Systematics and biogeography of the neotropical genus *Mabuya*, with special emphasis on the Amazonian skink *Mabuya nigropunctata*

(Reptilia, Scincidae). Molecular Phylogenetics and Evolution, 54, 857–869.

Moyle RG, Filardi CE, Smith CE, Diamond J (2009) Explosive Pleistocene diversification and hemispheric expansion of a great speciator. Proceedings of the National Academy of Sciences of the United States of America, 106, 1863–1868.

Mueller RL (2006) Evolutionary rates, divergence dates, and the performance of mitochondrial genes in Bayesian phylogenetic analysis. Systematic Biology, 55, 289–300.

Murphy RW, Fu JZ, Upton DE, De Lema T, Zhao EM (2000) Genetic variability among endangered Chinese giant salamanders, *Andrias davidianus*. Molecular Ecology, 9, 1539–1547.

Nishikawa K, Jiang JP, Matsui M (2011) Two new species of *Pachytriton* from Anhui and Guangxi, China (Amphibia: Urodela: Salamandridae). Current Herpetology, 30, 15–31.

Nogués-Bravo D (2009) Predicting the past distribution of species climatic niches. Global Ecology and Biogeography, 18, 521–553.

Novacek MJ (1999) 100 million years of land vertebrate evolution: the Cretaceous-Early Tertiary transition. Annals of the Missouri Botanical Garden, 86, 230–258.

Nylander JAA (2004) MrModeltest v2. Program distributed by the author. Evolutionary Biology Centre, Uppsala University. Available from http://www.abc.se/~nylander/ (Accessed June 20 2012)

Özeti N, Wake DB (1969) The morphology and evolution of the tongue and associated structures in salamanders and newts (Family Salamandridae). Copeia, 1969, 91–123.

Pamilo P, Nei M (1988) Relationships between gene trees and species trees. Molecular Biology and Evolution, 5, 568–583.

Patel S, Weckstein JD, Patane JSL, Bates JM, Aleixo A (2011) Temporal and spatial diversification of *Pteroglossus aracaris* (AVES: Ramphastidae) in the neotropics:

constant rate of diversification does not support an increase in radiation during the Pleistocene. Molecular Phylogenetics and Evolution, 58, 105–115.

Pounds JA, Bustamante MR, Coloma LA, Consuegra JA, Fogden MPL, Foster PN, La Marca E, Masters KL, Merino-Viteri A, Puschendorf R, Ron SR, Sanchez-Azofeifa GA, Still CJ, Young BE (2006) Widespread amphibian extinctions from epidemic disease driven by global warming. Nature, 439, 161–167.

Pybus OG, Harvey PH (2000) Testing macro-evolutionary models using incomplete molecular phylogenies. Proceedings of the Royal Society B: Biological Sciences, 267, 2267–2272.

Pybus OG, Rambaut A, Harvey PH (2000) An integrated framework for the inference of viral population history from reconstructed genealogies. Genetics, 155, 1429–1437.

Qian H, Ricklefs RE (2000) Large-scale processes and the Asian bias in species diversity of temperate plants. Nature, 407, 180–182.

Qiang XM, Yang XQ (2008) Onset and end of the first rainy season in south China. Chinese Journal of Geophysics, 51, 1333–1345.

Rambaut A (1995) Se–Al: sequence alignment program. Oxford University, Oxford, U.K. Available from http://tree.bio.ed.ac.uk/software/seal/ (Accessed June 20 2012)

Rambaut A, Drummond AJ (2007) Tracer v1.4, Available from http://beast.bio.ed.ac.uk/Tracer (Accessed June 20 2012)

Ravelo AC, Andreasen DH, Lyle M, Lyle AO, Wara MW (2004) Regional climate shifts caused by gradual global cooling in the Pliocene epoch. Nature, 429, 263–267.

Roelants K, Gower DJ, Wilkinson M, Loader SP, Biju SD, Guillaume K, Moriau L, Bossuyt F (2007) Global patterns of diversification in the history of modern amphibians. Proceedings of the National Academy of Sciences of the United States of America, 104, 887–892.

Rovito SM, Parra-Olea G, Vasquez-Almazan CR, Papenfuss TJ, Wake DB (2009)

Dramatic declines in neotropical salamander populations are an important part of the global amphibian crisis. Proceedings of the National Academy of Sciences of the United States of America, 106, 3231–3236.

Salzmann U, Haywood AM, Lunt DJ (2009) The past is a guide to the future? Comparing Middle Pliocene vegetation with predicted biome distributions for the twenty-first century. Philosophical Transactions of the Royal Society A: Mathematical, Physical and Engineering Sciences, 367, 189–204.

Salzmann U, Williams M, Haywood AM, Johnson ALA, Kender, S, Zalasiewicz, J (2011) Climate and environment of a Pliocene warm world. Palaeogeography, Palaeoclimatology, Palaeoecology, 309, 1–8.

Schalk CM, Luhring TM (2010) Vagility of aquatic salamanders: implications for wetland connectivity. Journal of Herpetology, 44, 104–109.

Shen Y, Shen D, Mo X (2008) A new species of salamander *Pachytriton archospotus* from Hunan Province, China (Amphibia, Salamandridae). Acta zoologica Sinica, 54, 645–652.

Shepard DB, Burbrink FT (2008) Lineage diversification and historical demography of a sky island salamander, *Plethodon ouachitae*, from the Interior Highlands. Molecular Ecology, 17, 5315–5335.

Song G, Qu YH, Yin ZH, Li SS, Liu NF, Lei FM (2009) Phylogeography of the *Alcippe morrisonia* (Aves: Timaliidae): long population history beyond late Pleistocene glaciations. BMC Evolutionary Biology, 9, 143.

Stamatakis A (2006) RAxML-VI-HPC: maximum likelihood-based phylogenetic analyses with thousands of taxa and mixed models. Bioinformatics, 22, 2688–2690.

Stuart SN, Chanson JS, Cox NA, Young BE, Rodrigues ASL, Fischman DL, Waller RW (2004) Status and trends of amphibian declines and extinctions worldwide. Science, 306, 1783–1786.

Tajima F (1989) The effect of change in population size on DNA polymorphism. Genetics, 105, 437–460.

Titus TA, Larson A (1995) A molecular phylogenetic perspective on the evolutionary radiation of the salamander family Salamandridae. Systematic Biology, 44, 125–151.

Utescher T, Bruch AA, Micheels A, Mosbrugger V, Popova S (2011) Cenozoic climate gradients in Eurasia—a palaeo-perspective on future climate change? Palaeogeography, Palaeoclimatology, Palaeoecology, 304, 351–358.

Van Bocxlaer I, Loader SP, Roelants K, Biju SD, Menegon M, Bossuyt F (2010) Gradual adaptation toward a range-expansion phenotype initiated the global radiation of toads. Science, 327, 679-682.

Vieites DR, Min MS, Wake DB (2007) Rapid diversification and dispersal during periods of global warming by plethodontid salamanders. Proceedings of the National Academy of Sciences of the United States of America, 104, 19903–19907.

Vieites DR, Nieto-Roman S, Wake DB (2009) Reconstruction of the climate envelopes of salamanders and their evolution through time. Proceedings of the National Academy of Sciences of the United States of America, 106, 19715–19722.

Wake DB (2009) What salamanders have taught us about evolution. Annual Review of Ecology, Evolution, and Systematics, 40, 333–352.

Wake DB (2012) Facing extinction in real time. Science, 335, 1052–1053.

Wake DB, Vredenburg VT (2008) Are we in the midst of the sixth mass extinction? A view from the world of amphibians. Proceedings of the National Academy of Sciences of the United States of America, 105, 11466–11473.

Weisrock DW, Macey JR, Ugurtas IH, Larson A, Papenfuss TJ (2001) Molecular phylogenetics and historical biogeography among salamandrids of the "true" salamander clade: rapid branching of numerous highly divergent lineages in *Mertensiella luschani* associated with the rise of Anatolia. Molecular Phylogenetics and Evolution, 18, 434–448.

Wu Y, Wang Y, Jiang K, Chen X, Hanken J (2010) Homoplastic evolution of external coloration in Asian stout newts (*Pachytriton*) inferred from molecular phylogeny. Zoologica Scripta, 39, 9–22.

Wu Y, Wang Y, Hanken J (2012a) Comparative osteology of the genus *Pachytriton* (Caudata: Salamandridae) from southeastern China. Asian Herpetological Research, 3, 83–102.

Wu Y, Wang Y, Hanken J (2012b) New species of *Pachytriton* (Caudata: Salamandridae) from the Nanling Mountain Range, southeastern China. Zootaxa, 3388, 1–16.

Xu J, Zou P, Wen C, Li S (2002) Ecological observation on *Pachytriton labiatus* in Nanling nature reserve of north Guangdong. Journal of Shaoguan University (Natural Science), 23, 83–86.

Zachos J, Pagani M, Sloan L, Thomas E, Billups K (2001) Trends, rhythms, and aberrations in global climate 65 Ma to present. Science, 292, 686–693.

Zhang H, Yan J, Zhang GQ, Zhou KY (2008a) Phylogeography and demographic history of Chinese black-spotted frog populations (*Pelophylax nigromaculata*): evidence for independent refugia expansion and secondary contact. BMC Evolutionary Biology, 8, 21.

Zhang P, Papenfuss TJ, Wake MH, Qu L, Wake DB (2008b) Phylogeny and biogeography of the family Salamandridae (Amphibia: Caudata) inferred from complete mitochondrial genomes. Molecular Phylogenetics and Evolution, 49, 586–597.

Zhao X, Zeng L, Zeng J, Lei Y (1994) Ecological study on *Pachytriton labiatus* in Yunshan Forest Park. Journal of Shaoyang College, 7, 147–149.

Zheng Y, Fu J, Li S (2009) Toward understanding the distribution of Laurasian frogs: a test of Savage's biogeographical hypothesis using the genus *Bombina*. Molecular Phylogenetics and Evolution, 52, 70–83.

Chapter 4

One species or four? An integrative perspective on species delimitation and speciation mechanism, with an example from Chinese salamanders

(Salamandridae: *Pachytriton brevipes* complex)

Abstract

Conceptualization of species as independently evolving lineages drives the development of coalescent-based methods that regard species delimitations as hypotheses, which can be tested with statistical rigor using probabilistic models and multi-locus DNA data. Black-spotted stout newts (*Pachytriton brevipes* complex) from montane streams of southeastern China represent an example where species are hard to delimit due to their conserved morphology and highly variable external color patterns. I applied two independent coalescent-based methods to assess evolutionary independence of four species in the complex, which are recognized primary from mitochondrial sequence data. The four-species taxonomy is significantly favored over the single-species taxonomy by two mitochondrial and two nuclear loci. Bayesian cluster and distance-based analyses also support the classification of multiple species, despite a signal of weak interspecific gene flow, which likely contributes to the conflict between the mitochondrial gene tree and species tree. I further statistically compare niches of the four species predicted by ecological niche modeling and multivariate analyses. Because species occupy different latitudes, their niches have undergone differentiation in ecological space. However, these montane salamanders exhibit strong evidence of niche conservatism. Given the non-overlapping geographic distribution among species, speciation most likely occurred through allopatric isolation of lineages that are restricted at high elevations, although I cannot rule out parapatric speciation with ongoing gene flow. My research provides an integrative perspective on species delimitation and study of the speciation mechanism. Coupling the two components yields important insights into species richness and the driving force for such richness in mountains of southeastern China, which harbors high

diversity of amphibians and plants.

Introduction

Species is the fundamental unit of systematic biology and the basis for classifying biological diversity. Until recently, no single definition of species was satisfactory and over 20 species concepts have been proposed (Mayden 1997), each addressing a different aspect of lineage separation (de Queiroz 2007). The lack of a stable species concept can lead to an unstable taxonomy, because depending on which definition is employed, taxonomists determine different boundaries and numbers of species. By extracting the common element of various contemporary species concepts, de Queiroz (1998) conceptualizes species as segments of independently evolving lineages, which refer to time-extended ancestor-descendant series. Those previously used species definition criteria, such as fixed phenotypic difference, intrinsic reproductive isolation or reciprocal phylogenetic monophyly, are now properties of lineages acquired during speciation (de Queiroz 2007). This general lineage species concept, which has gradually gained acceptance in systematic and phylogenetic studies (e.g., Pons *et al.* 2006; Leaché & Fujita 2010; Burbrink *et al.* 2011; Camargo *et al.* 2012), results in a shift in species delimitation from searching for diagnostic characters between lineages to testing the hypothesis of evolutionary independence (Fujita *et al.* 2012).

Allopatric speciation is the predominant mode of animal diversification (Mayr 1963; Barraclough & Vogler 2000). At the same time, species delimitation is most difficult and controversial in allopatric species, especially when morphology is highly conserved, because intrinsic reproductive isolation cannot readily be inferred (Fujita *et al.* 2012). Strong gene flow across geographic barriers suggests a homogeneous entity, and vice versa. By tracing the evolutionary history of alleles, advanced coalescent theory provides

a framework to directly estimate the status of lineage separation and gene flow. Coalescent-based species delimitation is therefore fundamentally distinct from traditional delimitation criteria in that it no longer depends on the interpretation of observed differences in characters (e.g., morphological, molecular, ecological or behavioral), or lack of them, as proxies for evolutionary independence among allopatric species (Fujita *et al.* 2012). Such interpretation can be biased among researchers unless it is quantified. Coalescent-based species delimitation uses multiple unlinked DNA loci and probabilistic models to directly test hypotheses of lineage divergence while allowing for gene tree discordance (Yang & Rannala 2010). Because species delimitation is derived from sequence data and explicit models, the resultant taxonomy is highly replicable and less prone to researcher bias (Fujita *et al.* 2012).

With the advent of analytical techniques associated with geographically explicit ecological niche modeling, there has been a recent focus on the role of ecology in speciation among closely related species (Warren *et al.* 2008; McCormack *et al.* 2010; Wien *et al.* 2010; Burbrink *et al.* 2011; Wooten & Gibbs 2011). Adaptation to different environmental conditions or resources (niche divergence) in geographically separated populations can promote allopatric or parapatric speciation (Kozak *et al.* 2008). Alternatively, niche conservatism, which describes the tendency of species to retain niche-related ecological traits over evolutionary timescales, may also drive geographic isolation of populations intervened by unsuitable areas and eventually lead to speciation (Wiens & Graham 2005; Wien *et al.* 2010). Niche conservatism has been proposed as the driving force for the rapid accumulation of numerous species of North American montane salamanders (Kozak & Wiens 2006; Kozak *et al.* 2006). However, testing for the two

patterns can be problematic (Warren *et al.* 2008; Wien *et al.* 2010). Owing to the strong spatial autocorrelation in climatic variables between regions where species occur, the predicted niches could appear different (even statistically significant) as a consequence of divergence between the two regional climates (Godsoe 2010; McCormack *et al.* 2010). In other words, species may have seemly distinct niches merely because they occupy separate geographic ranges (i.e., environmental backgrounds). But their niches could still be more similar than otherwise expected. Only when niche difference is significantly greater than the background divergence is niche divergence supported between taxa; a significantly smaller niche difference compared to the background divergence indicates niche conservatism (McCormack *et al.* 2010; Wooten & Gibbs 2011).

Southeastern China has a complex topography formed mostly before the middle Eocene (Guo 1998). Its unique climate is tightly associated with the development of the East Asian monsoon system (An *et al.* 2001). The old age of mountains, heterogeneous habitats and highly seasonal climate have generated high regional biodiversity. Phylogeographic analyses recover deep genetic structure in a broad range of organisms that are widely distributed in this area, including conifers, arthropods, fishes, non-migratory birds, and amphibians and reptiles (Murphy *et al.* 2000; Chang *et al.* 2007; Gao *et al.* 2007; Huang *et al.* 2007; Zhang *et al.* 2008; Li *et al.* 2009; Song *et al.* 2009; Lin *et al.* 2012). However, existence of cryptic species has not been tested with the coalescent-based species delimitation method and the driving force for speciation remains unexamined in most groups.

The black-spotted stout newt (*Pachytriton brevipes*) is a medium-sized aquatic salamandrid (total length 15 to 20 cm) that inhabits small montane streams in

southeastern China, primarily in the Nanling Mountains, Wuyi Mountains and coastal mountains of Zhejiang and Fujian provinces. The largest elevational difference between mountaintop and valley approaches 2000 m. The Nanling Mountains and Wuyi Mountains harbor high biological diversity, especially for Chinese amphibians, and are centers of plant endemism (Xie *et al.* 2007; Li *et al.* 2009; López-Pujol *et al.* 2011; Shih *et al.* 2011). Recently, deep phylogenetic divergence were revealed in *P. brevipes* from mitochondrial DNA sequences, which provided the basis to elevate three regional populations to full species, *P. feii*, *P. granulosus* and *P. xanthospilos* (Fig. 4-1; Nishikawa *et al.* 2011a, b; Wu *et al.* 2012). Consequently, *P. brevipes* now refers only to populations mainly distributed in the Wuyi Mountain Range. Species delimitation relying solely or even mainly on mitochondrial data could be problematic, however, because introgression or selection on mitochondrial genome may lead to inconsistency between a gene tree and its corresponding species tree (Ballard & Whitlock 2004; Meiklejohn *et al.* 2007). Although the mitochondrial gene tree strongly supports monophyly of each of the four species (Nishikawa *et al.* 2011a; Wu *et al.* 2012), two independent nuclear loci both identify admixture patterns among haplotypes of the same four species (Wu *et al.* 2013). External morphology is conserved in these salamanders, making species diagnosis difficult without the aid of DNA data. The only characters that exhibit conspicuous variation are dorsal and ventral color patterns, which have repeatedly evolved among populations and species (i.e., homoplasy; Wu *et al.* 2010). I regard the four species (*P. brevipes*, *P. feii*, *P. granulosus*, and *P. xanthospilos*) most appropriately as a species complex, in which traditional species delimitation may lead to disagreements in the taxonomy depending on operational criteria used. In contrast, coalescent-based species

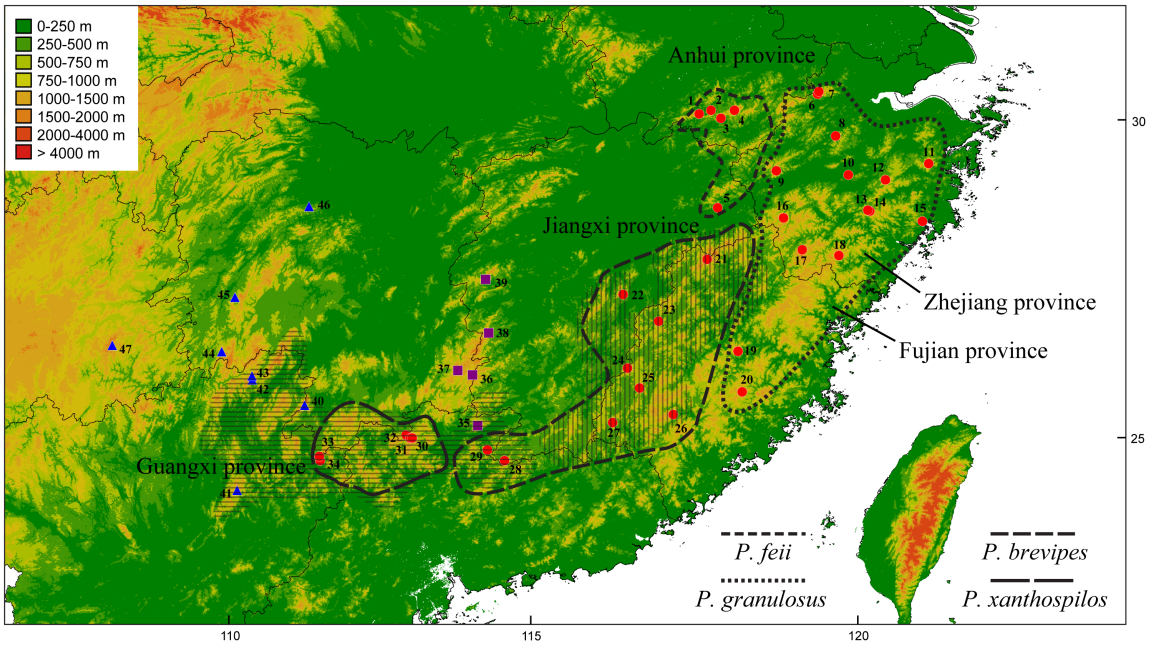

Figure 4-1. Geographic distribution of the genus *Pachytriton* in southeastern China. Red dots are samples of the *P. brevipes* complex: the range of *P. granulosus* is encircled by the shortest dashed line; *P. feii* by the second-shortest dashed line; *P. inexpectatus* by the longest dashed line; and *P. brevipes* by the second-longest dashed line. Purple squares denote *P. archospotus*. Blue triangles denote *P. inexpectatus* and *P. moi*. Numbers next to sampling sites are population IDs (Table 4-1). The Nanling Mountain Range and Wuyi Mountain Range are indicated by horizontal and vertical thin lines, respectively.

Table 4-1. Sampled populations used in the study.

Sampling Locality	Pop ID	Number of speciemens sampled	
		mtDNA dataset	nDNA dataset
Pachytriton feii			
Huangshan, Yixian, Huangshan city, Anhui	1	5	
Chayeshan, Yixian, Huangshan city, Anhui	2	3	
Huangshan, Shitai, Huangshan city, Anhui	3	Only used in ENM	
Huangshan, Jiaochun, Huangshan city, Anhui	4	3	3
Sanqingshan, Shangrao city, Jiangxi	5	5	
Pachytriton granulosus			
Pet market in China		7	
Tianmushan, Zaoxi county, Zhejiang	6	7	3
Longwangshan,Anji county, Zhejiang	7	4	
Baiyunyuan, Tonglu city, Zhejiang	8	2	
Qianligang, Quzhou city, Zhejiang	9	5	
Hutianshan, Jinhua city, Zhejiang	10	6	2
Tiantaishan, Ninghai county, Zhejiang	11	3	3
Dapanshan, Pan'an, Zhejiang	12	6	
Dayangshan, Jiyun county, Zhejiang (by KIZ)	13	Only used in ENM	
Dayangshan, Jiyun county, Zhejiang (by myself)	14	14	
Yandangshan, Leqing city, Zhejiang	15	6	
Jiulongshan, Lishui city, Zhejiang	16	7	
Longquanshan, Longquan city, Zhejiang	17	8	3
Shangshantou, Jingning county, Zhejiang	18	6	
Meixian, Youxi county, Fujian	19	6	3
Daiyunshan, Dehua county, Fujian	20	1	1
Pachytriton brevipes			
Wuyishan, Wuyishan city, Fujian	21	8	3
Junfengshan, Nanfeng county, Jiangxi	22	6	3
Jinraoshan, Jianning county, Fujian	23	4	
Jigongdong, Ninghua county, Fujian	24	8	3
Guanyinshi, Changting county, Fujian	25	8	
Tiangongshan, Longyan city, Fujian	26	8	3
Liangyeshan, Wuping county, Fujian	27	8	3
Jiulianshan, Qunan county, Jiangxi	28	1	
Chebaling, Shixing county, Guangdong	29	6	3
Pachytriton xanthospilos			
Babaoshan, Ruyuan city, Guangdong	30	Only used in ENM	
Mangshan, Yizhang county, Hunan (by KIZ)	31	3	
Mangshan, Yizhang county, Hunan (by myself)	32	6	3

Table 4-1 (continued)

Sampling Locality	Pop ID	Number of speciemens sampled	
		mtDNA dataset	nDNA dataset
Pachytriton xanthospilos			
Guposhan, Hezhou city, Guangxi (by KIZ)	33	3	
Guposhan, Hezhou city, Guangxi (by myself)	34	5	
Pachytriton archospotus			
Guanyindong, Shixing county, Guangdong	35	1	
Qiyunshan, Guidong county, Hunan	36	2	
Bamianshan, Guidong county, Hunan	37	1	
Jianggangshan, Jianggangshan city, Jiangxi	38	1	
Wugongshan, Pingxiang county Jiangxi	39	1	
Pachytriton inexpectatus			
Qianjiadong, Jiangyong county, Hunan	40	1	
Dayaoshan, Jinxiu county Guangxi	41	1	
Mao'ershan, Xin'an county Guangxi	42	2	
Shaping, Taoyuan county, Hunan	46	1	
Leigongshan, Leishan, Guizhou	47	1	
Pachytriton moi			
Mao'ershan, Xin'an county Guangxi (by KIZ)	43	1	

delimitation can effectively and objectively determine the number of independently evolving lineages using a hypothesis-testing framework (Fujita *et al.* 2012). Because all populations of the *P. brevipes* complex are restricted to montane habitats, this species complex also provides an opportunity to study the mechanisms underlying speciation on "sky islands" within a biodiversity center of southeastern China.

Using the *P. brevipes* complex as an example, I address the importance of an integrative perspective to couple the study of species delimitation and speciation process. The integration complements our understanding of two basic questions: how many species there are, and how they were formed. First, I test the existence of multiple species in the complex with coalescent-based species delimitation in conjunction with other statistical approaches. The coalescent theory is implemented in two independent methods: the General Mixed Yule Coalescent (GMYC) model (Pons *et al.* 2006) and the reversible-jump Markov chain Monte Carlo (rjMCMC) (Yang & Rannala 2010). Secondly, if those species represent independently evolving lineages, I reconstruct the species tree using two mitochondrial and two nuclear loci. Conflict between gene trees and the corresponding species tree suggests the presence of gene flow and/or incomplete lineage sorting. Third, because species of *Pachytriton* occupy similar habitats on sky islands, I investigate the potential role of niche conservatism in the origin of new species. Fourth, to understand demographic dynamics in each species, I estimate the extent of gene flow between geographically adjacent species and whether individual lineages underwent demographic expansion after speciation. Analyses used in this study may represent standard tools to be included in future research that assesses regional biodiversity.

Material and methods

Data collection

I collected 178 salamanders from 31 localities throughout the geographic range of the *Pachytriton brevipes* complex in southeastern China, including all four species: *P. brevipes*, *P. feii*, *P. granulosus*, and *P. xanthospilos* (Table 4-1). Respective type localities were included. Three to eight individuals (average 5.7 individuals) were sampled for each locality. Thirteen specimens that represent the remaining three species in the genus were included as phylogenetic outgroups. Total genomic DNA was extracted from ethanol-preserved liver or muscle tissue by using a DNeasy Blood and Tissue Kit (QIAGEN corp.). Two mitochondrial DNA (mtDNA) sequences, the *ND2* and *cytb* gene with flanking tRNAs (each with ~ 1200 base pairs, bp), were amplified for the complete dataset. Two additional nuclear DNA (nDNA) fragments were obtained from a subset of samples (14 localities), covering the 3' end of the *RAG-1* gene (~ 1200 bp) as well as a non-coding region of the tyrosinase gene (*NCRT*, 600 bp). The second nuclear marker was developed following the anonymous-loci development method (Espregueira Themudo *et al.* 2009). PCR primers and conditions for mtDNA and *RAG-1* were available from Wu *et al.* (2010). The *NCRT* fragment was amplified using the forward primer TYR-F (5'AGC GGT AGA CCT GTG GCT TC 3') and reverse primer TYR-R (5' TGC ACA CTG ATG GGG TTG GT 3'), under the condition of initial denaturation at 94 °C for 2 min, followed by 35 cycles of denaturation at 94 °C for 30 s, annealing at 60 °C for 45 s, extension at 72 °C for 60 s, and a final extension at 72 °C for 5 min. Amplified PCR products were examined on 1% agarose gels, successively purified with a

QIAquick PCR purification kit (QIAGEN corp.), and sequenced on an ABI 3730. The same PCR primers were also used for sequencing. DNA sequences were manually aligned in Se-Al 2.0 (Rambaut 1995). Nuclear haplotypes were inferred using Phase v2.1.1 (Stephens *et al.* 2001; Stephens & Donnelly, 2003) with default model settings and 100 iterations. Recombination with nuclear loci was examined using the algorithm implemented in IMgc Online (Woerner *et al.* 2007).

Gene tree reconstruction

Because in most cases the mitochondrial genome of vertebrates does not undergo recombination (Birky 2001), I concatenated the two mitochondrial genes to yield a single alignment (2357 bp) for gene tree reconstruction, which is conducted using the Bayesian inference in MrBayes 3.1.2 (Huelsenbeck & Ronquist 2001) and maximum-likelihood (ML) criterion in RAxML-HPC 7.3.1 (Stamatakis 2006; Stamatakis *et al*. 2008). Both analyses were performed in computer clusters through the CIPRES Science Gateway (Miller *et al.* 2010). Based on a comparison of partitioning strategies from Wu *et al.* (2012), mitochondrial sequences were tri-partitioned into first and second codon positions, third codon position and tRNAs. An independent GTR+G+I substitution model was selected for each partition by the Akaike Information Criterion implemented in MRMODELTEST 2.2 (Nylander 2004). The two nuclear loci were not partitioned and instead were assigned the HKY+I model. For the Bayesian inference, Markov Chain Monte Carlo (MCMC) was performed for 50-million generations sampled every 1000 generations. Chain convergence was assessed by the average standard deviation of split frequencies and in Tracer 1.5 (Rambaut & Drummond 2007). Trees sampled prior to

stationary distribution were discarded as burn-in. For the ML analysis, 1000 bootstrap replicates were performed to calculate nodal support.

Species delimitation

First, coalescent-based species delimitation was conducted for the complete sample with data from the two mitochondrial genes. I used the GMYC model (Pons *et al.* 2006) to infer the number of species by identifying a point of transition in branching process from between species divergence (i.e., speciation) to within-species coalescence on an ultrametric tree. The null hypothesis of no such transition was tested with a Likelihood Ratio (LR) Test. Before running GMYC, a mtDNA chronogram was estimated in BEAST 1.7.0 (Drummond & Rambaut 2007) under an uncorrelated relaxed-clock model, with a mean of 7.7×10^{-9} per site per year in *Pachytriton* (95% HPD: 5.9×10^{-9}–9.9×10^{-9}; Wu *et al.* 2013). This mitochondrial mutation rate is very close to the estimate for plethodontid salamanders (Mueller 2006). Bayesian MCMC was performed for 50-million generations with a sample frequency of 5000. The mtDNA chronogram was analyzed under the GMYC model implemented in the R package SPLITS (SPecies' LImits by Threshold Statistics, http://rforge.r-project.org/projects/splits/). I also tested the single-transition hypothesis against an alternative hypothesis that allows multiple independent transition points for different phylogenetic clades. Approximate 95% confidence intervals (CI) for the number of inferred species were calculated by finding solutions within two log-likelihood units of the maximum likelihood.

Secondly, I used the program Bayesian Phylogenetics & Phylogeography (BP&P; Yang & Rannala 2010) to estimate the posterior probability of potential species

delimitation. Because the four species in the *P. brevipes* complex are classified by mtDNA (Nishikawa *et al.* 2011a, b; Wu *et al.* 2012), the unlinked nuclear loci *RAG-1* and *NCRT* can provide an independent test to the evolutionary distinctness of these species. In contrast to the GMYC model, BP&P takes sequence data as input and accounts for uncertainties in gene-tree reconstruction as well as incomplete lineage sorting due to ancestral polymorphism (Yang & Rannala 2010). Although an explicit model of speciation with gene flow has not been incorporated into the current version of BP&P, model accuracy is virtually unaffected with small amount of gene flow (≤ 0.1 migrants per generation; Zhang *et al.* 2011). I used phased nuclear haplotype data and the rjMCMC in BP&P to delimit species based on a user-specified, fully resolved guide tree with each internal node representing a speciation event. Collapse of internal nodes produces alternative delimitations with fewer species. Leaché & Fujita (2010) report the impact of mis-specified guide trees on inference of species boundaries. To eliminate such impact, species delimitation was tested upon all 15 possible topologies for a four-species rooted tree. Followed a strategy similar to that used by Leaché & Fujita (2010), I used three combinations of priors of gamma distribution on ancestral population size (θ) and root age (τ) to represent different potential demographic histories: $\theta \sim G$ (2, 200) and $\tau \sim G$ (2, 100); $\theta \sim G$ (2, 2000) and $\tau \sim G$ (2, 1000); $\theta \sim G$ (2, 20000) and $\tau \sim G$ (2, 10000). Other divergence time parameters were assigned the Dirichlet process prior. The rjMCMC was run for 100,000 generations sampled every 2 generations. The first 20 percent of the run was discarded as burn-in. Both algorithms 0 and 1 were run multiple times with different starting trees and different fine-tune parameters to confirm the stability among runs.

I further applied a Bayesian approach implemented in STRUCTURE v.2.3.3 (Pritchard *et al.* 2000) to assess the genetic structure in the *P. brevipes* complex. Only single-nucleotide polymorphisms (SNP) in the phased nuclear data were used (strong linkage in mtDNA violates model assumptions). I ran a series of analyses to determine the optimal number of genetic distinct clusters (K), with K ranging from 1 to 10. In each analysis, individuals were probabilistically assigned either to a particular cluster or jointly to multiple populations if their genotypes suggest cluster admixture. The admixture model was chosen as the model for the ancestry of individuals. I assumed a correlated allele frequency model to improve grouping for closely related clusters. For each K, 10 replicates were performed using MCMC for 20,000 generations after a burn-in of 10,000 generations. The posterior probability of each K was calculated using the mean estimated log likelihood of the data (D) given the K [Ln P ($D|K$), averaging over 10 replicates] under the assumption of a uniform prior. An alternative criterion for choosing K employed the second order rate of change of the likelihood function with respect to K (ΔK), which has a mode at the true K (Evanno *et al.* 2005). Estimated membership coefficients for each individual in each cluster were plotted by Distruct 1.1 (Rosenberg 2004). I followed Weisrock *et al.* (2010) to discard membership coefficients with posterior probabilities less than 0.05 and assigned corresponding values proportionally to the other membership coefficients, so coefficients for each individual still sum to 1. An individual is considered of admixed ancestry if it has multiple membership coefficients between 0.1 and 0.9 (Vähä & Primmer 2005).

Lastly, I used distance-based methods to investigate the genetic structure within the *P. brevipes* complex. For the mtDNA data, analysis of molecular variance (AMOVA;

Excoffier *et al*. 1992) was performed in Arlequin version 3.1 (Excoffier *et al*. 2005) to evaluate the distribution of genetic variation at different hierarchical levels. Statistical significance of covariance associated with each level was calculated with 1000 permutations. For nuclear haplotypes, a statistical parsimony network was reconstructed in TCS v. 1.21 (Clement *et al.* 2000). Haplotypes were connected by mutational differences that do not exceed the parsimony connection limit, resulting in a 95% plausible network. Reticulations in the network were broken according to coalescent-based predictions on allele frequency and distribution (Posada & Crandall 2001).

Species tree reconstruction

I used two multi-locus approaches to estimate the species tree of the *P. brevipes* complex with data from mtDNA, *RAG-1*, and *NCRT*. First, I applied the hierarchical Bayesian model implemented in Bayesian Estimation of Species Trees (BEST) v. 2.3 (Liu & Pearl 2007; Liu 2008). Substitution models were the same as those used in gene tree reconstruction. Following Leaché (2009), a relatively large mean for the population size prior [$\theta = 0.01$, invgamma (3, 0.02)] was chosen to improve MCMC performance and achieve faster chain convergence. Mutation rate prior was set to a uniform distribution (0.15, 1.5) to accommodate the general ten-fold difference in mutation rates between mtDNA and nDNA (Ballard & Whitlock 2004). Gene tree topology, branch length, and mutation rates were unlinked across loci. *Pachytriton inexpectatus* and *P. archospotus* were used as outgroups. Two Bayesian MCMC runs were performed for 100-million generations and sampled every 1000 generations. Convergence and burn-in period were

determined by average standard deviation of split frequencies among runs (< 0.01) as well as in Tracer 1.5 (Rambaut & Drummond 2007). The posterior distribution of the species tree was summarized by the "sumt" command. The second approach for species-tree inference used the *BEAST option implemented in BEAST v1.7.0 (Drummond & Rambaut 2007; Heled & Drummond 2010). Unlike BEST, which estimates individual gene trees first and then infers the species tree with the marginal posteriors of gene trees, *BEAST uses a single Bayesian MCMC run to estimate gene trees and the species tree simultaneously (Heled & Drummond 2010). In practice, *BEAST is substantially more computationally efficient than BEST (Kubatko *et al.* 2011). To evaluate the impact of outgroup taxa, which may lead to erroneous estimation of the species tree (Heled & Drummond 2010), I performed analyses both with and without outgroups. Substitution models were the same as those used in BEST and in gene tree reconstruction. Bayesian MCMC was performed for 100-million generations with a sample frequency at every 1000 generations. Burn-in period was determined by Tracer 1.5 (Rambaut & Drummond 2007).

Ecological niche modeling

To evaluate the role of ecology in species formation in the *P. brevipes* complex, I reconstructed the potential niche for each species using spatially explicit environmental data and a maximum entropy model implemented in Maxent 3.3.3 (Phillips *et al.* 2006; Phillips & Dudík 2008). Nineteen bioclimatic variables derived from monthly temperatures and precipitation (1950–2000) were downloaded from the WorldClim database (http://www.worldclim.org; Hijmans *et al.* 2005) at a resolution of 30

arc-seconds (~1 km). Those variables describe annual trend, seasonality, and extreme environmental conditions. All 31 collecting localities were treated as occurrence data. Three additional localities, which have geographic coordinates and can be confidently assigned to species, were retrieved from the global database of natural history museums via HerpNET (http://www.herpnet.org). The dataset is undoubtedly small for model-based niche analyses (9 localities for *P. brevipes*, 5 for *P. feii*, 15 for *P. granulosus*, and 5 for *P. xanthospilos*; Table 4-1), but this dataset likely represents the most complete sampling of *Pachytriton* to date. Default settings with auto features were used, except that the number of maximum iterations was increased to 5000. Due to limited sample size, all occurrence data were designated for model training. Model accuracy was assessed using the area under the receiving operation characteristic curve (AUC), with values around 0.5 suggesting a random model and values greater than 0.7 indicating sufficient discrimination between suitable and unsuitable areas for the species (Swets 1988). The predicted niches were projected into DIVA-GIS 7.1.7 (http://www.diva-gis.org/) using the minimum training presence as the binary threshold for suitable and unsuitable habitat.

Niche overlap between species was assessed using both Schoener's *D* (Schoener 1968) and *I* statistic (Warren *et al.* 2008) in ENMTools (Warren *et al.* 2008). Both statistics range from 0 (i.e., complete different niches between species) to 1 (i.e., identical niche shared by species). Niche overlap was measured between each pair of the four species based on niches predicted by Maxent. To test whether niches of two species are significantly different from each other, I performed a niche-identity test, which randomizes the occurrence data between two species in 100 replicates to generate a null distribution of niche overlap as if they share the same ecological niche. Niche overlap

value generated from the actual data of each species was compared to the null distribution, and statistical significance was calculated using a 2-tailed one-sample *t*-test. Because niches could appear different as a result of divergence in the environmental background where species occur (McCormack *et al.* 2010), I performed a background test to further evaluate whether two predicted niches are more divergent (niche divergence) or similar (niche conservatism) than expected, given the difference or similarity between environmental backgrounds. For each pair of species, the niche of the first species was compared to the background of the second species (predicted from 50 random localities within the geographic range of the second species) in 100 replications. These random localities provide ecological information regarding the environmental background of the second species. A second comparison was performed from the opposite direction (i.e., the niche of the second species was compared to the environmental background of the first species). Each observed overlap value was compared to the null distribution, and statistical significance was calculated using a 2-tailed one-sample *t*-test. If an observed value is significantly smaller than the null distribution, niche divergence is inferred between the two species; if the observed value is significantly greater, niche conservatism is inferred.

To further understand how niches of the *P. brevipes* complex differentiate in the ecological space, I conducted a principal-component analysis (PCA) with varimax rotation in SPSS (ver. 16, Chicago, IL, USA) based on the 19 bioclimatic variables. Variable values at each collecting locality were extracted in DIVA-GIS. I applied a multivariate analysis of variance (MANOVA) to test if PC scores are statistically different among species. The niche of each species was plotted in the multi-dimensional

ecological space in which each axis represents one PC.

Demographic dynamics

To assess whether gene flow has contributed to the observed genetic structure in the *P. brevipes* complex, I estimated population migration rates among the four species with an isolation-with-migration model implemented in IMa2 (Hey & Nielsen 2004, 2007; Hey 2010). If the estimated migration rate approaches zero, then I concluded that speciation was achieved in allopatry without gene flow. Mitochondrial data were analyzed for the complete dataset and phased nuclear loci were analyzed for the subset dataset. The HKY substitution model was used for all DNA loci. Migration prior was set to zero between geographically isolated species (e.g., *P. feii* and *P. xanthospilos*) and set to 1 between geographically neighboring species (e.g., *P. brevipes* and *P. granulosus*). Preliminary runs determined that a burn-in period of 1 million steps was adequate for the MCMC convergence, after which 20,000 genealogies were stored. Each run included 20 chains and used a low heating scheme with the geometric model (ha = 0.96, hb = 0.9). Because IMa2 requires a user-specified phylogenetic tree for analysis with three or more species (Hey 2010), I also tested with alternative topologies and evaluated the associated impact on demographic parameter estimation.

After speciation, daughter species might undergo demographic expansion, resulting in a unimodal distribution of pairwise nucleotide difference between haplotypes (Rogers & Harpending 1992; Excoffier 2004). I used the mismatch distribution in Arlequin ver 3.1 (Excoffier *et al.* 2005) to test the signal of such expansions for each species using the full mtDNA dataset. Confidence intervals for the time of expansion (τ) were estimated

with 1000 coalescent simulations. Statistical significance of the mismatch distribution was assessed with the sum of squared deviations (SSD) between the observed and expected mismatch and the raggedness index.

Results

Mitochondrial and nuclear gene trees

The mtDNA gene tree produces fully resolved phylogenetic relationships among all known species of *Pachytriton* (Fig. 4-2). Monophyly is strongly supported for each species. Tree topologies are almost identical from Bayesian inference and ML analyses. A basal split separates the clade comprising *P. inexpectatus* and *P. moi* from the clade comprising *P. archospotus* and the *P. brevipes* complex. In the *P. brevipes* complex, *P. granulosus* is a sister taxon to the other three species, which form a well-supported clade. Deep mitochondrial lineages are recovered in all four species in the *P. brevipes* complex. Populations of *P. granulosus* from low elevations in central and eastern Zhejiang province constitute a strongly supported clade, which is separated from remaining populations from high mountains in Zhejiang and Fujian provinces. Notably, this star-like clade provides the only instance in which individuals from geographically separate mountains are admixed in the mtDNA gene tree. All other populations are reciprocally monophyletic. *Pachytriton brevipes* is divided into distinct northern and southern clades in the Wuyi Mountain Range. *Pachytriton feii* from Huangshan (sites 1–4, Anhui province) and Sanqingshan (site 5, Jiangxi province) are largely differentiated in mitochondrial sequences (~ 4% in uncorrected *p*-distance). The largest intraspecific divergences are observed in *P. xanthospilos* (> 6% in uncorrected *p*-distance), even when

Figure 4-2. The maximum-likelihood gene tree of *Pachytriton* derived from mtDNA gene. Double asterisks indicate posterior probability > 0.95 and bootstrap value > 90.

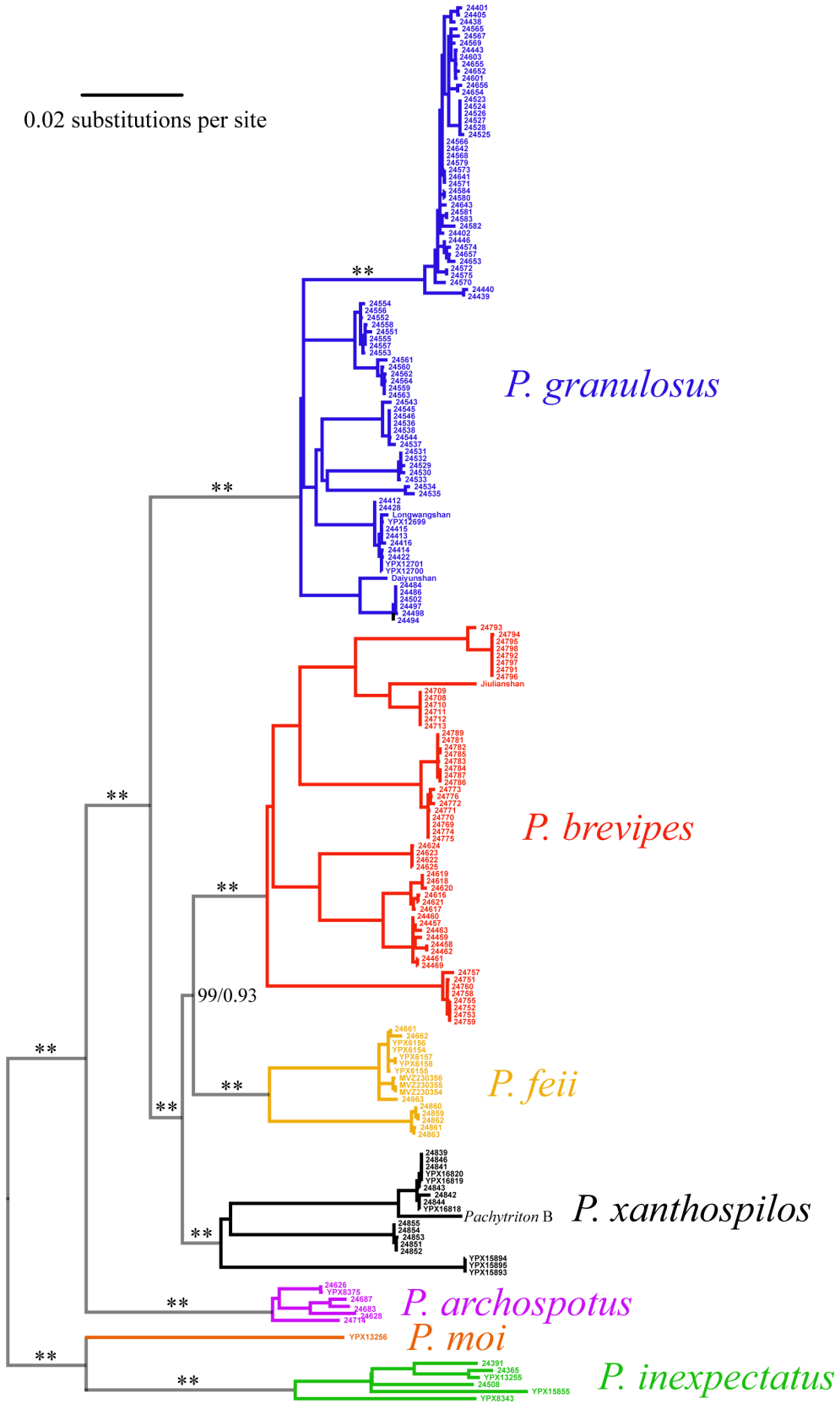

Figure 4-2 (continued)

two populations from Guposhan (sites 33 and 34, Guangxi province) are as close as 7 km in topographic distance. On the other hand, the two nuclear gene trees are much less resolved due to the low level of genetic variation (trees not shown). Monophyly of the *P. brevipes* complex is supported by *NCRT* but not by *RAG-1*. The latter gene implicates that the complex is paraphyletic with respect to *P. archospotus*. Relationships within the *P. brevipes* complex also differ between the two nuclear loci, although both loci indicate that haplotypes of the four species are admixed.

Species delimitation based on DNA data

The coalescent-based GMYC model posits the point of transition from species-level to population-level divergence at 0.59 Ma on the mtDNA chronogram of the *P. brevipes* complex generated by BEAST (Fig. 4-3). Using this threshold, 23 species are recognized in the complex (CI: 17–27; 8 in *P. brevipes*, 2 in *P. feii*, 9 in *P. granulosus*, and 4 in *P. xanthospilos*). Each phylogenetically deep lineage on the mtDNA gene tree corresponds to one species. The lineage-through-time (LLT) plot indicates a rapid increase in the number of evolutionary lineages shortly after the threshold. The GMYC model rejects the null model of a single species in the *P. brevipes* complex (LR = 34.04, d.f. = 3, $P = 1.94 \times 10^{-7}$). An alternative model that allows multiple independent thresholds for different clades does not fit the data statistically better than the single-threshold model (LR = 1.96, d.f. = 6, $P = 0.92$). Inclusion of other species of *Pachytriton* as outgroups in the chronogram yields identical estimates of the threshold and the number of species in the *P. brevipes* complex.

Using nuclear haplotype data, the Bayesian species delimitation strongly supports all

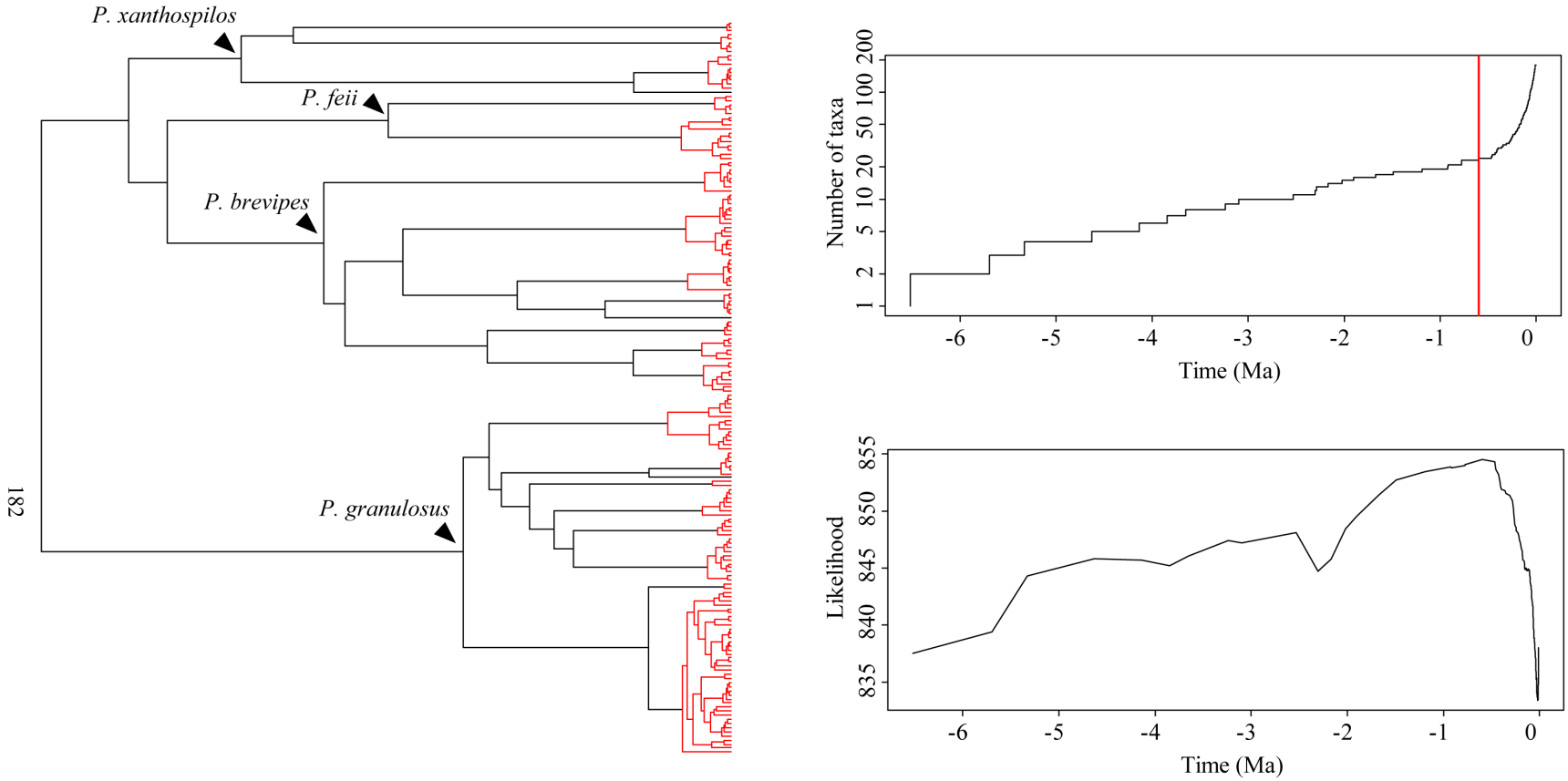

Figure 4-3. Left: Each red clade is recognized as a separate species by the GMYC analysis. Upper right: Lineage-through-time plot with the transitional threshold from species-level to population-level divergence (red line); bottom right: likelihood surface for this threshold.

15 guide trees when assuming four species in the *P. brevipes* complex. Speciation probabilities range from 0.98 to 1.0 at internal nodes, regardless of which combination of prior distributions is used (Fig. 4-4). Increasing chain length (500,000 generations) and using different algorithms and starting trees (i.e., rjMCMC started with one, two, three, or four species in the complex) do not affect the results. The Bayesian cluster analysis in STRUCTURE based on nuclear SNPs reveals a pattern of plateau in the Ln P ($D|K$) (averaged over 10 replicates for each K value) after $K = 5$ (Fig. 4-5). Assuming a uniform prior for K from 1 to 10, the posterior probability is 1.0 for $K = 7$. On the other hand, the ΔK criterion produces two peaks at $K = 2$ and $K = 5$. The first peak results from the dramatic increase in Ln P ($D|K$) from $K = 1$ to $K = 2$, suggesting that the single-species taxonomy is not sufficient to capture the basic hierarchical structure in the data (Weisrock *et al.* 2010). A comparison between nDNA clusters identified by $K = 5$ and $K = 7$ indicates that two additional clusters are split from *P. brevipes*. However, the two clusters do not represent more exclusive sets of individuals because most individuals have an admixed ancestry from multiple clusters. Therefore, I favor $K = 5$ as a conservative estimate of the number of clusters in my sample. The five nuclear clusters are only partially congruent with the four-species taxonomy classified based on the mtDNA gene tree. Among the four species, only *P. feii* is assigned to an exclusive cluster (yellow) with a membership coefficient of 1.0. This strongly supports this species as an independently evolving lineage. *Pachytriton granulosus* and *P. brevipes* each comprises three clusters, two of which (purple and green) are shared between the two species. A few specimens collected from Zhejiang group into a cluster (red) that is unique to *P. granulosus* but does not correspond to the mtDNA clade formed by low-elevation populations.Three individuals

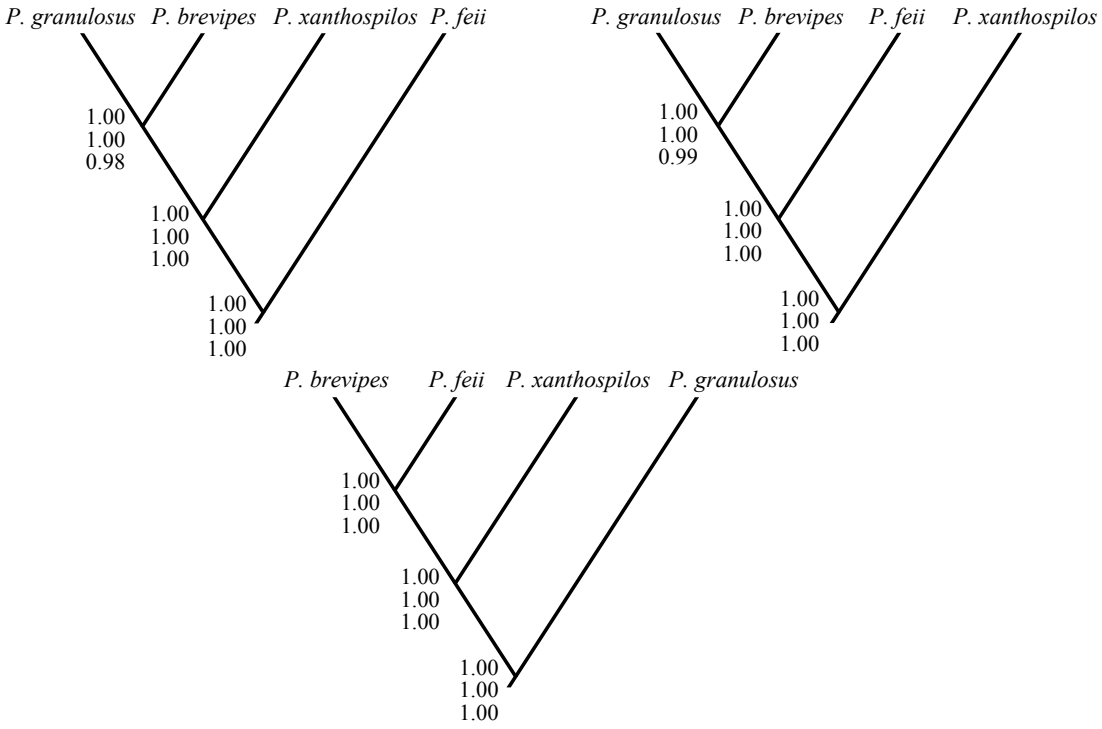

Figure 4-4. The BP&P analysis supports the four species in the *P. brevipes* complex as independently evolving lineages regardless of guide tree topologies. Upper left: topology of the BEST species tree; upper right: topology of the *BEAST species tree; bottom: topology of the mtDNA tree (Fig. 4-2)

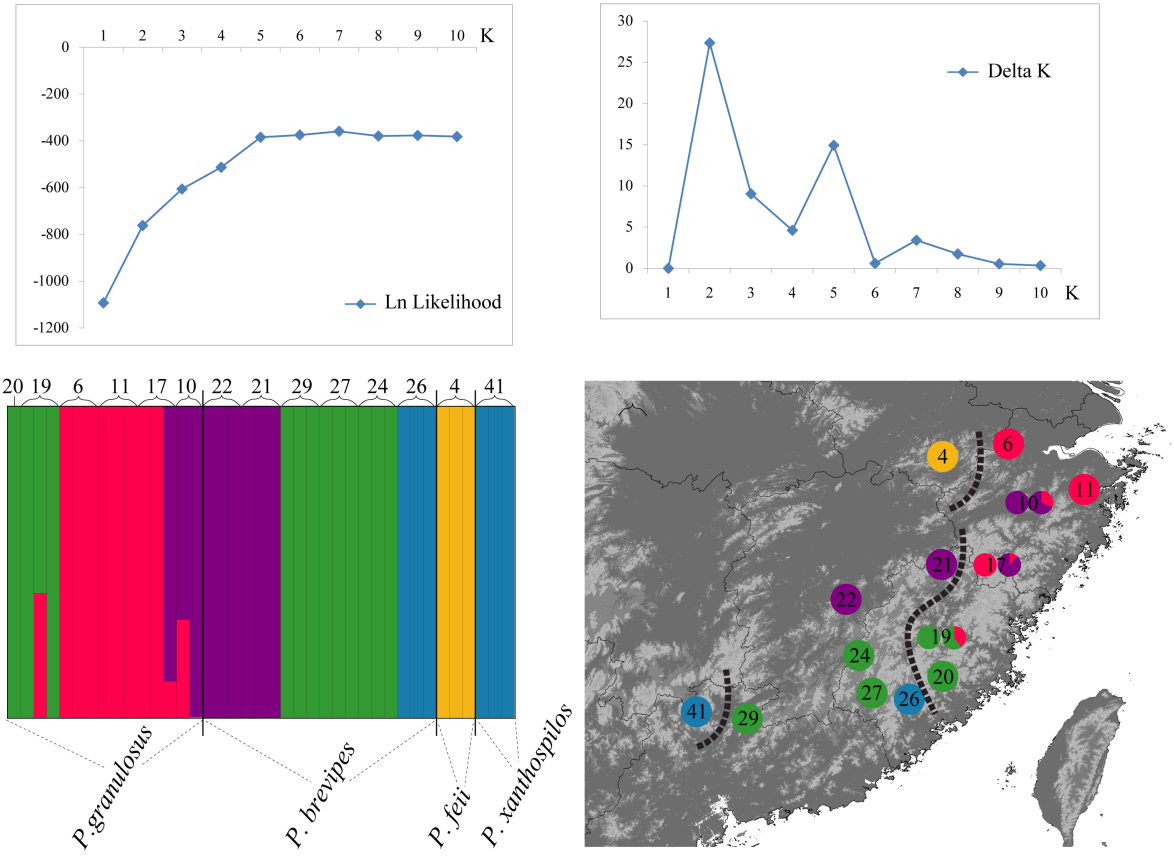

Figure 4-5. Upper left: Ln P (D|K) of different *K* values in STRUCTURE. The likelihood plateaus after *K* = 5. Bottom left: Δ*K* criterion produces two peaks at *K* = 2 and *K* = 5. Upper right: Nuclear DNA clusters for *K* = 5. Each color represents one cluster. Bottom right: the geographical distribution of nuclear DNA clusters. Numbers are population IDs (Table 4-1). Dashed lines are species boundaries. Individuals from sites 10, 17, and 19 are assigned either to a particular cluster or jointly to multiple clusters.

of *P. granulosus* collected across its geographic range are of admixed ancestry. None of the three clusters identified in *P. brevipes* is unique to this species. *Pachytriton brevipes* collected at Tiangongshan (site 26) does not cluster with other conspecific populations, but instead has a cluster assignment (blue) identical to *P. xanthospilos* with a membership coefficient of 1.0.

Distance-based methods suggest significant hierarchical genetic structure within the *P. brevipes* complex. For the mtDNA dataset, AMOVA partitioned almost all genetic variance (96.61%, $P < 0.001$) among collecting localities when assuming a single species, indicating that salamanders are genetically differentiated across localities. Only 3.39% of the overall variance is attributed to within-locality variation ($P < 0.001$). If localities are assigned to the four species, genetic structure is highly correlated with species boundaries; one half of the molecular variance is partitioned among species (50.35%, $P < 0.001$). For the nDNA dataset, the haplotype network recovers five clusters that are identical to those from the STRUCTURE analysis (Fig. 4-6). The red cluster unique to *P. granulosus* is connected to the purple and green clusters shared by *P. granulosus* and *P. brevipes*, and it is more closely related to the former cluster than to the latter. The yellow (*P. feii*) and blue clusters are distantly connected to the green cluster with multiple mutational steps.

Species tree inference

The sister relationship between *P. archospotus* and the *P. brevipes* complex, as well as the monophyly of the latter group, is well supported by both multi-locus methods. However, relationships within the *P. brevipes* complex are resolved differently (Fig. 4-7). The hierarchical model in BEST separates *P. feii* from the other three species, whereas the

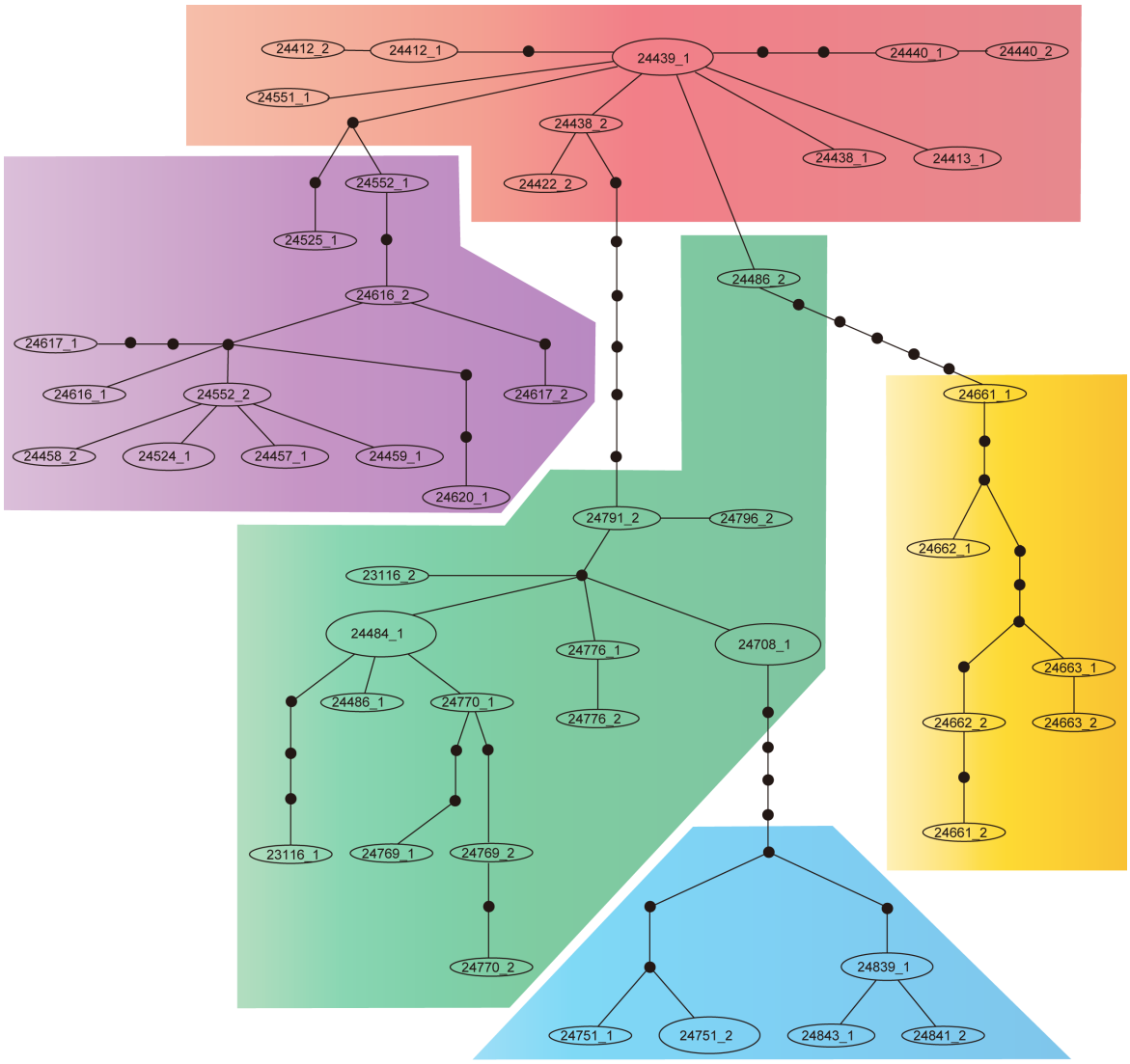

Figure 4-6. Nuclear haplotype map. Colors of clusters correspond to nuclear clusters in Fig. 4-5. Black dots denote missing haplotypes. Individuals are labeled by field numbers.

*BEAST analysis infers a basal split between *P. xanthospilos* and the remaining species. Regardless of inference methods, the multi-locus dataset consistently recovers a sister relationship between *P. granulosus* and *P. brevipes*, in contrast to the topology of the mtDNA gene tree, in which *P. granulosus* and *P. brevipes* are most divergent from each other. Excluding outgroup taxa (*P. inexpectatus* and *P. archospotus*) does not affect support for this sister relationship. Such discordance between gene tree and species tree reflects conflicting signals among mitochondrial and nuclear loci.

Ecological niche modeling

The reconstructed ecological niche for each species of the *P. brevipes* complex is shown in Fig. 4-8. Training AUC values range from 0.954 to 0.997, indicating high fitness of the model to the occurrence data. Among the 19 bioclimatic variables, precipitation seasonality is most important to the niche model of *P. granulosus*: permutation of this variable results in a dramatic decrease (76.8%) in the training AUC. Similarly, mean temperature of the wettest quarter, isothermality, and precipitation of the driest month are most important to the niche model of *P. brevipes* (58.4% decrease), *P. feii* (50.4% decrease), and *P. xanthospilos* (53.6% decrease), respectively. Using the minimum training presence as the binary threshold for suitable and unsuitable habitat, the predicted distribution of *P. brevipes* is much larger than the current surveyed range; the predicted distritbution occupies nearly the entire geographic distribution of the genus in southeastern China. On the other hand, predicted distributions of the other three species are highly consistent with their known geographic ranges, except for a few small areas predicted outside the core areas. The predicted occurrence of *P. feii* and *P. xanthospilos* is

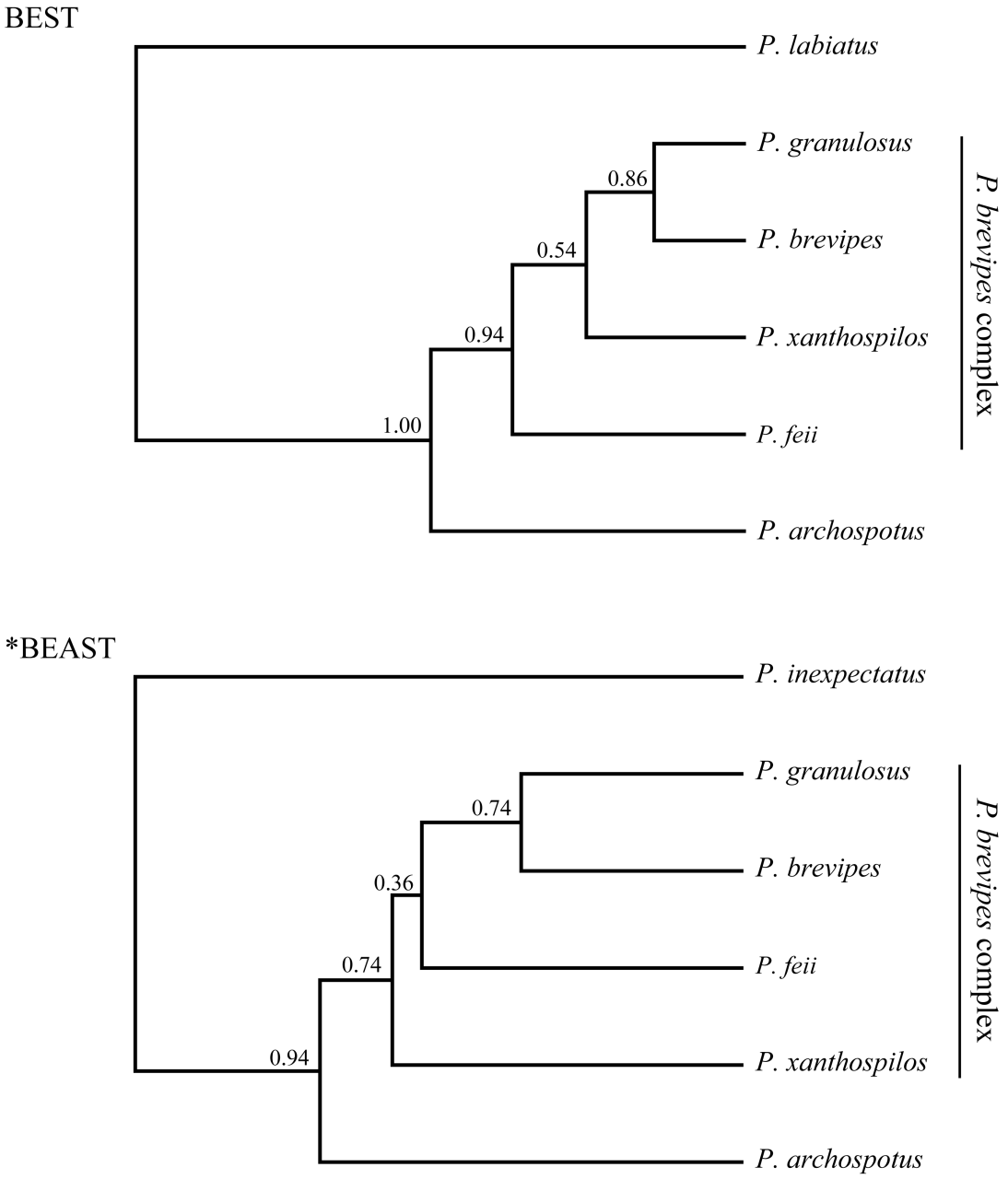

Figure 4-7. Species tree inferred based on mtDNA and nDNA by two different approaches (BEST and *BEAST). Numbers on branches are posterior probabilities.

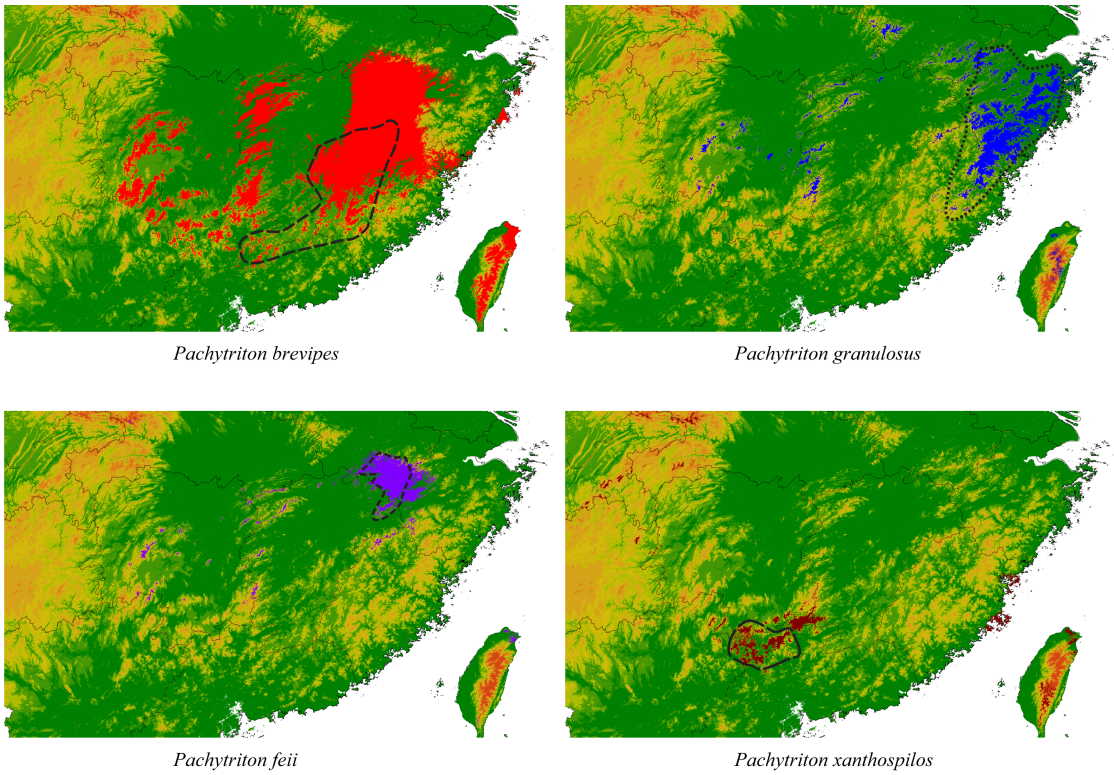

Figure 4-8. Predicted suitable habitat for each of the four species in the *P. brevipes* complex. Dashed line encircles the known geographic distribution of each species.

almost entirely included in that of *P. brevipes*, but the predicted occurrence of *P. granulosus* is parapatric to that of *P. brevipes*.

Niche overlap statistics reveal the largest overlap between *P. brevipes* and the remaining three species (D = 0.350–0.397, I = 0.626–0.669) and between *P. feii* and *P. granulosus* (D = 0.377, I = 0.638). Niches are most divergent between *P. feii* and *P. xanthospilos* (D = 0.123, I = 0.358). Pairwise niche-identity tests in ENMTool reveal that all overlap values observed among the four species are significantly lower than expected from the null distribution (Fig. 4-9, all $P < 0.0001$); each species occupies a distinct ecological niche. In multivariate PCA, the first three PCs (eigenvalues > 1) explain 36.67%, 22.88%, and 21.75% of the overall variance from the 19 bioclimatic variables. Based on the factor loadings (Table 4-2), PC 1 captures both daily and annual temperature changes and winter temperatures; PC 2 characterizes annual mean temperature and summer temperatures; PC 3 mostly represents annual mean precipitation and summer precipitations. The MANOVA using the three PC scores reveals significant niche difference among the four species (Wilk's $\lambda = 0.307$, $F_{9, 68} = 4.737$, $P < 0.001$). Specifically, PC 1 and PC 3 are significantly different among species ($F_{3, 30} = 8.177$, $P < 0.001$ and $F_{3, 30} = 3.829$, $P = 0.02$ respectively), whereas PC 2 is insignificant ($F_{3, 30} = 1.824$, $P = 0.164$). To present a species' niche as a multidimensional hypervolume (Hutchinson 1957), I plot the mean and associated 95% confidence intervals of the first three PC scores for each species in a three-dimensional ecological space, with each axis representing one PC (Fig. 4-10). Every point inside the hypervolume corresponds to a condition that allows the species to persist (Hutchinson 1957). The 95% confidence intervals of the four niches do not overlap, except that between *P. brevipes* and *P.*

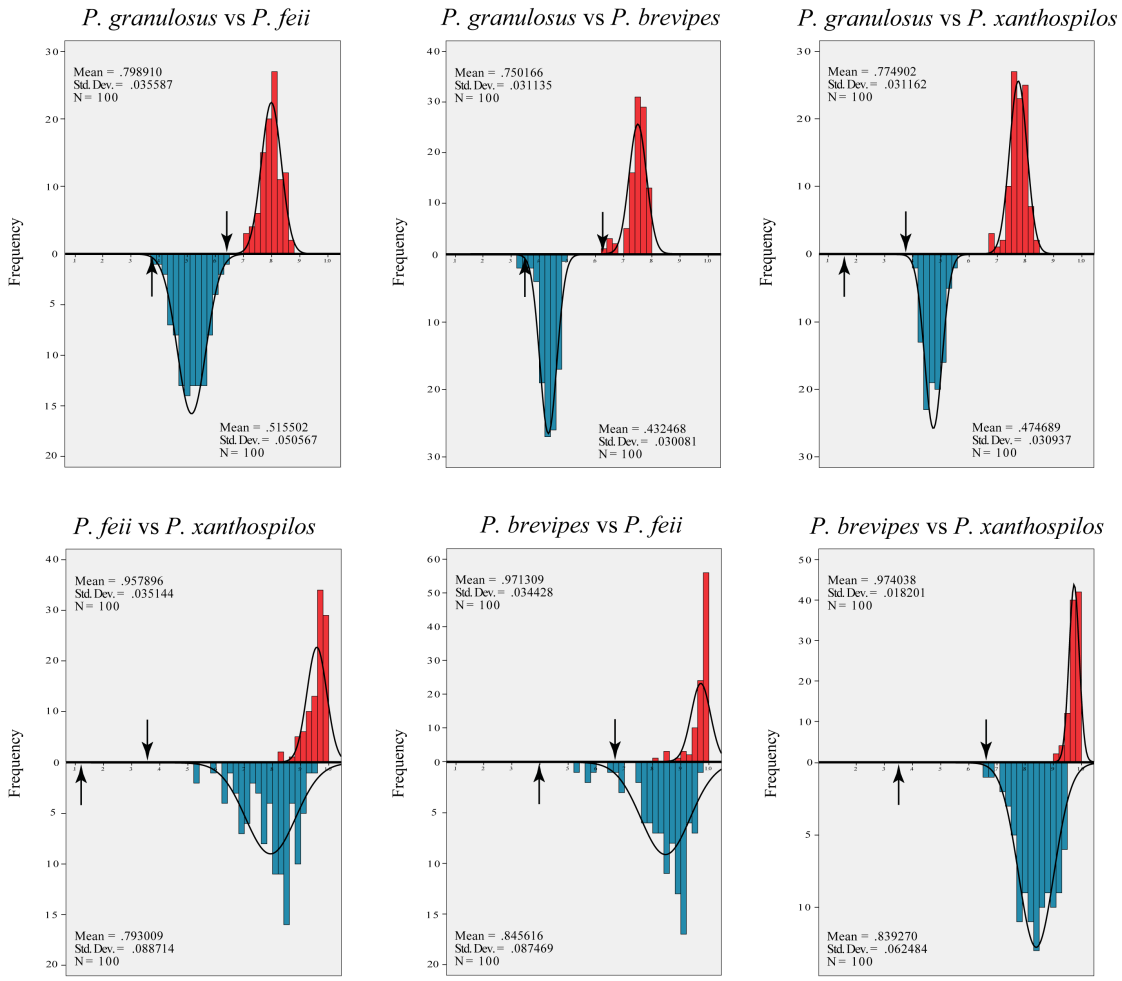

Figure 4-9. Pairwise niche-identity tests. Red columns are the null distribution of Schoener's *D* statistic; blue columns are the null distribution of the *I* statistic. Black arrows indicate values calculated from observed data.

Table 4-2. Varimax-rotated loadings of principal components.

Climatic Variables[ɠ]	Component 1	2	3	4
Bio1	0.553	0.821	0.062	-0.024
Bio2	0.402	0.544	0.127	0.467
Bio3	0.904	0.042	0.172	0.311
Bio4	-0.929	0.231	-0.194	-0.123
Bio5	-0.127	0.972	-0.098	-0.124
Bio6	0.838	0.493	0.108	-0.068
Bio7	-0.877	0.377	-0.182	-0.044
Bio8	0.083	0.375	-0.164	-0.831
Bio9	0.814	0.555	0.100	-0.048
Bio10	-0.104	0.961	-0.086	-0.143
Bio11	0.853	0.494	0.129	0.002
Bio12	0.096	-0.151	0.975	0.000
Bio13	0.237	-0.011	0.804	0.508
Bio14	-0.771	0.019	0.375	0.094
Bio15	0.658	0.115	0.250	0.617
Bio16	0.300	0.054	0.803	0.489
Bio17	-0.776	0.088	0.476	-0.336
Bio18	0.167	-0.516	0.724	-0.221
Bio19	-0.335	0.250	0.858	0.156

ɠ Bio1 = Annual Mean Temperature; Bio 2 = Mean Diurnal Range (Mean of monthly (max temp - min temp)); Bio 3 = Isothermality (Bio 2/ Bio 7) (* 100); Bio 4 = Temperature Seasonality (standard deviation *100); Bio 5 = Max Temperature of Warmest Month; Bio 6 = Min Temperature of Coldest Month; Bio 7 = Temperature Annual Range (Bio 5- Bio 6); Bio 8 = Mean Temperature of Wettest Quarter; Bio 9 = Mean Temperature of Driest Quarter; Bio 10 = Mean Temperature of Warmest Quarter; Bio 11 = Mean Temperature of Coldest Quarter; Bio 12 = Annual Precipitation; Bio 13 = Precipitation of Wettest Month; Bio 14 = Precipitation of Driest Month; Bio 15 = Precipitation Seasonality (Coefficient of Variation); Bio 16 = Precipitation of Wettest Quarter; Bio 17 = Precipitation of Driest Quarter; Bio 18 = Precipitation of Warmest Quarter; Bio 19 = Precipitation of Coldest Quarter

granulosus. The niche of *P. feii* is mainly characterized by small daily temperature change, generally low winter temperatures, and large annual temperature fluctuations, whereas *P. brevipes* and *P. xanthospilos* prefer areas with the opposite conditions. However, the habitat of *P. xanthospilos* receives significantly less precipitation and is cooler in summers compared to that of *P. brevipes*. *Pachytriton granulosus* has an intermediate niche among the four species.

Although identity tests and PCA support niche differentiation, pairwise background tests in ENMTool indicate that niche conservatism is the predominant pattern in the *P. brevipes* complex (Fig. 4-11): three of four species (*P. brevipes*, *P. feii*, and *P. xanthospilos*) share significantly more similar niches compared to their environmental background (i.e., overlap statistics are larger than null distributions generated from random localities, all $P < 0.0001$). When comparing the niche of *P. granulosus* to the environmental background of each of the other three species, significant evidence is found again for niche conservatism (all $P < 0.0001$). But when comparisons are made in the opposite direction, two of three comparisons support significant niche divergence (both $P < 0.0001$) and the third one indicates that the niche of *P. granulosus* is not different from its environmental background ($P = 0.1526$). Because montane habitats are heterogeneously distributed within the geographic range of *P. granulosus*, I performed additional tests that split the range of *P. granulosus* into a southern part with mostly high mountains (southern Zhejiang and Fujian province) and a northern part with a combination of mountains and large plains (central and northern Zhejiang province). Significant niche conservatism is found between the southern part of *P. granulosus* and the other three species, but is not between the northern part and the other three species.

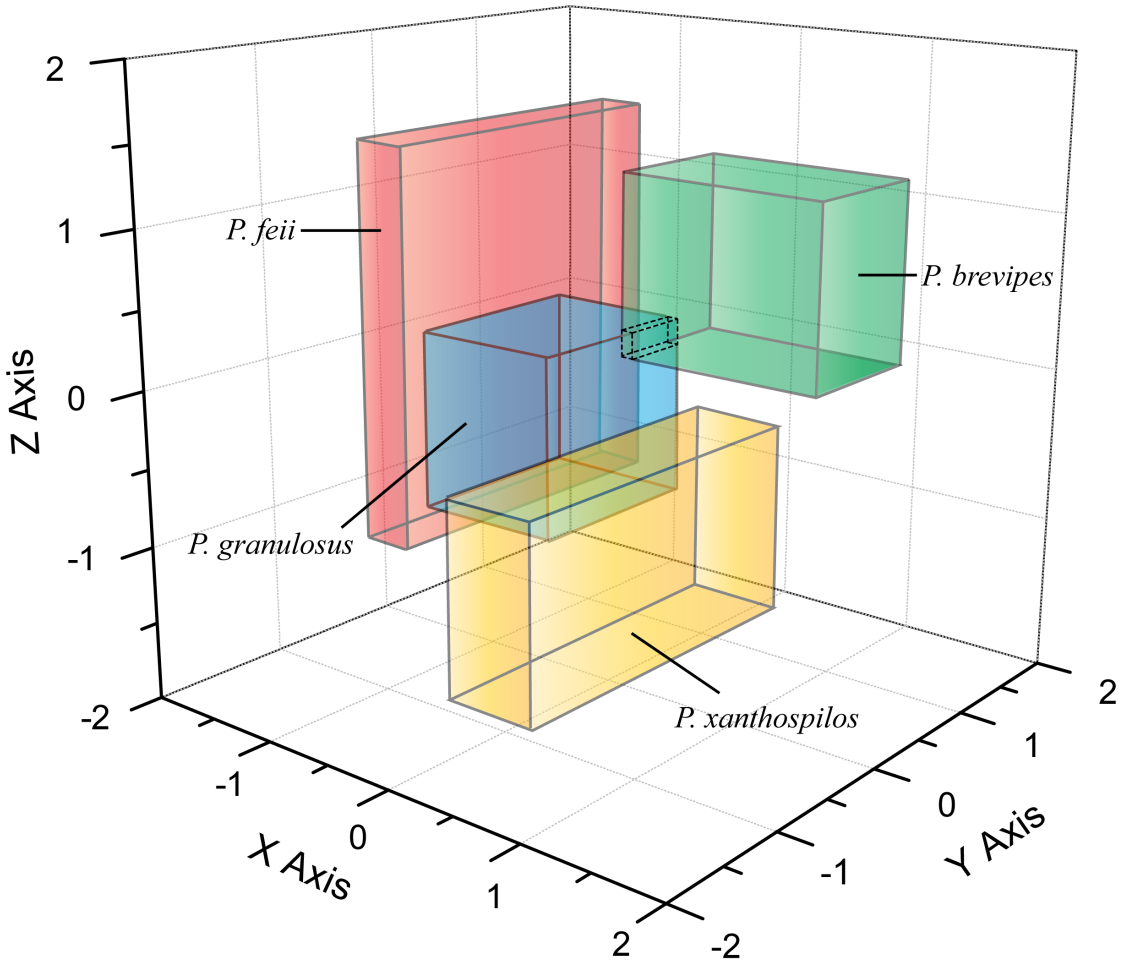

Figure 4-10. Niche space of species in the *P. brevipes* complex represented as hypervolumes. Each axis is a principal component. The 95% confidence intervals of *P. brevipes* and *P. granulosus* overlap slightly.

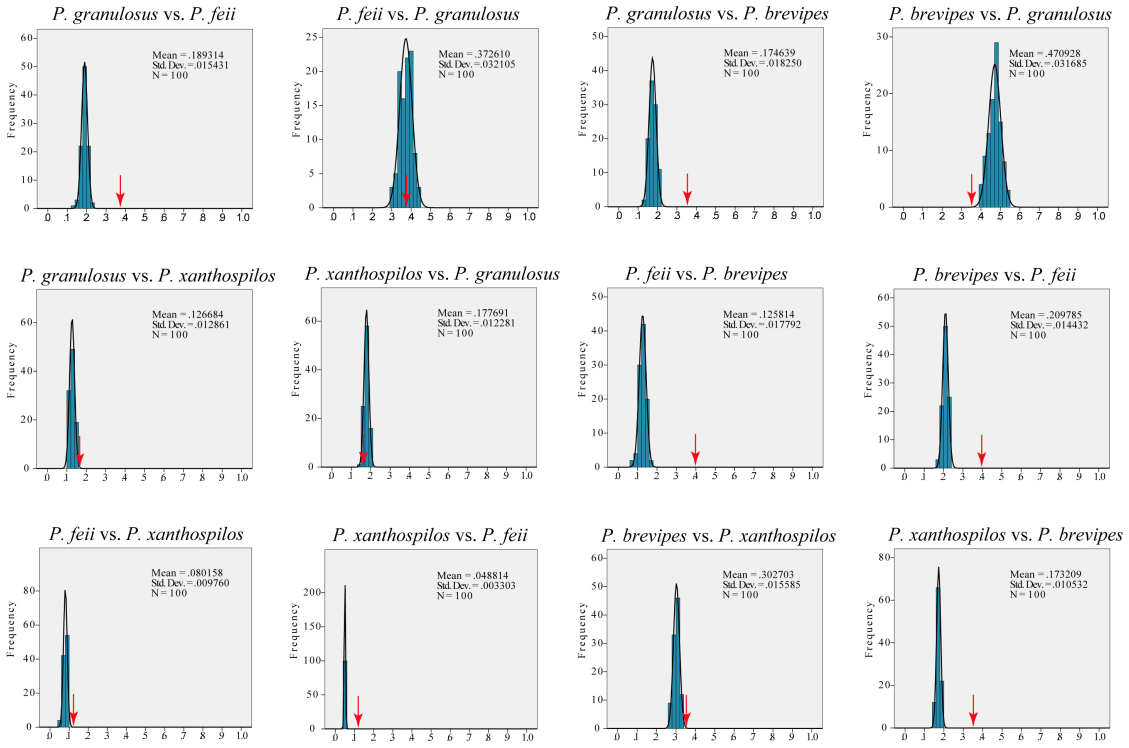

Figure 4-11. Pairwise background tests using Schoener's *D* statistic. Tests using the *I* statistic yield similar results and are not shown. Red arrows indicate observed values. Niche conservatism (i.e., observed values > 95% CI of the null distribution) is found among 9 of the 12 comparisons.

Demographic dynamics

The isolation-with-migration model was applied separately to mtDNA and phased nDNA datasets. Effective sample sizes for [P (D|G) + P (G)] (i.e., the sum of the posterior probability of the data given the genealogy and the prior probability of the genealogy) and all time parameters exceed 4000. Sufficient MCMC mixing is indicated by the absence of a long-term trend in the [P (D|G) + P (G)] plot and consistent estimates between the first and second halves of the run. Using the species tree estimated by BEST as the user-specified phylogeny, the likelihood-ratio test of Nielsen & Wakeley (2001) detects a significant non-zero population migration rate from *P. brevipes* to *P. xanthospilos* (2NM = 0.233) in mtDNA and from *P. brevipes* to *P. granulosus* (2NM = 0.223) in nDNA. Nuclear gene flow is further detected from *P. xanthospilos* to *P. brevipes* (2NM = 0.165), but it is not statistically significant. These results are highly congruent with the genetic clusters pattern recovered by STRUCTURE. Using alternative phylogenies based on the alternative species tree (by *BEAST) and the mtDNA gene tree consistently detects the same migration pattern and similar migration rates. However, estimates of effective population sizes and divergence times vary greatly depending on the topology. Because neither species tree is strongly supported by current data, discussion of results from IMa2 will be limited to the existence of interspecific gene flow.

Mismatch distribution analysis does not reject the null model of a demographic expansion in *P. granulosus* (P_{SSD} = 0.086, $P_{Raggedness}$ = 0.365), with the time of expansion τ = 84.9 (95% CI: 61.9–87.1) in mutational units. Expansion time in unit of years (t) is given by $t = \tau/(2\mu k)$, in which μ is the mutation rate per site per year and k is the total number of sites per sequence (Excoffier *et al.* 2005). Given the mtDNA mutation rate at

7.7×10^{-9} per site per year in *Pachytriton* (95% HPD: 5.9×10^{-9}–9.9×10^{-9}; Wu *et al.* 2013), the demographic expansion in *P. granulosus* occurred 2.33 Ma (95% CI: 1.32–3.12 Ma). However, the shape of the mismatch distribution is far from the expected unimodal (Fig. 4-12), indicating likely multiple expansions (Babik *et al.* 2005). Similarly, multiple modes are present in the distributions of the other three species, none of which offers significant evidence of demographic expansion.

Discussion

Using multi-locus genetic data, coalescent-based species delimitation identifies multiple species entities in the *P. brevipes* complex independent of morphology or other phenotypic characters. Due to its conserved morphology, traditional taxonomy recognized only a single species in this species complex for more than 130 years (Zhao & Hu 1984; Fei *et al.* 1999; Fei *et al.* 2006). Species are difficult to diagnose in the absence of DNA data. While additional new species are suggested by the mtDNA gene tree (i.e., the maternal genealogy), this gene tree is inconsistent with the inferred species phylogeny of the *P. brevipes* complex. Only with signals from multiple unlinked DNA loci can the hypothesis of evolutionary independence of each species (not just females) be tested explicitly. The resultant taxonomy is replicable if the same data and analyses are used (Fujita *et al.* 2012). I further show that study of ecological characteristics sheds light on mechanisms of formation of independent lineages, which are delimited by coalescent-based methods.

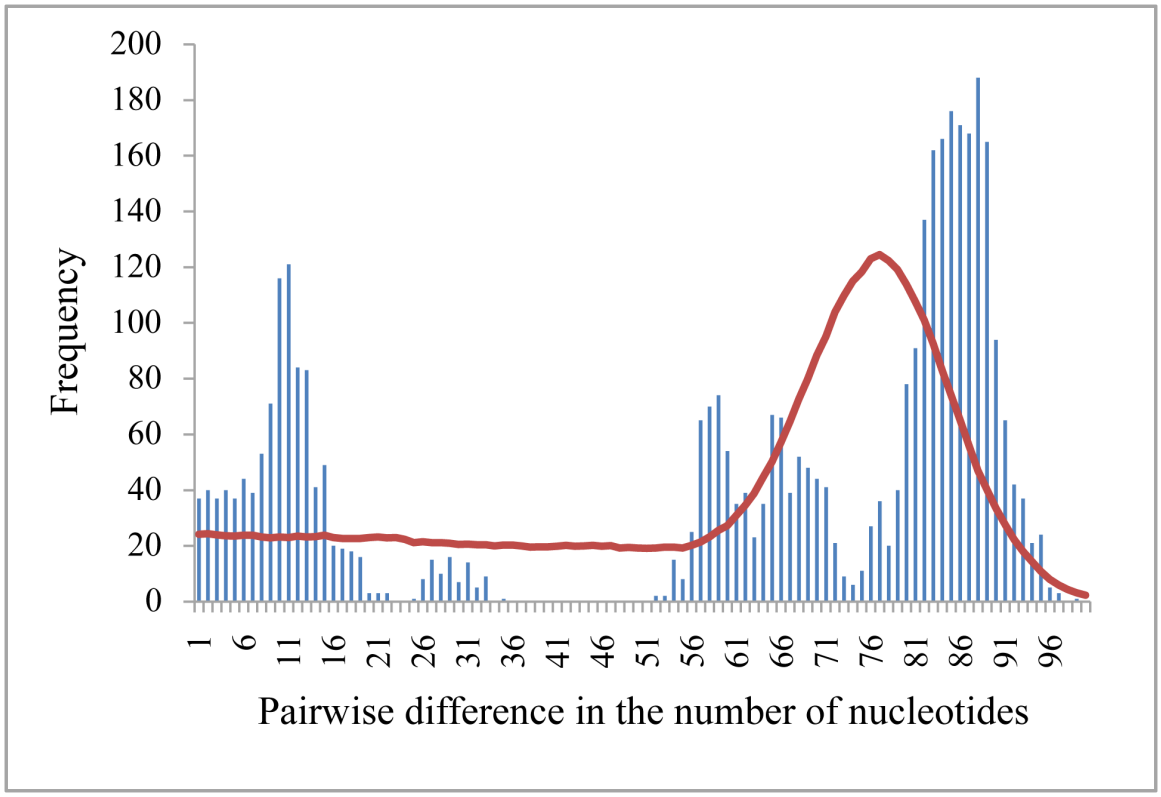

Figure 4-12. Mismatch distribution of mtDNA for *P. granulosus*, in which past demographic expansion was detected. Blue columns denote the observed pairwise difference. The red curve represents the null expectation of population growth.

Species delimitation in the **P. brevipes** *complex*

Both coalescent-based species delimitation methods from Pons *et al.* (2006) and Yang & Rannala (2010) statistically reject the single-species hypothesis. Because the GMYC model is applied to the two mitochondrial genes and the Bayesian approach in BP&P is applied to the two nuclear loci, these two analyses represent independent tests supporting the presence of multiple evolutionarily distinct lineages in the *P. brevipes* complex. Without a priori assumption of the number of species, the GMYC model recognizes 23 species (CI: 17–27) on the mtDNA gene tree. This delimitation is congruent with the four-species taxonomy but each named species is further split into 2–9 species. In agreement with previous results (Monaghan *et al.* 2009; Hendrich *et al.* 2010), the GMYC model tends to overestimate species numbers by considering genetically divergent populations as separate species. Salamanders generally have low dispersal ability and exhibit philopatry (Vieites *et al.* 2009); thus, large mtDNA divergences are expected among geographically separated populations (e.g., Martínez-Solano *et al.* 2007; Fu & Zeng 2008). Most of the inferred 23 species each corresponds to a population from a single mountain peak. The two populations of *P. xanthospilos* from Guposhan are recognized as different species even though they are extremely close in topographic distance. Guposhan has 25 high peaks (> 1000 m) that are interspersed among low valleys. On the other hand, the star-like clade in *P. granulosus* that occupies large areas of relatively low elevations in central and eastern Zhejiang comprises a single species, excluding two individuals from Tiantaishan (site 11). This contrasting pattern suggests a critical role for topography in shaping genetic structure in montane salamanders. Species status of the four species is again strongly supported by BP&P regardless of guide trees

and prior parameters used. Camargo *et al.* (2012) demonstrated that BP&P is most accurate in species delimitation compared to other new methods, including Approximate Bayesian Computation. Although intraspecific gene flow is not explicitly incorporated into the coalescent model of BP&P and my results reveal evidence of such events, species delimitation can be correctly inferred with a low migration rate (≤ 0.1 migrants per generation; Zhang *et al.* 2011), which is comparable to the level estimated among species of the *P. brevipes* complex (0.233 and 0.253 effective migrant gene copies per generation for mtDNA and nDNA, respectively).

The Bayesian cluster analysis and nuclear haplotype network further corroborate the presence of significant genetic structure in the *P. brevipes* complex. *Pachytriton feii* is unambiguously identified as a unique cluster. This confirms its species status. However, not every cluster necessarily represents a separate species. Reclassification of species boundaries according to nuclear clusters would require at least four mitochondrial introgression events involving all species except *P. feii* to explain the topology of the mtDNA gene tree. Furthermore, it is difficult to explain the contemporary separation of *P. xanthospilos* and salamanders at Tiangongshan if they belong to the same species. Alternatively, the presence of multiple nuclear clusters within *P. granulosus* and *P. brevipes* can be attributed to the retention of ancestral allelic polymorphisms and/or nuclear gene flow, which is detected between *P. brevipes* and *P. granulosus* and between *P. brevipes* and *P. xanthospilos*. Compared to mitochondrial introgression, nuclear gene flow offers a more parsimonious explanation (2 vs. 4 events) to the incongruence between mtDNA gene tree and nuclear cluster structure. Although gene flow is the counterforce for lineage separation, a low level of migration can occur continuously

between incipient species evolved in parapatry or ensue upon secondary contact after a long term of allopatric divergence (Niemiller *et al.* 2008; Nosil 2008). Hybridization between geographically neighboring species can spread alleles from source species to recipient species (Avise 1994).

Lastly, AMOVA results indicate that the four-species taxonomy provides a better estimate of the genetic structure in the mtDNA dataset than does the single-species taxonomy. Divergence among species accounts for half of the mtDNA variance. However, intraspecific divergences are still substantially large given the recognition of the four species. Despite the tendency to overestimate species number, the GMYC model suggests remarkable cryptic diversity in populations that are geographically isolated. Therefore, recognizing only the current four species could still be a conservative estimate of species diversity in the *P. brevipes* complex. Although the four species share a highly similar morphology, morphometric analysis based on linear measurements reveals significant differences in body proportions (Nishikawa *et al.* 2011a; Wu *et al.* 2012). Furthermore, breeding seasons could be separate among species to minimize gene flow. *Pachytriton granulosus* in Daiyunshan (site 20) lay eggs at early May (Fei *et al.* 2006), whereas *P. brevipes* from Wuyishan (site 21) still have mature ova in early July (Pope, 1931). In the Nanling Mountain Range, ovaries of *P. xanthospilos* develop from May to August and eggs are laid in September and October (Xu *et al.* 2002).

Conflicts between mtDNA gene tree and species tree

An accurate species phylogeny is essential for inference of speciation mechanisms. However, neither coalescent-based method (BEST and *BEAST) produced a robust

species tree using the multi-locus dataset. Disagreement is found regarding the relationship between *P. granulosus* and *P. brevipes*. The two species are most divergent in mitochondrial DNA sequences but share a majority of nuclear haplotypes. Regardless of analytical methods, inferred species trees corroborate the nDNA in recovering *P. granulosus* and *P. brevipes* as sister species.

Conflicts between individual gene trees and the underlying organismal phylogeny can be generated by incomplete sorting of ancestral polymorphisms; hybridization between geographically neighboring species also rearranges phylogenetic relationships on gene trees (Moore 1995). Existing methodology is most challenged when both processes have contributed to the evolutionary history of a group of closely related organisms (Jacobsen & Omland 2011). In the *P. brevipes* complex, I find evidence of mitochondrial and nuclear gene flow. Current species-tree inference methods attribute all discordance between gene trees and the species tree to incomplete lineage sorting and assume no post-speciation hybridization (Liu *et al.* 2009). This inference could be misleading if extensive exchange of migrants occurs between non-sister taxa (Jacobsen & Omland 2011). When gene flow occurs between sister species or an introgressing gene region is only a small portion of the genome, an accurate species tree may still be recovered using multiple independent loci (Liu *et al.* 2008). Because the inferred gene flow is weak and species trees integrate phylogenetic signals from all loci including mtDNA, I favor the sister relationship between *P. granulosus* and *P. brevipes* over the topology of the mtDNA gene tree.

Ecological niche conservatism and differentiation

Nine of the twelve comparisons in background tests suggest that observed divergences between niches are significantly smaller than divergences in their environmental backgrounds. This provides strong evidence for ecological niche conservatism in the *P. brevipes* complex (Warren *et al.* 2008). The predicted habitat of *P. brevipes* occupies nearly the entire known geographic ranges of all other species in the genus except *P. granulosus*. This pattern could either indicate niche similarities between *P. brevipes* and congeneric species or be the result of model overprediction. The latter alternative is not uncommon especially, when training occurrence data are limited (Loiselle *et al.* 2008; Giovanelli *et al.* 2010). If *P. brevipes* is excluded from the background test, half of the comparisons still unambiguously support niche conservatism in this group of salamanders. Even between *P. feii* and *P. xanthospilos*, which have the most distinct niches based on overlap statistics and the multivariate PCA, the background test confirms that their niches are more similar than expected. Predicted distributions of the two species closely conform to their known geographic ranges.

Three exceptions that do not support niche conservatism occur when the background of *P. granulosus* is used to simulate the null distribution for comparisons with the other three species. The simplest explanation is that habitat availability is heterogeneous in the geographic range of *P. granulosus*, which comprises mostly continuous high mountains in the south and a combination of mountains and large plains in the north. Two thirds of the occurrence data for *P. granulosus* are from the northern mountains due to limited accessibility to the southern region. When species appear to occupy a subset of available habitat in a heterogeneous environmental background, background tests tend to suggest

that niches are more similar than expected in one direction and less so in the opposite direction (Nakazato *et al.* 2010). Splitting the geographic range of *P. granulosus* in the background test finds that southern *P. granulosus* share significantly similar niches with the other three species whereas northern *P. granulosus* do not. This result does not necessarily suggest niche divergence within a single species, but instead reflects the broad range of niches occupied by *P. granulosus*.

Niche conservatism does not preclude niche differentiation (Wiens & Graham 2005; Warren *et al.* 2008). In other words, while still preferring a similar type of habitat, allopatric or parapatric species gradually adapt to slightly different environments as a consequence of occupying regions that do not overlap geographically (McCormack *et al.* 2010). Both niche-identity test and multivariate PCA support significant niche separation among the four species. Consistent with previous studies (Kozak & Wiens 2006, 2010), temperature fluctuations likely play a critical role in determining the distribution of terrestrial as well as aquatic montane salamanders. My results further indicate the importance of winter temperatures that set the distributional limit in the *P. brevipes* complex. Together, these two categories of climate variables generate the greatest niche differentiation, which can be explained by the distribution pattern that exhibits a latitudinal gradient (Fig. 4-1). *Pachytriton xanthospilos* and a few populations of *P. brevipes* are distributed at the southern limit of the geographic range of the genus in the Nanling Mountain Range, which is characterized by subtropical evergreen broadleaf forest with average winter temperatures of 7–9 °C and limited temperature fluctuations (Fang 2001). On the other hand, *P. feii* occurs only in the north at Huangshan and nearby mountains, where the forest zone is replaced by warm-temperate mixed

deciduous-evergreen forest (Fang 2001). In Huangshan, winter temperature could drop below -20 °C (average ~2 °C) and the annual temperature range reaches nearly 50 °C (Wang *et al.* 2008). Therefore, the first PC axis separates *P. feii* from *P. brevipes* and *P. xanthospilos*, whereas *P. granulosus*, which occupies middle latitudes, has intermediate values. Other niche separation includes differential precipitations, which are highest in the geographic range of *P. brevipes* and lowest in that of *P. xanthospilos*. Interestingly, even though the annual mean temperature and summer temperatures (PC 2) explain considerable climate variance among sampling localities, these variables do not contribute to niche differentiation in the *P. brevipes* complex. My result is consistent with the concept that niches are hypervolume spaces, in which species are differentiated along some axes but remain conserved along others (Hutchinson 1957; McCormack *et al.* 2010).

Speciation mode in the P. brevipes *complex*

As the predominant pattern observed in the *P. brevipes* complex, niche conservatism may have played a critical role in the origin of new species. Because contemporary distributions do not overlap among species, speciation most likely occurred through allopatric isolation of lineages that are constrained in their conserved niches at high elevations (Barraclough & Vogler 2000; Kozak & Wiens 2006). Although weak gene flow has been detected, results from BP&P suggest that species maintain their identities as independently evolving lineages.

Major mountains in southeastern China were uplifted before the middle Eocene (Guo 1998). This date is much earlier than the split between the *P. brevipes* complex and

its sister species *P. archospotus* at 6.8 Ma (4.5–9.1 Ma, Wu *et al.* 2013). Vicariance within the *P. brevipes* complex is unlikely the consequence of mountain orogeny. Alternatively, elevational shift of montane climatic conditions may promote vicariance and allopatric speciation in montane salamanders (Kozak & Wiens 2006, 2010). Ancestors of those salamanders, which could occupy both lowland and montane habitats when the climate was cooler and wetter, were forced to move to higher elevations as the climate changed (i.e., temperature increased or precipitation reduced). After range contraction, populations tend to be constrained within montane habitats by niche conservatism, which likely stems from their limited physiological tolerance (Bernardo & Spotila 2006). Ancestral populations are thus isolated on sky islands, between which migration is restricted. Phylogeographic studies demonstrate that contemporary climatic conditions at lowlands are always hotter and drier than those of montane habitats; absence of suitable habitat at lowlands precludes the occurrence of montane organisms (Kozak & Wiens 2006; Shepard & Burbrink 2008, 2009; Burbrink *et al.* 2011). Signals of gene flow do not invalidate the climate shift hypothesis, because migration could occur when environmental conditions at lowlands were suitable again after initial divergence (Weisrock & Larson 2006). In support of this hypothesis in the *P. brevipes* complex, there is evidence for a Pliocene global warming (3–5 Ma), which occurred after the origination of the ancestor of the *P. brevipes* complex. The warming period contrasted with the otherwise prevailing trend towards global cooling that existed since the late Miocene (Zachos *et al.* 2001; Ravelo *et al.* 2004). Salamanders would have been eliminated from low to middle elevations by increased environmental temperature. Furthermore, the unique East Asian summer monsoon, which likely triggered the initial diversification of

Pachytriton (Wu *et al.* in prep), exhibits considerable variability (An *et al.* 2001; Wang *et al.* 2010). When precipitation is reduced at a regional scale as a result of weakened summer monsoon, salamanders may retreat to montane habitats, where water level remains constantly high compared to lowlands (Viviroli *et al.* 2003). However, processes other than climate change (e.g., genetic drift, sexual selection, or adaptive mutation, etc) can also lead to reproductive isolation between incipient allopatric species (McCormack *et al.* 2010).

One potential exception to the dominant mode of allopatric speciation is found between *P. granulosus* and *P. brevipes*, which, given their sister relationship, evidence of gene flow, and geographically neighboring distributions, could represent an example of parapatric speciation in the face of gene flow. Alternatively, hybridization occurred only when species that diverged in allopatry came into secondary contact through range expansion. The timing of gene flow critically differentiates the two speciation modes (Nosil 2008; Burbrink *et al.* 2011). One approach introduced by Won & Hey (2005) records timing of migration during coalescent simulations in IMa2 and has been applied to infer parapatric speciation in cave salamanders (Niemiller *et al*. 2008). But Strasburg & Rieseberg (2011) suggests that confidence intervals of migration time estimated by this approach are too wide to be reliable, leading to spurious conclusion of speciation with ongoing gene flow. On the other hand, ecological divergence along environmental gradients is generally expected in parapatric speciation, because local adaptation can overcome the homogenizing effect of gene flow (Kozak & Wiens 2006; Nosil 2008). I did not find such evidence of ecological divergence between *P. brevipes* and *P. granulosus*. Multivariate PCA analysis reveals that 95% confidence intervals of the

niches of the two species overlap in ecological space. Background test also suggests that the two species from Fujian province, where the contemporary contact zone is located, share highly conserved niches. Furthermore, *P. granulosus* preserves signals of past demographic expansions based on mtDNA data. If demographic growth was also accompanied by range expansions, then the contemporary parapatric distribution could be a consequence of secondary contact. Therefore, speciation would be allopatric through niche conservatism. In order to confidently infer speciation mode in parapatric sister species such as *P. brevipes* and *P. granulosus*, novel methods are needed to accurately determine the timing of gene flow as well as to establish null expectations of niche characteristics when species indeed underwent parapatric speciation.

Lastly, I cannot rule out the possibility that the mtDNA gene tree is closer to the true organismal phylogeny than are the inferred species trees. If this is so, *P. brevipes* and *P. granulosus* are not sister species and their abutting distributions are more likely shaped by competitive interactions. *Pachytriton brevipes* would instead comprise the sister taxon to *P. feii*. These two species are contemporarily isolated by a large plain in northeastern Jiangxi province, indicating that speciation occurred in allopatry. However, the suitable habitat of *P. brevipes*, if not overpredicted, encompasses that of *P. feii* as well as the intervening lowlands, suggesting that factors other than the 19 climatic variables used for ecological niche modeling are involved in lineage separation (Kozak & Wiens 2006).

Conclusions

My study on the *P. brevipes* complex integrates species delimitation with study of speciation mechanism. The two components complement each other, providing a more

comprehensive understanding of the number and formation of independently evolving lineages than either does alone. Coalescent-based methods sufficiently delimit species in the *P. brevipes* complex using multi-locus data. Both mtDNA and nDNA statistically reject the single-species taxonomy, despite signals of weak gene flow. The *P. brevipes* complex represents one single example in which species richness is underestimated. In southeastern China, deep genetic structure is frequently encountered in widespread organisms. Future phylogeographic studies in this region should incorporate analysis on species delimitation for a better assessment of regional biodiversity. Understanding the species richness is the cornerstone to understand mechanisms that generate such diversity. Coalescent-based species delimitation is particularly useful when phenotypic characters exhibit either little (e.g., conserved morphology) or too much (e.g., homoplasy) variability. Although multivariate analyses reveal niche differentiation in the *P. brevipes* complex, niche modeling indicates that conservatism is the predominant pattern. The tendency for those salamanders to retain in similar montane habitats may play a critical role in driving and maintaining vicariance that leads to allopatric speciation. Crucially, niche characteristics need to be studied from more organisms from southeastern China to determine whether niche conservatism is a general pattern shared by montane endemics on "sky islands" in this region (i.e., Wuyi Mountain Range and Nanling Mountain Range). Such generality may explain the high diversity of Chinese amphibians and plants harbored in this hotspot. An additional speciation mode in the *P. brevipes* complex may include parapatric speciation, depending on the timing of gene flow.

References

An Z, Kutzbach JE, Prell WL, Porter SC (2001) Evolution of Asian monsoons and phased uplift of the Himalayan Tibetan plateau since Late Miocene times. Nature, 411, 62–66.

Avise JC (1994) Molecular Markers, Natural History and Evolution. Chapman and Hall Press, New York.

Babik W, Branicki W, Cranobrnja-Isailovic J, Cogalniceanud D, Sas I, Olgun K, Poyarkov NA, García-París M, Arntzen W (2005) Phylogeography of two European newt species: discordance between mtDNA and morphology. Molecular Ecology, 14, 2475–2491.

Ballard JWO, Whitlock MC (2004) The incomplete natural history of mitochondria. Molecular Ecology, 13, 729–744.

Barraclough TG, Vogler AP (2000) Detecting the geographical pattern of speciation from species-level phylogenies. The American Naturalist, 155, 419–434.

Bernardo J, Spotila JR (2006) Physiological constraints on organismal response to global warming: Mechanistic insights from clinally varying populations and implications for assessing endangerment. Biology Letters, 2, 135–139.

Birky CW (2001) The inheritance of genes in mitochondria and chloroplasts: laws, mechanisms, and models. Annual Review of Genetics, 35, 125–148.

Burbrink FT, Yao H, Ingrasci M, Bryson RW Jr., Guiher TJ, Ruane S (2011) Speciation at the Mogollon Rim in the Arizona mountain kingsnake (*Lampropeltis pyromelana*). Molecular Phylogenetics and Evolution, 60, 445–454.

Camargo A, Morando M, Avila LJ, Sites JW Jr. (2012) Species delimitation with ABC and other coalescent-based methods: a test of accuracy with simulations and an empirical example with lizards of the *Liolaemus darwinii* complex (Squamata: Liolaemidae). Evolution, 66, 2834–2849.

Chang J, Song D, Zhou K (2007) Incongruous nuclear and mitochondrial

phylogeographic patterns in two sympatric lineages of the wolf spider *Pardosa astrigera* (Araneae: Lycosidae) from China. Molecular Phylogenetics and Evolution, 42, 104–121.

Clement M, Posada D, Crandall KA (2000) TCS: a computer program to estimate gene genealogies. Molecular Ecology, 9, 1657–1659.

de Queiroz K (1998) The general lineage concept of species, species criteria, and the process of speciation: A conceptual unification and terminological recommendations. Pages 57–75 *in* Endless forms: Species and speciation (D. J. Howard, and S. H. Berlocher, eds.). Oxford University Press, New York.

de Queiroz K (2007) Species concepts and species delimitation. Systematic Biology, 56, 879–886.

Drummond AJ, Rambaut A (2007) BEAST: Bayesian evolutionary analysis by sampling trees. BMC Evolutionary Biology, 7, 214.

Espregueira Themudo G, Babik W, Arntzen JW (2009) A combination of techniques proves useful in the development of nuclear markers in the newt genus *Triturus*. Molecular Ecology Resources, 9, 1160–1162.

Evanno G, Regnaut S, Goudet J (2005) Detecting the number of clusters of individuals using the software STRUCTURE: a simulation study. Molecular Ecology, 14, 2611–2620.

Excoffier L (2004) Patterns of DNA sequence diversity and genetic structure after a range expansion: lessons from the infinite-island model. Molecular Ecology, 13, 853–864.

Excoffier L, Laval G, Schneider S (2005) Arlequin version 3.0: an integrated software package for population genetics data analysis. Evolutionary Bioinformatics Online, 1, 47–50.

Excoffier L, Smouse PE, Quattro JM (1992) Analysis of molecular variance inferred from metric distances among DNA haplotypes: applications to human mitochondrial DNA restriction data. Genetics, 131, 479–491.

Fang J (2001) Re-discussion about the forest vegetation zonation in East China. Acta Botanica Sinica, 43, 522–533.

Fei L, Hu S, Ye C, Huang Y eds (2006) Fauna Sinica, Amphibia Vol. 1. Beijing, China: Science Press.

Fei L, Ye C, Huang Y, Liu M (1999) Atlas of amphibians of China. Zhengzhou, China: Henan Science and Technical Press.

Fu J, Zeng X (2008) How many species are in the genus *Batrachuperus*? A phylogeographical analysis of the stream salamanders (family Hynobiidae) from southwestern China. Molecular Ecology, 17, 1469–1488.

Fujita MK, Leaché AD, Burbrink FT, McGuire JA, Moritz C (2012) Coalescent-based species delimitation in an integrative taxonomy. Trends in Ecology and Evolution 27, 480–488.

Gao LM, Möller M, Zhang X-M, Hollingsworth ML, Liu J, Mill RR, Gibby M, Li D-Z (2007) High variation and strong phylogeographic pattern among cpDNA haplotypes in *Taxus wallichiana* (Taxaceae) in China and North Vietnam. Molecular Ecology, 16, 4684–4698.

Giovanelli JGR, de Siqueira MF, Haddad CFB, Alexandrino J (2010) Modeling a spatially restricted distribution in the Neotropics: How the size of calibration area affects the performance of five presence-only methods. Ecological Modelling, 221, 215–224.

Godsoe W (2010) Regional variation exaggerates ecological divergence in niche models. Systematic Biology, 59, 298–306.

Guo F (1998) Meso-cenozoic Nanhua (South China) orogenic belt: subaerial tridirectional orogeny. Acta Geologica Sinica, 72, 22–33.

Heled J, Drummond AJ (2010) Bayesian inference of species trees from multilocus data. Molecular Biology and Evolution, 27, 570–580.

Hendrich L, Pons J, Ribera I, Balke M (2010) Mitochondrial cox1 sequence data reliably uncover patterns of insect diversity but suffer from high lineage-idiosyncratic error rates. PLoS ONE, 5, e14448.

Hey J (2010) Isolation with migration models for more than two populations. Molecular Biology and Evolution, 27, 905–920.

Hey J, Nielsen R (2004) Multilocus methods for estimating population sizes, migration rates and divergence time, with applications to the divergence of *Drosophila pseudoobscura* and *D. persimilis.* Genetics, 167, 747–760.

Hey J, Nielsen R (2007) Integration within the Felsenstein equation for improved Markov chain Monte Carlo methods in population genetics. Proceedings of the National Academy of Sciences of the United States of America, 104, 2785–2790.

Hijmans RJ, Cameron SE, Parra JL, Jones PG, Jarvis A (2005) Very high resolution interpolated climate surfaces for global land areas. International Journal of Climatology, 25, 1965–1978.

Huang S, He S, Peng Z, Zhao K, Zhao E (2007) Molecular phylogeography of endangered sharp-snouted pitviper (*Deinagkistrodon acutus*: Reptilia, Viperidae) in Mainland China. Molecular Phylogenetics and Evolution, 44, 942–952.

Huelsenbeck JP, Ronquist F (2001) MRBAYES: Bayesian inference of phylogenetic trees. Bioinformatics, 17, 754–755.

Hutchinson GE (1957) Concluding remarks. Cold Spring Harbor Symposia on Quantitative Biology, 22, 415–427.

Jacobsen F, Omland KE (2011) Species tree inference in a recent radiation of orioles (Genus *Icterus*): multiple markers and methods reveal cytonuclear discordance in the northern oriole group. Molecular Phylogenetics and Evolution, 61, 460–469.

Kozak KH, Weisrock DW, Larson A (2006) Rapid lineage accumulation in a non-adaptive radiation: phylogenetic analysis of diversification rates in eastern North American woodland salamanders (Plethodontidae: *Plethodon*). Proceedings of the Royal Society B: Biological Sciences, 273, 539–546.

Kozak KH, Wiens JJ (2006) Does niche conservatism promote speciation? A case study in North American salamanders. Evolution, 60, 2604–2621.

Kozak KH, Wiens JJ (2010) Niche conservatism drives elevational diversity patterns in Appalachian salamanders. The American Naturalist, 176, 40–54.

Kubatko LS, Gibbs HL, Bloomquist, EW (2011) Inferring species-level phylogenies and taxonomic distinctiveness using multilocus data in *Sistrurus* rattlesnakes. Systematic Biology, 60, 393–409.

Leaché AD (2009) Species tree discordance traces to phylogeographic clade boundaries in North American fence lizards (*Sceloporus*). Systematic Biology, 58, 547–559.

Leaché, AD, Fujita MK (2010) Bayesian species delimitation in West African forest geckos (*Hemidactylus fasciatus*). Proceedings of the Royal Society B: Biological Sciences, 277, 3071–3077.

Li G, Shen Z, Ying T, Fang J (2009) The spatial pattern of species richness and diversity centers of gymnosperm in China. Biodiversity Science, 17, 272–279.

Li SH, Yeung CKL, Feinstein J, Han LX, Manh HL, Wang CX, Ding P (2009) Sailing through the Late Pleistocene: unusual historical demography of an East Asian endemic, the Chinese Hwamei (*Leucodioptron canorum canorum*), during the last glacial period. Molecular Ecology, 18, 622–633.

Lin L, Qu Y, Li H, Zhou K, Ji X (2012) Genetic structure and demographic history should inform conservation: Chinese cobras currently treated as homogenous show population divergence. PLoS ONE, 7, e36334.

Liu L (2008) BEST: Bayesian estimation of species trees under the coalescent model. Bioinformatics, 24, 2542–2543.

Liu L, Pearl DK (2007) Species trees from gene trees: reconstructing Bayesian posterior distributions of a species phylogeny using estimated gene tree distributions. Systematic Biology, 56, 504–514.

Liu L, Pearl DK, Brumfield RT, Edwards SV (2008) Estimating species trees using multiple-allele DNA sequence data. Evolution, 62, 2080–2091.

Liu L, Yu LL, Kubatko L, Pearl DK, Edwards SV (2009) Coalescent methods for estimating phylogenetic trees. Molecular Phylogenetics and Evolution, 53, 320–328.

Loiselle BA, Jorgensen PM, Consiglio T, Jimenez I, Blake JG, Lohmann LG, Montiel OM (2008) Predicting species distributions from herbarium collections: does climate bias in collection sampling influence model outcomes? Journal of Biogeography, 35, 105–116.

López-Pujol J, Zhang MF, Sun HQ, Ying TS, Ge S (2011) Centres of plant endemism in China: Places for survival or for speciation? Journal of Biogeography, 38, 1267–1280.

Martínez-Solano I, Jockusch EL, Wake DB (2007) Extreme population subdivision throughout a continuous range: phylogeography of *Batrachoseps attenuatus* (Caudata: Plethodontidae) in western North America. Molecular Ecology, 16, 4335–4355.

Mayden RL (1997) A hierarchy of species concepts: The denouement in the saga of the species problem. Pages 381–424 in Species: The units of biodiversity (M. F. Claridge, H. A. Dawah, and M. R.Wilson, eds.). Chapman and Hall, London.

Mayr E (1963) Animal species and evolution. Cambridge, MA: Harvard University Press.

McCormack JE, Zellmer AJ, Knowles LL (2010) Does niche divergence accompany allopatric divergence in *Aphelocoma* jays as predicted under ecological speciation?: insights from tests with niche models. Evolution, 64, 1231–1244.

Meiklejohn CD, Meiklejohn KL, Rand DM (2007) Positive and negative selection on the mitochondrial genome. Trends in Genetics, 23, 259–263.

Miller MA, Pfeiffer W, Schwartz T (2010) Creating the CIPRES Science Gateway for inference of large phylogenetic trees. Proceedings of the Gateway Computing

Environments Workshop (GCE), 14 Nov. 2010, New Orleans, LA pp 1–8.

Monaghan MT, Wild R, Elliot M, Fujisawa T, Balke M, Inward DJ, Lees DC, Ranaivosolo R, Eggleton P, Barraclough TG, Vogler AP (2009) Accelerated species inventory on Madagascar using coalescent-based models of species delineation. Systematic Biology, 58, 298–311.

Moore WS (1995) Inferring phylogenies from mtDNA variation: mitochondrial-gene tree versus nuclear-gene tree. Evolution, 49, 718–726.

Mueller RL (2006) Evolutionary rates, divergence dates, and the performance of mitochondrial genes in Bayesian phylogenetic analysis. Systematic Biology, 55, 289–300.

Murphy RW, Fu JZ, Upton DE, De Lema T, Zhao EM (2000) Genetic variability among endangered Chinese giant salamanders, *Andrias davidianus*. Molecular Ecology, 9, 1539–1547.

Nakazato T, Warren DL, Moyle LC (2010) Ecological and geographic modes of species divergence in wild tomatoes. American Journal of Botany, 4, 680–693.

Nielsen R, Wakeley J (2001) Distinguishing migration from isolation: a Markov chain Monte Carlo approach. Genetics, 158, 885–896.

Niemiller ML, Nosil P, Fitzpatrick BM (2008) Recent divergence-with-gene-flow in Tennessee cave salamanders (Plethodontidae: *Gyrinophilus*) inferred from gene genealogies. Molecular Ecology, 17, 2258–2275.

Nishikawa K, Jiang J, Matsui M (2011a) Two new species of *Pachytriton* from Anhui and Guangxi, China (Amphibia: Urodela: Salamandridae). Current Herpetology, 30, 15–31.

Nishikawa K, Jiang J, Matsui M, Mo Y (2011b) Unmasking *Pachytriton labiatus* (Amphibia: Urodela: Salamandridae), with description of a new species of *Pachytriton* from Guangxi, China. Zoological Science, 28, 453–461.

Nosil P (2008) Speciation with gene flow could be common. Molecular Ecology, 17, 2103–2106.

Nylander JAA (2004) MrModeltest v2 [Computer software and manual]. Program distributed by the author. Evolutionary Biology Centre, Uppsala University. Available via http://www.abc.se/~nylander/

Phillips SJ, Anderson RP, Schapire RE (2006) Maximum entropy modeling of species geographic distributions. Ecological Modelling, 190, 231–259.

Phillips SJ, Dudík M (2008) Modeling of species distributions with Maxent: new extensions and a comprehensive evaluation. Ecography, 31, 161–175.

Pons J, Barraclough TG, Gomez-Zurita J, Cardoso A, Duran DP, Hazell S, Kamoun S, Sumlin WD, Vogler AP (2006) Sequence-based species delimitation for the DNA taxonomy of undescribed insects. Systematic Biology, 55, 595–609.

Pope CH (1931) Notes on amphibians from Fukien, Hainan, and other parts of China. Bulletin of the American Museum of Natural History, 61, 397–611.

Posada D, Crandall KA (2001) Intraspecific gene genealogies: Trees grafting into networks. Trends in Ecology and Evolution, 16, 37–45.

Pritchard JK, Stephens M, Donnelly P (2000) Inference of population structure using multilocus genotype data. Genetics, 155, 945–959.

Rambaut A (1995) Se–Al: Sequence alignment program. Oxford University, Oxford, U.K. Available from http://tree.bio.ed.ac.uk/software/seal/ (Accessed May 20, 2012)

Rambaut A, Drummond AJ (2007) Tracer v1.4, Available from http://beast.bio.ed.ac.uk/Tracer (Accessed May, 20, 2012)

Ravelo AC, Andreasen DH, Lyle M, Lyle AO, Wara MW (2004) Regional climate shifts caused by gradual global cooling in the Pliocene epoch. Nature, 429, 263–267.

Rogers AR, Harpending H (1992) Population growth makes waves in the distribution of pairwise genetic differences. Molecular Biology and Evolution, 9, 552–569.

Rosenberg NA (2004) Distruct: a program for the graphical display of population structure. Molecular Ecology Notes, 4, 137–138.

Schoener TW (1968) The *Anolis* lizards of Bimini – resource partitioning in a complex fauna. Ecology, 49, 704–726.

Shepard DB, Burbrink FT (2008) Lineage diversification and historical demography of a sky island salamander, *Plethodon ouachitae*, from the Interior Highlands. Molecular Ecology, 17, 5315–5335.

Shepard DB, Burbrink FT (2009) Phylogeographic and demographic effects of Pleistocene climatic fluctuations in a montane salamander, *Plethodon fourchensis*. Molecular Ecology, 18, 2243–2262.

Shih HT, Zhou XM, Chen GX, Chien IC, Ng PKL (2011) Recent vicariant and dispersal events affecting the phylogeny and biogeography of East Asian freshwater crab genus *Nanhaipotamon* (Decapoda: Potamidae). Molecular Phylogenetics and Evolution, 58, 427–438.

Song G, Qu YH, Yin ZH, Li SS, Liu NF, Lei FM (2009) Phylogeography of the *Alcippe morrisonia* (Aves: Timaliidae): long population history beyond late Pleistocene glaciations. BMC Evolutionary Biology, 9, 143.

Stamatakis A (2006) RAxML-VI-HPC: maximum likelihood-based phylogenetic analyses with thousands of taxa and mixed models. Bioinformatics, 22, 2688–2690.

Stamatakis A, Hoover P, Rougemont J (2008) A rapid bootstrap algorithm for the RAxML web servers. Systematic Biology, 57, 758–771.

Stephens M, Donnelly P (2003) A comparison of Bayesian methods for haplotype reconstruction from population genotype data. American Journal of Human Genetics, 73, 1162–1169.

Stephens M, Smith N, Donnelly P (2001) A new statistical method for haplotype reconstruction from population data. American Journal of Human Genetics, 68, 978–989.

Strasburg JL, Rieseberg LH (2011) Interpreting the estimated timing of migration events between hybridizing species. Molecular Ecology, 20, 2353–2366.

Swets JA (1988) Measuring the Accuracy of Diagnostic Systems. Science, 240, 1285–1293.

Vähä JP, Primmer CR (2005) Efficiency of model-based Bayesian methods for detecting hybrid individuals under different hybridization scenarios and with different numbers of loci. Molecular Ecology, 15, 63–72.

Vieites DR, Nieto-Roman S, Wake DB (2009) Reconstruction of the climate envelopes of salamanders and their evolution through time. Proceedings of the National Academy of Sciences of the United States of America, 106, 19715–19722.

Viviroli D, Weingartner R, Messerli B (2003) Assessing the hydrological significance of the world's mountains. Mountain Research and Development, 23, 32–40.

Wan SM, Tian J, Steinke S, Li AC, Li TG (2010) Evolution and variability of the East Asian summer monsoon during the Pliocene: Evidence from clay mineral records of the South China Sea. Palaeogeography Palaeoclimatology Palaeoecology, 293, 237–247.

Wang X, Yang B, Zhang J, Zhang S, Yang H (2008) Study on climate change at Huangshan Mountain in recent 50 years. Resource Development and Market, 24, 834–836.

Warren DL, Glor RE, Turelli M (2008) Environmental niche equivalency versus conservatism: quantitative approaches to niche evolution. Evolution, 62, 2868–2883.

Weisrock DW, Larson A (2006) Testing hypotheses of speciation in the *Plethodon jordani* species complex with allozymes and mitochondrial DNA sequences. Biological Journal of the Linnean Society, 89, 25-51.

Wiens JJ, Ackerly DD, Allen AP, Anacker BL, Buckley LB, Cornell HV, Damschen EI, Davies TJ, Grytnes JA, Harrison SP, Hawkins BA, Holt RD, McCain CM, Stephens PR (2010) Niche conservatism as an emerging principle in ecology and conservation biology. Ecology Letters, 13, 1310–1324.

Wiens JJ, Graham CH (2005) Niche conservatism: integrating evolution, ecology, and conservation biology. Annual Review of Ecology Evolution and Systematics, 36, 519–539.

Woerner AE, Cox MP, Hammer MF (2007) Recombination-filtered genomic datasets by information maximization. Bioinformatics, 23, 1851–1853.

Won YJ, Hey J (2005) Divergence population genetics of chimpanzees. Molecular Biology and Evolution, 22, 297–307.

Wooten JA, Gibbs HL (2011) Niche divergence and lineage diversification among closely related *Sistrurus* rattlesnakes. Journal of Evolutionary Biology, 25, 317–328.

Wu Y, Wang Y, Jiang K, Chen X, Hanken J (2010) Homoplastic evolution of external coloration in Asian stout newts (*Pachytriton*) inferred from molecular phylogeny. Zoologica Scripta, 39, 9–22.

Wu Y, Wang Y, Hanken J (2012) New species of *Pachytriton* (Caudata: Salamandridae) from the Nanling Mountain Range, southeastern China. Zootaxa, 3388, 1–16.

Wu Y, Wang Y, Jiang K, Hanken J (2013) Significance of pre-Quaternary climate change for montane species diversity: Insights from Asian salamanders (Salamandridae: *Pachytriton*). Molecular Phylogenetics and Evolution, 66, 380–390.

Xie F, Lau MWN, Stuart SN, Chanson JS, Cox NA, Fischman DL (2007) Conservation needs of amphibians in China: a review. Science in China Series C, Life Sciences, 50, 265–276.

Xu J, Zou P, Wen C, Chen J (2002) Sexual dimorphism and female reproduction of *Pachytriton labiatus* in the north of Guangdong. Journal of Shaoguan University (Natural Science), 23, 1–6.

Yang Z, Rannala B (2010) Bayesian species delimitation using multilocus sequence data. Proceedings of the National Academy of Sciences of the United States of America, 107, 9264–9269.

Zachos J, Pagani M, Sloan L, Thomas E, Billups K (2001) Trends, rhythms, and aberrations in global climate 65 Ma to present. Science, 292, 686–693.

Zhang C, Zhang D, Zhu T, Yang Z (2011) Evaluation of a Bayesian coalescent method of species delimitation. Systematics Biology, 60, 747–761.

Zhang H, Yan J, Zhang GQ, Zhou KY (2008) Phylogeography and demographic history of Chinese black-spotted frog populations (*Pelophylax nigromaculata*): Evidence for independent refugia expansion and secondary contact. BMC Evolutionary Biology, 8, 21.

Zhao E, Hu Q (1984) Studies on Chinese tailed amphibians. Chengdu, China: Sichuan Scientific and Technical Publishing House.